$\mathrm{A}\,\mathrm{A}\,\mathrm{E}$ ▶━━

AERONAUTICAL
AND ASTRONAUTICAL
ENGINEERING DEPARTMENT

ENGINEERING EXPERIMENT STATION, COLLEGE OF ENGINEERING, UNIVERSITY OF ILLINOIS, URBANA

TRAILING EDGE FLOW CONDITIONS

AS A FACTOR IN AIRFOIL DESIGN

by

A.I. Ormsbee and Mark D. Maughmer

ABSTRACT

Some new developments relevant to the design of single-element airfoils using potential flow methods are presented. In particular, the role played by the non-dimensional trailing edge velocity in design is considered and the relationship between the specified value and the resulting airfoil geometry is explored. In addition, the ramifications of the unbounded trailing edge pressure gradients generally present in the potential flow solution of the flow over an airfoil are examined, and the conditions necessary to obtain a class of airfoils having finite trailing edge pressure gradients developed. The incorporation of these conditions into the inverse method of Eppler is presented and the modified scheme employed to generate a number of airfoils for consideration. The detailed viscous analysis of airfoils having finite trailing edge pressure gradients demonstrates a reduction in the strong inviscid-viscid interactions generally present near the trailing edge of an airfoil.

TABLE OF CONTENTS

APPENDICES

CHAPTER I

INTRODUCTION

Low-Speed, Single-Element Airfoil Design

Much of the current research effort applied to low-speed airfoils is directed toward the analysis and design of multi-element sections, which incorporate high-lift devices such as multiple-slotted flaps and movable leading edge slats. The use of such airfoils permits a broad range of performance through the integration of an airfoil that is suitable for high-speed cruise with a configuration capable of high-lift for take-off and landing. In spite of the strong interest in the complicated flow phenomena connected with the multi-element design, considerable motivation remains for the study of single-element wing sections. For example, a number of practical applications exist, including low-speed recreational aircraft, sailplanes, helicopter and windmill rotors, and aircraft in the expanding arena of remotely piloted vehicles (RPV's), for which either the cost and mechanical complexity of a high-lift system cannot be justified, or such a section is unnecessary in that a broad performance envelope is not a design requirement. Furthermore, much of the increased understanding resulting from the study of single-element airfoils is directly applicable to the individual components of the multi-element designs.

As detailed by various authors, most notably Wortmann [1]-[4], Eppler [5]-[7], and Miley [8], the modern methodology of low-speed airfoil design involves relating the aerodynamic performance features sought to particular characteristics of the boundary layer and, in turn, specifying the velocity

(pressure) distribution around the airfoil necessary to achieve those boundary layer characteristics which give rise to the desired performance. Once the required velocity distribution has been established, the airfoil is obtained by means of any one of a number of inverse (design) procedures such as the exact potential flow methods, based on complex functions, developed by Lighthill [9], Eppler [5] and Arlinger [10]. Whereas in the direct (analysis) problem every airfoil has a corresponding velocity distribution, the inverse problem is complicated by the fact that every velocity distribution does not necessarily have a corresponding airfoil. Thus, in the design process it is necessary to allow some flexibility in the prescribed velocity distirbution such that a physically reasonable airfoil can be obtained. Also, in some inverse methods, including those of Lighthill [9] and Eppler [5], the velocity distribution is specified through parameters which are rather indirect. Consequently, these methods usually require some amount of iteration in order to determine what parameter values actually achieve the desired velocity distribution.

One particular low-speed airfoil research subject which has received considerable attention is concerned with the theoretically interesting question of how much lift can be generated by a single-element airfoil without using active means of boundary layer control. In order to make the problem more tractable, most efforts in the area have considered only flows which are fully attached. Typically, airfoils in application achieve maximum lift when the lift increase due to an increase in angle of attack is just equalled by the lift losses due to separation; and consequently, the production of high lift is usually accompanied by relatively high drag. Thus, by limiting the maximum lift airfoil problem to fully attached flows, not only are the

complications of analyzing separated flows eliminated, but the desirable
result that the airfoils generated attain high lift with comparatively low
drag is also achieved.

As discussed by Smith [11] and Liebeck [12], the velocity distribution
formulated for the purposes of maximizing the lift generated by a single-
element airfoil having fully attached flow is of the form shown in Figure 1.
On the lower surface, the desired velocity distribution is simply that which
is as close to stagnation over as much of the lower surface as is possible.
On the upper surface, it is dictated that the flow accelerate rapidly from the
leading edge stagnation point to a level of constant velocity (rooftop
velocity) that is to be maintained as far aft as possible and still permit
pressure recovery over the rear of the airfoil without introducing flow
separations due to an excessive adverse pressure gradient. As first adopted
for airfoils by Liebeck and Ormsbee [13], the theoretical recovery that allows
the longest rooftop by achieving the recovery of a given pressure in the
shortest distances possible is the zero skin friction approximation of
Stratford [14]. The notion of zero skin friction implies that separation is
everywhere imminent along the Stratford distribution. The ideal maximum lift
velocity distribution was further defined by Ormsbee and Chen [15] in that the
optimum relationship between the maximum velocity on the upper surface, the
rooftop velocity, and the trailing edge velocity was determined. This
relationship, however, does not specify the magnitude of either the rooftop
velocity or the trailing edge velocity, but only the optimum ratio between the
two. As a consequence, disregarding the small adjustment in rooftop length
necessary because the local Reynolds number in that region changes, increasing
the value of the trailing edge to free-stream velocity ratio, V_{TE}/U, allows

the level of the entire upper surface velocity distribution to increase while
the margin against separation offered by the Stratford distribution is
unchanged. Thus, increasing V_{TE}/U is an extremely effective means of
increasing the amount of lift generated by a particular design. At this
point, however, although there is no doubt that for practical airfoils the
value of V_{TE}/U must have an upper bound, it is not evident what that bound is.
Because of its strong influence on the amount of lift generated, and because
its specification can be connected to minimizing drag through the attainment
of fully attached flow, it would be of some benefit to low-speed airfoil
design to better understand the influences that the specification of V_{TE}/U has
on the aerodynamic characteristics of an airfoil, as well as how the
specification physically impacts the geometry of the profile which results.

Consideration of Flow Conditions in the Vicinity of the Trailing Edge

In surveying the available literature to better understand what limits
exist on the value of V_{TE}/U, it is found that conventional airfoils, such as
those catalogued by Abbott and von Doenhoff [16], exhibit a trailing edge
velocity in the neighborhood of eight to nine-tenths of the free-stream
value. Liebeck [12], indicates that the bounding value for V_{TE}/U in potential
flow is unity. This conclusion is advanced through the argument that for a
cusped trailing edge, symmetrical airfoil at zero angle of attack, the
trailing edge velocity approaches that of the free-stream as the thickness of
the airfoil goes to zero, i.e., a flat plate. Thus, it is supposed that any
thickness or lift generation requires that the trailing edge velocity be less
than free-stream. While no disagreement is taken with these notions, which
can be demonstrated using the familiar Joukowsky transformation, it remains to

develop them in a more general manner and to indicate how the physical characteristics of an airfoil are affected by the specified value of V_{TE}/U.

Another characteristic of the flow in the vicinity of the trailing edge which warrants further consideration, and will be developed in detail later, is the fact that, in general, the complex pressure gradient, $p_x - ip_y$, at the trailing edge is infinite. That p_{xt} is infinite is readily confirmed by noting the vertical slope that occurs at the trailing edge in the pressure distributions of Joukowsky airfoils, for example. Although not as readily observable, the value of p_{yt} exhibits similar behavior.

In addition to the presence of infinite trailing edge pressure gradients, there are numerous examples in the literature, including References [17]-[19], of airfoils in which the potential flow velocity distribution is characterized by a large velocity differential between the upper and lower surfaces over the aft portions of the airfoil and in the region of the trailing edge. As is demonstrated by Figure 2, this large velocity differential is introduced as it increases the area enclosed by the velocity distribution and the resulting increase in aft pressure loading on the airfoil manifests itself through increased lift production. While it might appear, in some cases, that the velocity distribution is closed by a vertical slope connecting the upper and lower surface velocities, because potential flow theory requires that each point in the flow field have a unique velocity then, as discussed by Nonweiler [20], there can be no difference between the upper and lower surface flow velocities at the point where they meet and flow into the wake. Thus, although the recovery distributions of a number of airfoils appearing in the literature, including that of Figure 2, have been formulated using a value of V_{TE}/U in excess of unity, in actuality, the value used is not that of the

trailing edge but, rather, corresponds to a portion on the upper surface slightly upstream of the trailing edge. From this point, the fluid is decelerated very rapidly to the actual velocity at the trailing edge. This value is in common with that resulting from accelerating the flow on the lower surface in the immediate vicinity of the trailing edge through a steep, favorable pressure gradient. While it is quite clear that the viscous effects prevent the full realization of the lift gains predicted by potential flow methods, exper _____ results have indicated, in some applications, that the proper implementation of large velocity differentials between the upper and lower surfaces to very near the trailing edge can be of some benefit.

An interesting example of an airfoil designed to exploit the benefits of a large amount of aft loading is that of Kennedy and Marsden [18]. The potential flow analysis of this airfoil, shown in Figure 2, yields a lift coefficient of 3.81, resulting from the design velocity distribution based on a upper surface trailing edge velocity of 1.2U. While experimentally, the lift coefficient at the design conditions was found to be an impressive 2.64, it was obtained at the expense of relatively high drag resulting in a maximum lift-to-drag ratio notably less than those obtained for other high lift designs. It was also found experimentally that viscous effects reduced the upper surface velocity just upstream of the trailing edge from its potential flow design value to 1.07U. To further demonstrate the viscous influences, Figure 3 compares an off-design potential flow velocity distribution of the Kennedy and Marsden airfoil with one obtained experimentally, Reference [18]. In addition, the figure includes results obtained using the GRUMFOIL code developed by Mead and Melnik [21]. In the classical method of correcting inviscid flow results for the effects of viscosity, the displacement thickness

of the boundary layer on the airfoil is calculated and added to the original profile. This results in an equivalent body which can be analyzed to approximately account for the influence of the boundary layer. This procedure, however, ignores additional viscid-inviscid interactions, each of which has an influence on the inviscid result equal to that of the displacement thickness. The GRUMFOIL code remedies the deficiencies of previous methods for the analyses of the flow over an airfoil by incorporating a complete interacting boundary layer formulation which, in consideration of application to low-speed flows, includes the effects of the boundary layer displacement thickness on the airfoil and in the wake, wake curvature effects arising from the turning of low momentum fluid in the wake along curved streamlines, and the effects of strong viscous interactions in the vicinity of the trailing edge. As Figure 3 demonstrates, the potential flow velocity distribution over the airfoil is modified considerably by viscous effects. In particular, the steep trailing edge velocity gradient is rounded off to the extent that the actual trailing edge velocity of .94U is easily identified. It is also evident from Figure 3 that, because the viscous influences are amplified in high lift situations, the conscientious design of high lift airfoils for actual applications must involve the integration of viscous flow analysis with the potential flow design method.

In the potential flow inverse scheme of Eppler [5], an attempt is made to achieve the lift-increasing benefits of a large upper and lower surface velocity differential near the trailing edge and also, in a somewhat qualitative manner, account for the viscous effects. While the potential flow formulation requires that the upper and lower surfaces have equal velocities at the trailing edge, the manner in which geometrical closure of the airfoil

is achieved allows for large velocity differences between the upper and lower surfaces to a point very near the trailing edge. Consequently, this trailing edge treatment allows for velocity distributions which, in the vicinity of the trailing edge, are very similar to those which occur when viscous influences are considered. While this model is clearly an improvement on the usage of the nearly infinite trailing edge gradie' , the question arises as to what is the permissible extent of recovery before the steepened portion of the distribution causes flow separation problems. For example, if a Stratford distribution is specified for recovery on the upper surface, then, even in the best of situations, separation would occur where the velocity gradient steepens due to the closure contribution. As is demonstr-ed by both the experimental and viscous analysis results shown in Figure 3, the loss of loading near the trailing edge that occurs when viscous effects are considered generally causes the overall recovery gradients to be somewhat steeper than indicated by inviscid results. Thus, it is a possibility that the steeper gradients will cause severe separation problems. Even in the case of more practical airfoils, not pushing recovery limits as does a Stratford distribution, only the gentlest distributions will have sufficient momentum in the boundary layer to overcome the very steep adverse pressure gradient introduced in the vicinity of the trailing edge by the presence of large amounts of aft loading. To reduce these problems, Eppler [5] discusses the fact that, while it is desirable to reduce the upper surface adverse pressure gradient in the closure region as much as possible by increasing the value of the trailing edge velocity ratio, such relief is limited. As the value of V_{TE}/U is increased, a point is reached for which any additional increase causes the upper and lower surfaces of the airfoil to intersect one another

ahead of the trailing edge. In addition, Nonweiler [20] notes that even if it were possible to completely eliminate the upper surface adverse pressure gradient due to closure by accelerating the lower surface flow through a strong favorable gradient and discharging the flows from both surfaces into the wake at a velocity corresponding to a smooth continuation of the upper surface recovery distribution that, as this dumping velocity would be greater than th..t of the free stream, some deceleration of the flow in the wake would be required. This situation is also likely to have an upstream influence manifested as separation on the upper surface ahead of the trailing edge.

A demonstration of the problems that might occur usirg the trailing edge treatment of Eppler [5] is provided by the high-lift, single-design-point airfoils of Thompson [19]. These airfoils make use of the Stratfod recovery distribution on the upper surface. As shown in Figure 4, the closure contribution at the trailing ed$_c$e of these airfoils extends over such a narrow portion of chord length that, like the Kennedy and Marsden airfoil of Figure 2, it appears as though the large velocity difference between the upper and lower surfaces is adjusted at the trailing edge through an infinite velocity gradient. As illustrated in the insets of Figure 4, however, it is found that the value of V_{TE}/U used to generate the upper surface recovery distribution is actually an upstream po'.nt at which is initiated a very rapid deceleration of the flow around the small protuberance located at the rear of the airfoil. Thus, the actual V_{TE}/U is considerably less than the value in excess of unity which was employed in formulating the Stratford distribution. Consequently, rather than the desired velocity distribution, which includes recovery through a Stratford distribution extending to the wake, the airfoil generated has recovery through a Stratford distribution followed by a violent recompression

at a point near the trailing edge. Not only might this result lead to flow separation problems and a thicker wake than is necessary, but more importantly, the discrepancies that exist between the intended velocity distribution and that obtained introduces a degree of uncertainty into the design procedure which is undesirable. While a part of these problems can be attributed to erroneous interpretations in the human-computer iteration process which is necessary with the inverse method used for these designs, a more significant element was the fact that the values of V_{TE}/U used in formulating the desired velocity distributions were much too high. While this possibility was clearly acknowledged, it was also emphasized by Thompson [19] that the literature contained very little information to aid in the selection of this important parameter.

Objectives of the Present Investigation

As part of the desired velocity distribution, the value of the trailing edge velocity ratio must be specified in most airfoil design procedures; however, there is little information in the existing literature to guide in its choice. Consequently, as has been discussed by several authors, including McMasters and Henderson [22], V_{TE}/U is perhaps one of the most difficult of the required parameters to determine. While in many design exercises, such as those directed at low drag, the situation is less critical in that the desired aerodynamic characteristics are less sensitive to an optimum selection of V_{TE}/U, the difficulty is heightened in the maximum lift problem because of the strong dependency of the lift generated to the value specified. Thus, in order to provide some guidance for selecting the value of V_{TE}/U in the design of low-speed, high-lift airfoils, the first part of the present investigation

considers the relationship between the maximum values of V_{TE}/U obtainable and profile characteristics such as thickness and camber.

Considering the modification of the potential flow maximum lift velocity distributions by viscous effects, there is clearly a trade-off between the lift gained by maintaining a large velocity differential between the upper and lower surfaces in the vicinity of the trailing edge and the lift lost by separation. While there are examples of potential flow designed airfoils that achieve some portion of their design goals, Kennedy and Marsden [18] and Sivier, et. al. [23], there are others, such as the designs of Thompson [19] experimentally investigated by Moore [24], which exhibit extremely poor performance attributed primarily to widespread flow separation. In the context of designing airfoils having predictable characteristics, the inconsistency of results for airfoils which make use of large velocity differentials near the trailing edge leaves much to be desired. Thus, until additional guidance is available, the design process is limited in not knowing precisely to what extent the potential flow results in the vic nity of the trailing edge will be modified by viscous interactions. In order to eliminate some of the uncertainty in using potential flow airfoil design methods, the second part of this research is directed toward the development of a class of airfoils in which the viscous interactions in the trailing edge region are minimized by the introduction of a condition to insure that the pressure gradients at the trailing edge are bounded. Not only does the enforcement of this condition permit the fluid on the airfoil to flow smoothly into the wake; but in addition, it typically excludes the possibility of the closure contribution causing steep upper surface adverse pressure gradients in the vicinity of the trailing edge. The practical implementation of this condition

is achieved through modification of the airfoil design code of Eppler and Somers [25]. While unquestionably viscous effects alter the flow in the trailing edge region, it is hoped that the application of the condition for finite trailing edge pressure gradients modify the viscous influences to the extent that the results obtained using potential flow design methods are more reliable.

The final phase of the research effort to be presented is directed toward exploring the influences on the geometry and aerodynamic characteristics caused by the introduction of the finite trailing edge pressure gradients condition into the design process. To facilitate this exploration, a number of airfoils having finite trailing edge pressure gradients are presented and compared to airfoils which are as similar as possible but having unbounded trailing edge pressure gradients.

CHAPTER II

MAXIMUM TRAILING EDGE VELOCITIES

Preliminary Remarks

As the ratio of the trailing edge to free-stream velocity, V_{TE}/U, has a
global influence on the lifting capability of a given airfoil, it is important
to determine the maximum value that this ratio can attain and how its
specification affects other airfoil design considerations. While, as it has
been noted, there are assertions in the literature regarding a potential flow
upper bound of V_{TE}/U equal to unity for a flat plate at zero angle of attack,
Reference [12] for example, these are apparently based on results formulated
through the use of the Joukowsky transformation. A survey of the literature
has not revealed an extension of this conclusion for the more general
transformation mapping a circle into an airfoil. In order to develop such a
demonstration, a series of truncations of the general transformation, the so-
called von Mises transformations, will be used to show that the addition of a
finite number of extra terms to the series does not alter the flat plate
results. While this does not result in a general proof concerning the
ultimate value that V_{TE}/U can attain, it does indicate that the upper bound
for the very broad class of von Mises airfoils is indeed unity. More
importantly, however, the development provides some insight into how the
specification of V_{TE}/U influences the geometry of an airfoil.

In the course of numerical design studies in which it was attempted to
raise V_{TE}/U to as high of value as possible, it was found that while the
potential flow formulation of the problem places no restrictions on the upper

bound of V_{TE}/U, the resulting airfoils are physically restricted in that as increases are made in V_{TE}/U, a point is eventually reached for which further increases cause the upper and lower surface to cross one another such that a profile .iaving a region of negative thickness is generated. Thus, this situation indicates that an additional constraint must be imposed such that the problem becomes that of finding the largest value of V_{TE}/U for which a physically realizable airfoil is possible.

Transformation of a Circle into an Airfoil

The method of conformal mapping may be employed to analyze the flow over airfoils by transforming the known flow field about a circular cylinder into that about an airfoil as depicted in Figure 5. In this formulation, $\zeta = \mu$ denotes the center of the circle, r its radius, and the function $\zeta_c = \mu + re^{i\phi}$ describes the circle. The complex potential for the flow about the circular cylinder with circulation Γ can be expressed as

$$F(\zeta) = U(\zeta-\mu)e^{-i\alpha} + \frac{U\,r^2}{(\zeta-\mu)}\,e^{i\alpha} + \frac{i\Gamma}{2\pi}\,\ln\frac{(\zeta-\mu)}{re^{i\alpha}} \qquad (2\text{-}1)$$

and the complex velocity in the ζ-plane is

$$w(\zeta) = \frac{dF(\zeta)}{d\zeta} = Ue^{-i\alpha} - Ur^2e^{i\alpha}\frac{1}{(\zeta-\mu)^2} + \frac{i\Gamma}{2\pi}\frac{1}{(\zeta-\mu)} \qquad (2\text{-}2)$$

The complex velocity in the airfoil plane is then given by

$$w(z) = \frac{dF}{d\zeta} \Big/ \frac{dz}{d\zeta} = w(\zeta)/z' \qquad (2\text{-}3)$$

where $z(\zeta)$ is the mapping function which takes the circle into the airfoil. This function will, in general, possess a certain number of critical points which are defined by the solution of the equation $(dz/d\zeta) = 0$. A profile having a sharp trailing edge requires that one of these critical points be on the circle while all of the others are contained in the interior of the circle. Thus, the critical point on the circle, ζ_T, maps to the trailing edge of the airfoil while the regions external to the circle and the airfoil are everywhere conformal.

The amount of circulation present in equation (2-1) may be determined by introducing the Kutta condition, which requires that the flow velocity at the trailing edge be finite and continuous. From equation (2-3), the complex velocity at the trailing edge is given

$$w_T = w(z_T) = w(\zeta_T)/z_T' \qquad (2-4)$$

Because a sharp trailing edge requires that z_T' be zero, the requirement that w_T be finite necessitates that $w(\zeta_T)$ also be zero. The circulation which fixes this stagnation point at $\zeta_T = re^{-i\beta} + \mu$ is found from equation (2-2) to be

$$\Gamma = 4\pi RU \sin(\alpha + \beta) \qquad (2-5)$$

As presented in Karamcheti [26], a non-zero trailing edge closure angle requires a stagnation point at the trailing edge of the airfoil. Thus, in investigating upper bounds of V_{TE}/U, it is necessary to consider airfoils whose trailing edges close in a cusp and thereby have non-zero trailing edge

velocities. In order to obtain an expression for the trailing edge velocity of this class of airfoils, L'Hopital's rule is applied to the indeterminate form obtained from equation (2-4) such that

$$V_{TE} = |w(z_T)| = \lim_{\zeta \to \zeta_T} \frac{|w'(\zeta)|}{|z''(\zeta)|} = \frac{|w'(\zeta_T)|}{|z_T''|} \tag{2-6}$$

and, using equations (2-2) and (2-5) to obtain

$$w_T' = \frac{2U\ e^{2i\beta}}{r} \cos(\alpha + \beta) \tag{2-7}$$

the trailing edge to free-stream velocity ratio is found to be given by

$$\frac{V_{TE}}{U} = \frac{2\ |\cos(\alpha + \beta)\ |}{|z_T''|r} \tag{2-8}$$

For the Joukowsky transformation,

$$z = \zeta + \frac{b^2}{\zeta} \tag{2-9}$$

where, as can be verified by consideration of Figure 5,

$$b = \frac{r}{(1 + \epsilon)} \cos \beta \tag{2-10}$$

the trailing edge velocity ratio is then given by

$$\frac{V_{TE}}{U} = \left|\ \frac{\cos \beta}{(1 + \epsilon)}\ \right|\ |\cos(\alpha + \beta)\ | \tag{2-11}$$

As shown in Reference [26], as well as in any one of a number of classical aerodynamic texts, the thickness of the Joukowsky airfoil is increased as the magnitude of ϵ is increased, while increases in β increase the amount of camber. Thus, from equation (2-11), it is clear that for the case of the Joukowsky transformation, the presence of any thickness or camber reduces V_{TE}/U from the value of unity which exists for the flat plate at zero angle of attack.

The Von Mises Transformation

The general transformation which maps a circle into an airfoil is expressed as

$$z = z(\zeta) = \zeta + \sum_{n=1}^{\infty} \frac{c_n}{\zeta^n} \tag{2-12}$$

where, as can be seen in Figure 5, $z = x + iy$, $\zeta = \xi + i\eta$, and, in general, the c_n's are complex quantities. Note that the mapping function, $z(\zeta)$, satisfies the requirement of not altering the flow field at infinity.

Now, consider a truncated form of the general transformation which, after differentiation, is written as

$$\frac{dz}{d\zeta} = 1 - \sum_{n=1}^{N} \frac{n c_n}{\zeta^{n+1}} \tag{2-13}$$

This transformation must not possess any singular points outside the generating circle, although one singular point, denoted by ζ_T, must be on the circle. Since the remaining singular points, given by $\zeta_2, \zeta_3, \ldots, \zeta_N$, are zeros of equation (2-13), in factored form, that equation becomes

$$\frac{dz}{d\zeta} = \left(1 - \frac{\zeta_T}{\zeta}\right)\left(1 - \frac{\zeta_2}{\zeta}\right)\left(1 - \frac{\zeta_3}{\zeta}\right)\ldots\left(1 - \frac{\zeta_N}{\zeta}\right) \qquad (2\text{-}14)$$

where the zero locations are indicated by

$$\zeta_n = \xi_n + i\eta_n \qquad (2\text{-}15)$$

At this point, it is seen that the mapping function may be generated by
postulating the locations of the N zeros which lie, along with the origin,
within a circle of radius r in the ζ-plane. Without loss of generality, the
zero on the circle, ζ_T, which transforms to the trailing edge of the airfoil,
may be fixed at the location (1,0). By choosing different sets of zeros and
different generating circles, a great deal of flexibility exists in the shapes
of airfoils which can be obtained. Profiles which are generated by these
means are known as von Mises airfoils and the mappings obtained by expanding
equation (2-14) and integrating the result are known as von Mises
transformations.

The coefficients of the transformation, the c_n's, can be related to the
zero locations, the ζ_n's, by expanding equation (2-14) and equating that
result with equation (2-13). In this manner, it is found that the coefficient
of the ζ^{-1} term must vanish. Hence, the relation

$$\zeta_T + \sum_{n=2}^{N} \zeta_n = 0 \qquad (2\text{-}16)$$

indicates that the origin of the ζ-plane must be the centroid of the zeros
located at ζ_T, ζ_2, ζ_3, ... ζ_N. The coefficients for von Mises transformations

of up to six terms, $N < 6$, are related to the zero locations as follows:

$$c_0 = \varsigma_T + \varsigma_2 + \varsigma_3 + \varsigma_4 + \varsigma_5 + \varsigma_6 = 0 \qquad (2\text{-}17)$$

$$c_1 = \{\varsigma_T^2 - \varsigma_2(\varsigma_3 + \varsigma_4 + \varsigma_5 + \varsigma_6) - \varsigma_3(\varsigma_4 + \varsigma_5 + \varsigma_6)$$

$$- \varsigma_4(\varsigma_5 + \varsigma_6) - \varsigma_5\varsigma_6\} \qquad (2\text{-}18)$$

$$c_2 = \frac{1}{2}\{\varsigma_T[\varsigma_2(\varsigma_3 + \varsigma_4 + \varsigma_5 + \varsigma_6) + \varsigma_3(\varsigma_4 + \varsigma_5 + \varsigma_6)$$

$$+ \varsigma_4(\varsigma_T + \varsigma_6) + \varsigma_5\varsigma_6] + \varsigma_2[\varsigma_3(\varsigma_4 + \varsigma_5 + \varsigma_6)$$

$$+ \varsigma_4(\varsigma_5 + \varsigma_6) + \varsigma_5\varsigma_6] + \varsigma_3[\varsigma_4(\varsigma_5 + \varsigma_6) + \varsigma_5\varsigma_6] + \varsigma_4\varsigma_5\varsigma_6\} \qquad (2\text{-}19)$$

$$c_3 = -\frac{1}{3}\{\varsigma_T[\varsigma_2(\varsigma_3\varsigma_4 + \varsigma_3\varsigma_5 + \varsigma_3\varsigma_6 + \varsigma_4\varsigma_5 + \varsigma_4\varsigma_6 + \varsigma_5\varsigma_6)$$

$$+ \varsigma_3(\varsigma_4\varsigma_5 + \varsigma_4\varsigma_6 + \varsigma_5\varsigma_6) + \varsigma_4\varsigma_5\varsigma_6] + \varsigma_2[\varsigma_3(\varsigma_4\varsigma_5$$

$$+ \varsigma_4\varsigma_6 + \varsigma_5\varsigma_6) + \varsigma_4\varsigma_5\varsigma_6] + \varsigma_3\varsigma_4\varsigma_5\varsigma_6\} \qquad (2\text{-}20)$$

$$c_4 = \frac{1}{4}\{\varsigma_T[\varsigma_2(\varsigma_3\varsigma_4\varsigma_5 + \varsigma_3\varsigma_4\varsigma_6 + \varsigma_3\varsigma_5\varsigma_6 + \varsigma_4\varsigma_5\varsigma_6)$$

$$+ \varsigma_3\varsigma_4\varsigma_5\varsigma_6] + \varsigma_2\varsigma_3\varsigma_4\varsigma_5\varsigma_6\} \qquad (2\text{-}21)$$

$$c_5 = -\frac{1}{5}\{\varsigma_T\varsigma_2\varsigma_3\varsigma_4\varsigma_5\varsigma_6\} \qquad (2\text{-}22)$$

For a two term transformation, $N=2$, equation (2-17) indicates that $\zeta_2 = -\zeta_T$ and equation (2-14) reduces to the familiar Joukowsky case,

$$\frac{dz}{d\zeta} = \left(1 - \frac{\zeta_T^2}{\zeta^2}\right) \qquad (2-23)$$

From equation (2-13), $c_1 = \zeta_T^2$ and the Joukowsky transformation is obtained in the form of equation (2-12) as

$$z = \zeta + \frac{\zeta_T^2}{\zeta} \qquad (2-24)$$

While Joukowsky airfoils are limited to a circular arc camberline and a maximum thickness at approximately the quarter-chord position, such restrictive limitations do not exist for von Mises airfoils. By appropriately locating the generating zeros and the origin of the transformation circle, it is possible to approximate a desired shape through an extremely wide range of airfoil geometries. While the zero locations govern the basic thickness distribution and camberline shape, the center location of the generating circle can be used to influence the overall amounts of thickness and camber as in the case of Joukowsky airfoils. Displacements of the circle in the direction of the real axis, μ_R, primarily influences the thickness of von Mises airfoils while displacements in the direction of the imaginary axis, μ_I, the camber.

A few examples of the profile variations possible using the von Mises transformation are provided by the airfoils shown in Figures 6 and 7, generated using four term transformations, and those shown in Figures 8 and 9, obtained using six terms. The zero locations used to generate these airfoils

and the resulting transformation coefficients are indicated in the figures
with the complex number pairs denoted by the Z_n's and the C_n's,
respectively. The real and imaginary components of the origin of the
generating circle are given in the figures, respectively, as UR and UI.

Because the von Mises transformations provide for such a wide range of
possibilities, and airfoils of practical interest can generally be
characterized by relatively few inflections in the thickness distribution and
camberline shape, the conclusions developed using the von Mises
transformations are considered to be applicable over a broad range of
airfoils. In addition, the development is conducted using a relatively small
number of terms in the transformation because, as demonstrated by the examples
presented, large variatons in profile geometries are possible without a large
number of terms. This is further justified by the fact that the contributions
made to the resulting airfoil shape by terms of increasing order rapidly
become insignificant compared to the influence of the first few terms.

Maximum Trailing Edge Velocity Ratios for Physically Realizable Airfoils

From equation (2-8), it is seen that V_{TE}/U is inversely proportional
$|z_T''|$ and r. Thus, the maximum value of V_{TE}/U occurs when $|z_T''|$ is minimized
and r is fixed at a minimum value for the given $|z_T''|$ which insures that the
airfoil generated is free of any regions of negative thickness. Denoting the
complex coefficients of the transformation function as $c_n = a_n + ib_n$, taking
$\zeta_T = (1,0)$, and performing the necessary operations on the truncated form of
equation (2-12), $|z_T''|$ is found to be

$$|z_T''| = [(\sum_{n=1}^{N-1} n(n+1)\ a_n)^2 + (\sum_{n=1}^{N-1} n(n+1)b_n)^2]^{1/2} \qquad (2-25)$$

Because the second term or the right of this expression is positive, the minimum value of $|z_T''|$, for a given set of a_n's, occurs when the second term is zero. While there are non-zero values of the b_n's that can achieve this, the second term always disappears for symmetrical airfoils which are generated when μ_I and all of the b_n's are zero. Consequently, as developed further in Appendix A, for determining the maximum value of V_{TE}/U pos. ble for an airfoil generated by a fixed set of a_n's, it is sufficient to consider only the symmetrical profile which can result. While there may be non-symmetrical sections having a value of V_{TE}/U as large, there can be none for which the value is larger. By eliminating the need to consider other than symmetrical airfoils, the determination of the maximum attainable values of V_{TE}/U for physically realizable airfoils of the von Mises family is significantly simplified in that the thickness distributions, which must exclude negative thicknesses, are dependent only upon μ_R and the a_n's. Through these considerations, the problem of determining the conditions insuring that a transformation yield an airfoil which does not cross-over itself is reduced to that of finding the minimum value of r for which the upper surface coordinates of the generated profile are all non-negative.

To proceed in this development, the representation of the generating circle in the complex ζ-plane, as previously noted, is given by

$$\zeta = \xi + i\eta = re^{i\phi} + \mu \qquad (2-26)$$

Thus, the coordinates of the circle are

$$\xi = r\cos\phi + \mu_R \qquad (2\text{-}27)$$

$$\eta = r\sin\phi + \mu_I \qquad (2\text{-}28)$$

where, with $\zeta_T = (1,0)$, it is evident from Figure 5 that

$$r = |1 - \mu| = [(1-\mu_R)^2 + \mu_I^2]^{1/2} \qquad (2\text{-}29)$$

Setting μ_I to zero and defining

$$f = (1 - \cos\phi) \qquad (2\text{-}30)$$

allows the preceding relationships to be written as

$$r = 1 - \mu_R \qquad (2\text{-}31)$$

$$\xi = 1 - rf \qquad (2\text{-}32)$$

$$\eta = r\sin\phi \qquad (2\text{-}33)$$

The relationship between the real part of the transformation
coefficients, the a_n's, and the radius of the generating circle insuring that
the symmetrical airfoil developed is characterized by positive thickness
everywhere has been analytically determined for von Mises transformations of
up to six terms. Before this case is considered, however, it is instructive
to examine the derivation with only three terms as the key points of the

development are retained while the algebra is simplified considerably.

The three-term von Mises transformation having real coefficients is written as

$$z = \zeta + \frac{a_1}{\zeta} + \frac{a_2}{\zeta^2} \tag{2-34}$$

For the symmetrical airfoil generated to have non-negative thickness everywhere, it is required that

$$Im(z) = y \geqslant 0 \tag{2-35}$$

for $0 \leqslant \phi \leqslant \pi$. Substitution of equation (2-26) into (2-34), and making use of the condition given by equation (2-35), yields

$$\eta - \frac{a_1 \eta}{\left(\xi^2 + \eta^2\right)} - \frac{2a_2 \xi \eta}{\left(\xi^2 + \eta^2\right)^2} \geqslant 0 \tag{2-36}$$

which may be rearranged to give

$$\left(\xi^2 + \eta^2\right)^2 - a_1\left(\xi^2 + \eta^2\right) - 2a_2 \xi \geqslant 0 \tag{2-37}$$

Using equations (2-32) and (2-33), the quantities required in equation (2-37) are found to be:

$$\xi^2 = r^2 f^2 - 2rf + 1 \tag{2-38}$$

$$\eta^2 = r^2 \sin^2 \phi \tag{2-39}$$

$$\left(\xi^2 + \eta^2\right) = 2 \, rf(r-1) + 1 \tag{2-40}$$

$$\left(\xi^2 + \eta^2\right)^2 = 4rf(r-1)\left[rf(r-1) + 1\right] + 1 \tag{2-41}$$

Substitution of the above quantities into equation (2-37) gives

$$4rf(r-1)\left[rf(r-1) + 1\right] + 1 - a_1\left[2rf(r-1) + 1\right]$$

$$- 2a_2\left[1 - rf\right] > 0 \tag{2-42}$$

The terms in this expression which are independent of r and f, that is, $1-a_1-2a_2$, may be eliminated by making use of the Kutta condition which requires, for the general case, that

$$z_T' = 1 - \sum_{n=1}^{N-1} n \, a_n = 0 \tag{2-43}$$

For N=3, this expression indicates that

$$1 - a_1 - 2a_2 = 0 \tag{2-44}$$

Applying this result and factoring rf from what remains, equation (2-42) becomes

$$2r(r-1)^2 f + 2(r-1) - a_1(r-1) + a_2 > 0 \tag{2-45}$$

As the first term in this expression is non-negative, given that r is non-negative, the most critical situation for meeting the condition of the inequality occurs when $f = 0$, i.e., when $\cos\phi = 1$. For this case, equation (2-45) becomes

$$4(r-1) - 2a_1(r-1) + 2a_2 > 0 \qquad (2-46)$$

Using this result, it is found that in order to prevent the airfoil obtained through the mapping function from having regions of negative thickness, it is necessary to require that

$$r > \frac{2 - a_1 - a_2}{2 - a_1} \qquad (2-47)$$

In addition, the value of $|z_T''|$, from equation (2-25), is given by the expression

$$|z_T''| = | 2a_1 + 6a_2 | \qquad (2-48)$$

Using equation (2-8), the maximum value of V_{TE}/U which can be obtained from a given three-term transformation is

$$\frac{V_{TE}}{U} = \frac{2 \cos\alpha}{|z_T''| r_{min}} = \frac{2(2-a_1)\cos\alpha}{|2a_1 + 6a_2|(2-a_1 - a_2)} \qquad (2-49)$$

For this case, the maximum V_{TE}/U clearly occurs when the angle of attack, α, is zero. To determine the transformation which affords the largest V_{TE}/U overall, equations (2-18) and (2-19) are used to relate the coefficients to

the locations of the generating zeros. Thus, for symmetrical airfoils generated with all of the generating zeros located on the real axis such that the n_n's are all zero, the coefficients are given by

$$a_1 = 1 - \xi_2 \xi_3 \qquad (2\text{-}50)$$

$$a_2 = \frac{1}{2} \xi_2 \xi_3 \qquad (2\text{-}51)$$

Substitution of these relations into equations (2-49) and setting α equal to zero yields

$$\frac{V_{TE}}{U} = \frac{1 + \xi_2 \xi_3}{\left(1 + \frac{1}{2}\xi_2 \xi_3\right)^2} \qquad (2\text{-}52)$$

and using equation (2-17), it is found that

$$\xi_3 = - (1 + \xi_2) \qquad (2\text{-}53)$$

Equation (2-52) thus becomes

$$\frac{V_{TE}}{U} = \frac{4(\xi_2^2 + \xi_2 + 1)}{(\xi_2^2 + \xi_2 - 2)^2} \qquad (2\text{-}54)$$

Maximizing V_{TE}/U with respect to ξ_2 indicates that the overall largest value of V_{TE}/U occurs when $\xi_2 = -1$ and $\xi_3 = 0$ or $\xi_2 = 0$ and $\xi_3 = -1$. While it is also possible to generate symmetrical airfoils with non-zero values of the n_n's, for example, when ξ_2 and $\xi_3 = -.5$ and $n_2 = - n_3$, it is found that the value of V_{TE}/U is maximum when $n_2 = -n_3 = 0$. Thus, for determining the

bounding values of V_{TE}/U, it is sufficient to consider the case of having the η_n's set to zero. Thus, for the three-term von Mises transformation, the maximum V_{TE}/U occurs when the third term is zero and the remaining terms are equivalent to those of the Joukowsky transformation which yield the flat plate airfoil.

Now consider the case of the six-term von Mises transformations having real coefficients, as given by

$$z = \zeta + \sum_{n=1}^{5} \frac{a_n}{\zeta^n} \qquad (2-55)$$

A physically realizable symmetrical airfoil is insured provided that

$$\text{Im}\left\{\xi + i\eta + \sum_{n=1}^{5} \frac{a_n(\xi - i\eta)^n}{(\xi^2 + \eta^2)^n}\right\} > 0 \qquad (2-56)$$

Proceeding as in the case of the three term transformation, this equation is expanded to obtain

$$(\xi^2 + \eta^2)^5 - a_1(\xi^2 + \eta^2)^4 - 2a_2\xi(\xi^2 + \eta^2)^3 + a_3(\eta^2 - 3\xi^2)(\xi^2 + \eta^2)^2$$

$$+ 4a_4\xi(\eta^2 - \xi^2)(\xi^2 + \eta^2) + a_5(10\xi^2\eta^2 - 5\xi^4 - \eta^4) > 0 \qquad (2-57)$$

After making the proper substitutions and expanding, the terms in the resulting equation which are independent of r and f are again eliminated by use of the Kutta condition, equation (2-43). Factoring $2rf$ from the remaining expression yields an inequality of the form

$$Af^4 + Bf^3 + Cf^2 + Df + E \geqslant 0 \tag{2-58}$$

where expressions for the coefficients are given in Appendix B. For $0 < \phi < \pi$, f, given by equation (2-30), is never negative. Hence, when A, B, C, and D are non-negative, the inequality will be satisfied as f goes to zero provided that E is non-negative. Additionally, for the case when A, B, C, and D are not all non-negative, it has been demonstrated numerically that requiring E to be non-negative is still sufficient to guarantee that the condition of the inequality is met. From these results, the attainment of a non-negative thickness distribution on an airfoil resulting from a six-term von Mises transformation requires that

$$r \geqslant \frac{5 - 4a_1 - 7a_2 - 9a_3 - 10a_4 - 10a_5}{5 - 4a_1 - 6a_2 - 5a_3 + 10a_5} \tag{2-59}$$

It should be noted that the expression degenerates into the appropriate forms for transformations having fewer than six terms.

The results of maximizing V_{TE}/U for transformations of up to six terms in a manner analogous to that used for three terms suggests that for $\zeta_T = (1,0)$, a specified ξ_2 location, and any number of remaining zeros, say k, that V_{TE}/U achieves a maximum when the k zeros are all positioned at the location defined by

$$\xi_n = - \frac{1}{k} (\xi_2 + 1) \tag{2-60}$$

Furthermore, the value of V_{TE}/U is found to increase as the value of ξ_2

approaches -1.0 from either direction. When ξ_2 is equal to -1.0, the maximum value of V_{TE}/U reaches unity and requires that all of the other zeros be located at $\xi_n = 0$ and consequently, have no influence. Again, this indicates that the largest possible value of V_{TE}/U for a physically reasonable airfoil is unity and occurs when the profile is a flat plate at zero angle of attack.

Numerical Results and Discussion

In order to simplify the determination of the minimum generating circle radius for which an allowable airfoil is obtained, the development in the preceding section considered only symmetrical profiles in order to uncouple the thickness distribution from the b_n's. Note, however, that if the airfoils under consideration have neither excessive camber or thickness, the resulting condition provides an approximation which is still useful to insure the generation of physically realizable airfoils. For non-symmetrical profiles, due to the fact that a chordwise location from an upper portion of the generating circle, $x(\theta)$, does not correspond to the same location transformed from the lower portion, $x(-\theta)$, the thickness distribution becomes coupled to the b_n's. If the airfoil is not excessively cambered, however, then $x(\theta)$ will be approximately equal to $x(-\theta)$ and consequently, the thickness distribution is only weakly influenced by the non-zero b_n's. Thus, the positive thickness condition remains approximately correct. Similarly, in practice, it has been found that the condition is reasonably valid for small, non-zero values of μ_I, and only excessively cambered profiles actually might have regions of negative thickness even though the positive thickness condition is satisfied. Thus, for most practical purposes, the condition developed is useful in generating physically realizable von Mises airfoils whether or not they are symmetrical.

To further understand the utility of the positive thickness condition, a digital computer program was written to calculate the transformation coefficients and airfoil coordinates resulting from an input generating circle and a set of zeros. As previously indicated, on the figures to be discussed, the zero locations and the transformation coefficients are each listed as a complex number pair denoted by the Z_n's and C_n's, respectively. Considering the condition on the minimum allowable radius such that $\mu_{Rmax} = 1 - r_{min}$, the value of URMAX presented in the figures is the maximum allowable real axis location of the generating circle center which results in a reasonable airfoil. Depending on which situation is most critical, this value is based on either the positive thickness condition, as determined from equation (2-59), or, on the requirement that all of the zeros lie within the generating circle. The radius of the mapping circle used to generate the airfoil shown is denoted in the figures as R, while the real and imaginary components of its center are UR and UI, respectively. The value of V_{TE}/U for the airfoil is identified by VTE.

To demonstrate the relationship of camber and thickness to the value of V_{TE}/U, a comparison of the airfoil shown in Figure 10 to that shown in Figure 7 is informative. The symmetrical airfoil of Figure 10 has been generated by locating the zeros such that the b_n's are all zero, while the a_n's have essentially the same values as those of the section shown in Figure 7. As the transformation for the cambered airfoil was determined so that $\sum_{n=1}^{N-1} n(n+1) b_n$ is zero, the value of $|z_T''|$ is the same for both airfoils as can be seen from equation (2-25). Thus, with both airfoils having the same r, the values of V_{TE}/U from equation (2-8) are equal. In essence then, the airfoil of Figure 7 has traded an appropriate amount of thickness for camber such that there is no

reduction in V_{TE}/U. As is also demonstrated by the expression for the value

of V_{TE}/U in the case of Joukowsky airfoils, equation (2-11), the trading of

some amount of thickness for camber is possible in all cases provided that

some thickness is available to trade. Hence, in the case of the flat plate it

is not possible to obtain a cambered plate while V_{TE}/U remains equal to

unity.

The effect of varying μ_R on the airfoil resulting from a given

transformation is exemplified by Figures 9, 11 and 12. The airfoil of Figure

9 is developed using the maximum value of μ_R as determined from the condition

for positive thickness, which is approximately correct for the cambered

profile shown. Thus, it can be considered that the point where the upper and

lower surfaces cross is located at the trailing edge of this profile. As the

value of μ_R is made greater than μ_{Rmax}, the point of cross-over moves from the

trailing edge toward the leading edge. The airfoil shown in Figure 11, using

the same set of generating zeros as the profile of Figure 9, exhibits this

behavior. As the value of μ_R is increased above the value used in Figure 11,

the point of cross-over on the resulting airfoil moves further and further

forward. In some cases, this continues until the cross-over point reaches the

leading edge, after which, further increases in μ_R cause the thickness

distribution of the resulting airfoil to be totally negative. In this

situation, the upper parts of the generating circle are mapped to the lower

surface of the airfoil, and the lower parts of the circle to the upper surface

of the airfoil. An alternative possibility exists as, in some cases, before

the cross-over point reaches the leading edge, a value of μ_R is used which

causes one of the generating zeros, in addition to that at the trailing edge,

to lie on the circle. This results in an additional cusp appearing on the

boundary of the airfoil. A further increase in μ_R then results in a zero
becoming situated outside of the circle and the mapping of the flow field is
no longer conformal.

While moving the origin of the generating circle in the positive
direction causes the resulting airfoil to become thinner, Figure 12 shows that
moving it in the opposite direction causes it to thicken. To the extent that
the positive thickness condition is an approximation for non-symmetrical
airfoils, the examples of Figure 9, 11 and 12 demonstrate that generating a
profile with μ_R equal to μ_{Rmax} results in the thinnest uncrossed airfoil
possible for a given set of zeros.

The next group of figures is included to show quantitatively how an
additional non-zero term in the transformation influences the shape of the
profile and the value of V_{TE}/U. Figure 13 depicts the Joukowsky flat plate
airfoil at zero angle of attack. As indicated in the figure, this airfoil has
the limiting value for V_{TE}/U of unity. By moving a third generating zero a
small distance away from the origin in either direction, Figures 14 and 15, it
is seen that the profile thickness increases slightly while V_{TE}/U becomes less
than unity.

Figure 16 depicts an airfoil having the highest attainable value of V_{TE}/U
using a six-term transformation and $\xi_2 = -.6$ as the specified location of the
second generating zero. The locations of the other zeros for this airfoil are
prescribed by equation (2-60). As before, Figure 17 indicates that a decrease
in V_{TE}/U results when the zeros are moved slightly from the maximizing
locations used to obtain the airfoil of Figure 16.

Figures 18 and 19 present plots of the zero-lift, maximum values of V_{TE}/U
and the symmetrical airfoil thickness ratios as they depend on the zero

location, ξ_2. Figure 18 is produced using a three-term von Mises

transformation, while Figure 19 a six-term transformation. For both cases,

the zeros other than the trailing edge zero, ζ_T, and the given zero, ξ_2, are

positioned using equation (2-60) in order to maximize the value of V_{TE}/U. The

symmetrical behavior about $\xi_2 = -.5$ of the plots shown in Figure 18 is due to

the fact that, with only three terms, equation (2-60) requires that $\xi_3 = -$

$(\xi_2 + 1)$. Thus, the Joukowsky flat plate results that occurs when $\xi_2 = -1$ and

$\xi_3 = 0$ also occurs when $\xi_2 = 0$ and $\xi_3 = -1$. It is interesting to note that

this behavior disappears, as shown in Figure 19, when additional terms are

employed in the transformation. In comparing the two figures in the region of

$\xi_2 = 0$, it is apparent that the presence of more terms allows higher values of

V_{TE}/U to occur for a given thickness ratio.

As an aid in airfoil design studies, Figure 20 summarizes the manner in

which the maximum, zero-lift trailing edge velocity ratios are limited by the

airfoil thickness ratio. It is important to note, however, that the

relationship shown should not be regarded as absolute potential flow limits

as, by moving the zeros off the real-axis, it is possible to obtain

symmetrical profiles of larger thickness ratios which produce higher values of

V_{TE}/U than those indicated. As the profiles generating these results have

excessively blunted or concave noses, and otherwise radical shapes, these

cases were excluded from the results presented in Figure 20.

Because the specification of V_{TE}/U is necessary in a number of airfoil

design techniques, it is anticipated that the preceding results will be

useful. For example, in the fully laminar airfoil designs of Sappuppo and

Archer [27], the value of $V_{TE}/U = .97$ was selected "as high as possible so as

to obtain high lift". As consistent with Figure 20, the thickness ratio of

the symmetrical airfoil resulting from the surface singularity inverse procedure employed was 9.7%. On the introduction of camber, however, difficulties were reported in retaining a reasonable thickness ratio and that of the resulting airfoil was only 4.2%. While it was concluded that the thinness of these profiles was due to the low Reynolds number specification and employment of the fully laminar Stratford recovery distribution, the present investigation indicates that it is, more likely, a result of the high value of V_{TE}/U specified. Furthermore, in light of the discussion regarding the trade-off of thickness and camber necessary to maintain a given value of V_{TE}/U, the difficulties encountered when camber was introduced are to be expected.

As already noted, another area in which insight into the factors influencing the selection of V_{TE}/U would be most valuable is in the high lift airfoil design procedure detailed by Thompson [19]. In this method, the formulation of the Stratford recovery distribution for the upper surface is initiated by selecting the value of V_{TE}/U. As has been discussed, the literature provided little guidance for choosing reasonable values of V_{TE}/U, and those used by Thompson were unreasonably high. Thus, the present work provides the means by which the specification of V_{TE}/U can be made with greater understanding.

CHAPTER III

AIRFOILS WITH FINITE TRAILING EDGE PRESSURE GRADIENTS

Conditions Required for Finite Trailing Edge Pressure Gradients

In considering the results of interacting boundary layer theory to model the real flow around an airfoil, it is found that the displacement thickness of the boundary layer and of the wake increase rapidly in the vicinity of the trailing edge, and a discontinuity generally exists where they join at the trailing edge. This behavior has been considered in numerous references, such as the classical papers of Preston, et. al., [29]-[31], as well as in more modern sources such as Reference [32], and, as shown by Melnik, et. al., [33] is attributable to singularities which occur at the trailing edge of the inviscid solution. These unbounded quantities, present in the case of any airfoil carrying a non-zero load at the trailing edge, lead to a breakdown of the boundary layer approximations such that, in the vicinity of the trailing edge, the assumption that pressure is constant across the boundary layer is no longer valid. Thus, the elimination of these singularities should allow the viscous flow on an airfoil to be more reliably predicted using conventional boundary layer theory. More significantly, because of the reduction in the strong viscous effects at the trailing edge, it is reasonable to expect that airfoil aerodynamics might be enhanced as the level of performance achaved in the real flow field would more closely approach the high levels predicted using potential flow methods. Finally, because the manner in which the flow approaches the trailing edge should be globally influenced by the removal of the trailing edge singularities, it is anticipated that the possibility of

large upper and lower surface velocity differentials in the vicinity of the trailing edge would be eliminated. Thus, separation problems introduced by the steep adverse pressure gradient that typically exists on the upper surface near the trailing edge when such velocity differentials exist would be mitigated.

In order to examine the flow in the vicinity of the trailing edge in detail, consider the transformation of the unit circle centered at the origin of the ζ-plane into an airfoil in the z-plane as shown in Figure 21. The complex potential function for the unit circle having circulation Γ and an angle of attack α is

$$F(\zeta) = U \, e^{-i\alpha} - U \, e^{i\alpha}\zeta^{-1} - \frac{\Gamma}{2\pi i} \ln \zeta \tag{3-1}$$

and the complex velocity is

$$\omega(\zeta) = \frac{dF(\zeta)}{d\zeta} = U \, e^{-i\alpha} - U \, e^{i\alpha}\zeta^{-2} + \frac{i\Gamma}{2\pi} \zeta^{-1} \tag{3-2}$$

Imposing the Kutta condition, the circulation necessary to fix the stagnation point at $\zeta = \zeta_T = 1$ in the circle plane is found to be

$$\Gamma = 4\pi \, U \sin \alpha \tag{3-3}$$

Thus,

$$\frac{w(\zeta)}{U} = e^{-i\alpha} - e^{i\alpha}\zeta^{-2} + 2i\zeta^{-1} \sin \alpha \tag{3-4}$$

which may be written

$$\frac{w(\zeta)}{U} = \left(e^{-i\alpha} + e^{i\alpha}\zeta^{-1}\right)\left(1 - \zeta^{-1}\right) \qquad (3\text{-}5)$$

The velocity in the airfoil plane is

$$w(z) = u - iv = \frac{dF}{d\zeta}\frac{d\zeta}{dz} = w(\zeta) \, / \, z'(\zeta) \qquad (3\text{-}6)$$

To preclude the presence of a stagnation point at the trailing edge of the airfoil, z_T, it is necessary that the trailing edge of the airfoil be cusped. This requires that

$$z_T'(\zeta) = 0 \qquad (3\text{-}7)$$

Because the velocity at the trailing edge, from equation (3-6), is of an indeterminant form, L'Hopital's rule can be invoked to yield

$$w(z_T) = \frac{w'\left(\zeta_T\right)}{z_T''} \qquad (3\text{-}8)$$

At this point, the complex pressure gradient is defined as

$$R = \frac{\partial p}{\partial x} - i\,\frac{\partial p}{\partial y} = p_x - ip_y \qquad (3\text{-}9)$$

Using the Bernoulli equation, the pressure at a point on an airfoil, p, may be related to the free-stream conditions such that

$$p = p_\infty + \frac{1}{2}\rho\left[U^2 - \left(u^2 + v^2\right)\right] \qquad (3\text{-}10)$$

which is differentiated to give

$$p_x = -\rho \left(uu_x + vv_x \right) \qquad (3\text{-}11)$$

$$p_y = -\rho \left(uu_y + vv_y \right) \qquad (3\text{-}12)$$

By substituting equations (3-11) and (3-12) into equation (3-9), it is found that

$$R = -\rho \left[u\left(u_x - iu_y \right) + v\left(v_x - iv_y \right) \right] \qquad (3\text{-}13)$$

Continuity and irrotationality require that $v_x = u_y$ and $u_x = -v_y$. Thus, equation (3-13) may be written

$$R = -\rho \left[u\left(u_x - iv_x \right) + v\left(u_y - iv_y \right) \right]$$

$$= -\rho \left[uw' + v\left(iw' \right) \right]$$

$$= -\rho \left[u + iv \right] w' \qquad (3\text{-}14)$$

or, more simply

$$R = -\rho \, \overline{w}(z) \, w'(z) \qquad (3\text{-}15)$$

where $\overline{w}(z)$ is the complex conjugate of $w(z)$. At the trailing edge, the complex pressure gradient is given by

$$R_T = -\rho \, \overline{w}\left(z_T \right) \, w'\left(z_T \right) \qquad (3\text{-}16)$$

In order to evaluate equation (3-16), an expression for $w'(z_T)$ is required. Note that the result of differentiating equation (3-8),

$$w'(z_T) = \lim_{\zeta \to \zeta_T} \frac{d}{dz}\left[\frac{w(\zeta)}{z'}\right] = \lim_{\zeta \to \zeta_T}\left\{\frac{w'(\zeta)z' - w(\zeta)z''}{(z')^3}\right\} \tag{3-17}$$

is of an indeterminant form such that L'Hopital's rule is applicable. Because $w(\zeta_T)$ and z_T' are both zero, this yields

$$w'(z_T) = \lim_{\zeta \to \zeta_T} \frac{w''(\zeta)z' - w(z)z'''}{3(z')^2 z''} \tag{3-18}$$

which is still of an indeterminant form. Using L'Hopital's rule again gives

$$w'(z_T) = \lim_{\zeta \to \zeta_T}\left[\frac{w''(\zeta)z'' - w'(\zeta)z'''}{6(z')(z'')^2 + 3(z')^2 z'''}\right] \tag{3-19}$$

Now, because the denominator of this expression is zero, $w'(z_T)$ will be unbounded unless the numerator is also zero. Thus, for $w'(z_T)$ to be finite, it is necessary that

$$w''(\zeta_T)z_T'' - w'(\zeta_T)z_T''' = 0 \tag{3-20}$$

If this condition is satisfied, then equation (3-19) will be of an indeterminant form and the use of L'Hopital's rule again yields

$$w'(z_T) = \frac{w'''(\zeta_T)z_T'' - w'(\zeta_T)z_T^{iv}}{3(z_T'')^3} \tag{3-21}$$

Now, substituting the above relation, along with the conjugate of equation

(3-8), into equation (3-16), the value of the complex trailing edge pressure gradient, provided that equation (3-20) is satisfied, is given by

$$R_T = -\rho \frac{\overline{w'(z_T)}}{3 \, \overline{z_T}''(z_T'')^3} \left[z_T'' \, w'''(\zeta_T) - z_T^{iv} \, w'(\zeta_T) \right] \tag{3-22}$$

To further evaluate equations (3-20) and (3-22), equation (3-5) may be differentiated successively and evaluated at the trailing edge giving

$$\frac{w'(\zeta_T)}{U} = \frac{\overline{w'(\zeta_T)}}{U} = 2\cos\alpha \tag{3-23}$$

$$\frac{w''(\zeta_T)}{U} = -6\cos\alpha - 2i\sin\alpha \tag{3-24}$$

$$\frac{w'''(\zeta_T)}{U} = 24\cos\alpha + 12i\sin\alpha \tag{3-25}$$

By writing equation (3-20) as

$$\frac{z_T'''}{z_T''} = \frac{w''(\zeta_T)}{w'(\zeta_T)} \tag{3-26}$$

and making use of equations (3-23) and (3-24), the condition required for the complex trailing edge pressure gradient to be finite on an airfoil may be expressed as a condition on the transformation function requiring that

$$\frac{z_T'''}{z_T''} = -3 - i\tan\alpha \tag{3-27}$$

While the ramifications of this requirement will be considered later, note that the imaginary part can only be satisfied for a particular airfoil at only

a single angle of attack. At any other angle of attack, the complex trailing
edge pressure gradient is unbounded.

Using equations (3-23) and (3-25) in equation (3-22), the value of the
complex trailing edge pressure gradient is given by

$$R_T = - \frac{4\rho U^2}{3(\overline{z_T''})} \frac{\cos \alpha}{(z_T'')^3} \left[6z_T''(2\cos\alpha + i\sin\alpha) - z_T^{iv}\cos\alpha \right] \tag{3-28}$$

provided that the condition of equation (3-27) is satisfied. Non-
dimensionalizing equation (3-28), where ℓ is the chord length of the airfoil,
yields

$$\frac{R_T}{\rho U^2/2\ell} = C_{pXT} - i\, C_{pYT}$$

$$= - \frac{8\,\ell\,\cos\alpha}{3(\overline{z_T''})(z_T'')^3} \left[6z_T''(2\cos\alpha + i\sin\alpha) - z_T^{iv}\cos\alpha \right] \tag{3-29}$$

By considering a circle of radius r and center location μ in the ζ-plane,
rather than a unit circle centered at the origin, the results of this analysis
can be made applicable to the von Mises airfoils previously considered. In
that case, it is interesting to note that all of the symmetrical airfoils
generated using the minimum circle radius which generates a physically
realizable airfoil, r_{min}, satisfy the condition for a finite complex trailing
edge pressure gradient. In order to explain this, consider that, in the case
of overlapping airfoils, the point of cross-over moves aft as the generating
circle radius, r, is increased. When $r = r_{min}$, the cross-over point is at the
trailing edge. Thus, the trailing edge of the airfoil is locally like the
flat plate at zero angle of attack and, evidently, the flow behavior is

similar. As an example of such an airfoil, the von Mises profile depicted in Figure 22 has trailing edge pressure gradient values of $C_{pXT} = -1.37$, while, as is the case for all non-lifting symmetrical airfoils, $C_{pYT} = 0$. For comparison, the airfoil of Figure 16 has $C_{pXT} = -.12$ and $C_{pYT} = 0$. It should be noted that because having $r = r_{min}$ in the case of two generating zeros yields the Joukowsky flat plate, Figure 13, that this is the only Joukowsky airfoil which can satisfy the condition for bounded trailing edge pressure gradients. This fact explains the presence of the "hooked" shape observed at the trailing edge of Joukowsky airfoil velocity distributions.

The Eppler Airfoil Design Method

In order for airfoils to be developed which make use of the conditon for finite trailing edge pressure gradients, it is necessary to incorporate the necessary condition into some airfoil design methodology. To this end, the inverse scheme developed by Eppler was selected as being the most suitable for this purpose. The theoretical details of this design procedure are presented in Eppler [5], and also summarized in References [8], [17], and [19], while a description of the code and its usage are documented by Eppler and Somers [25]. As modifications required to allow the method to design airfoils having finite trailing edge pressure gradients are significant, before considering these changes, a summary of the method will also be included here.

As depicted in Figure 21, the Eppler airfoil design procedure is based on the conformal mapping of the flow field exterior to a unit circle in the ζ-plane into the flow field exterior to an airfoil in the z-plane. The complex velocity for the flow about the unit circle is given by equation (3-5) where,

to be consistent with the derivation of Eppler, the free-stream velocity is taken to be unity. The mapping function, $z(\zeta)$, must, as detailed in the discussion of the von Mises transformation, preserve the flow conditions at infinity. Thus, it is required that

$$z(\infty) = \infty \quad \text{and} \quad \left(\frac{dz}{d\zeta}\right)_\infty = 1 \tag{3-30}$$

Most generally, these requirements are met by the power series

$$z(\zeta) = \beta_1 \zeta + \sum_{\nu=0}^{\infty} \beta_{-\nu} \zeta^{-\nu} \qquad \left(\beta_1 \neq 0, \text{ real}\right) \tag{3-31}$$

where the β_ν's are limited to values for which the series is convergent when $|\zeta| > 1$. As consistent with equation (3-6), the velocity in the airfoil plane is given by

$$w(z) = v e^{-i\theta} = \frac{dF}{dz} = \frac{dF}{d\zeta}\frac{d\zeta}{dz} \tag{3-32}$$

This relationship, for reasons discussed by Lighthill [9], is more conveniently represented by

$$\ln w(z) = \ln v - i\theta = \ln \frac{dF}{d\zeta} - \ln \frac{dz}{d\zeta} \tag{3-33}$$

Because $\ln \frac{dF}{d\zeta}$ is known from equation (3-5), then if $v(\phi)$ is specified, the real part of $\ln \frac{dz}{d\zeta}$ follows directly. Furthermore, because $\ln \frac{dF}{dz}$ is analytic in the exterior of the unit circle then, using the real part which is known on the boundary, $\zeta = e^{i\phi}$, the imaginary part can be determined. Thus, the

function $\frac{dz}{d\zeta}$, which maps the circle into the airfoil, can be solved for from

equation (3-33) and z obtained by integration. The advances which are

represented by the Eppler method include the development of an algorithm for

the numerical computations required by the procedure just outlined, and the

introduction of a form for $v(\phi)$ which allows practical airfoils to be obtained

in a straightforward manner.

The numerical algorithm of the method is based on the introduction of

$\ln \frac{dz}{d\zeta}$ in the form given by

$$\ln \frac{dz}{d\zeta} = \ln \left(1 - \frac{1}{\zeta}\right) + \sum_{m=0}^{\infty} \left(a_m + ib_m\right)\zeta^{-m} \qquad (3-34)$$

This form is advantageous in that it isolates the singularity which occurs on

the boundary, $\zeta = e^{i\phi}$. Operating on equation (3-34) yields

$$\frac{dz}{d\zeta} = \left(1 - \frac{1}{\zeta}\right) e^{\sum_{m=0}^{\infty} \left(a_m + ib_m\right)\zeta^{-m}} \qquad (3-35)$$

This result must be consistent with equation (3-31). Thus, differentiating

equation (3-31) and comparing terms having like-powers of ζ to those of the

preceding expression, it is found that compatibility requires

$$b_0 = 0 \qquad (3-36)$$

$$a_1 = 1 \qquad (3-37)$$

$$b_1 = 0 \qquad (3-38)$$

Equation (3-36) is necessary in order that there is no rotation of the

free-stream velocity at infinity. Equations (3-37) and (3-38) make

the ζ^{-1} term vanish and, as a consequence, ensure that the profile will close

at the trailing edge. Additionally, the requirement that velocity of unity be

preserved at infinity, as given by equation (3-30), necessitates that

$$a_0 = 0 \qquad\qquad (3-39)$$

Evaluating equation (3-33) on the circle boundary, $\zeta = e^{i\phi}$, and rearranging

the result gives

$$\left[\ln \frac{dz}{d\zeta} - \ln\left(1 - \frac{1}{\zeta}\right)\right]_{\zeta=e^{i\phi}} = -\ln v(\phi) + i\theta$$

$$+ \ln \left(\frac{dF}{d\zeta}\right)_{\zeta=e^{i\phi}} - \ln\left(1 - e^{-i\phi}\right)$$

$$= P(\phi) + i\, Q(\phi) \qquad\qquad (3-40)$$

$P(\phi)$ and $Q(\phi)$ are defined as the real and imaginary parts, respectively, of

this expression. The use of equations (3-5) and (3-34) allows $P(\phi)$ to be

expressed as

$$P(Q) = \sum_{m=0}^{\infty} \left(a_m \cos m\phi + b_m \sin m\phi\right) = -\ln\left[\frac{v(\phi)}{2|\cos(\frac{\phi}{2} - \alpha)|}\right] \qquad (3-41)$$

so that the coefficients, the a_m's and b_m's, are determinable in the same

manner as those of a real Fourier series. Consequently, using the formulas

for the evaluation of Fourier coefficients, and noting that the term

containing b_0 disappears in the expansion of equation (3-41), the requirements

of equation (3-37)-(3-39) generate three integral constraints,

$$\pi\, a_0 = \int_0^{2\pi} P(\phi)\, d\phi = 0 \qquad (3\text{-}42)$$

$$\pi\, a_1 = \int_0^{2\pi} P(\phi)\cos\phi\, d\phi = \pi \qquad (3\text{-}43)$$

$$\pi\, b_1 = \int_0^{2\pi} P(\phi)\sin\phi\, d\phi = 0 \qquad (3\text{-}44)$$

which must be satisfied by the specified velocity distribution, $v(\phi)$. In the actual method, it is not necessary to determine the remaining series coefficients but, rather, necessary only to calculate the conjugate harmonic funtion, $Q(\phi)$. Thus, using Poisson's formula, $Q(\phi)$ is given by

$$Q(\phi) = \sum_{m=0}^{\infty} \left(b_m \cos m\phi - a_m \sin m\phi\right) = \frac{1}{2\pi}\int_0^{2\pi} P(\psi)\operatorname{ctn}\frac{\psi-\phi}{2}\, d\psi \qquad (3\text{-}45)$$

Substituting equation (3-41) into equation (3-40) and simplifying yields

$$\left(\frac{dz}{d\zeta}\right)_{\zeta=e^{i\phi}} = 4i\sin\frac{\phi}{2}\left|\cos\left(\frac{\phi}{2}-\alpha\right)\right|\frac{1}{v(\phi)}\, e^{i\left(Q-\frac{\phi}{2}\right)} \qquad (3\text{-}46)$$

and, for $d\zeta = ie^{i\phi}\, d\phi$,

$$\frac{dz}{d\phi} = ie^{i\phi}\left(\frac{dz}{d\zeta}\right)_{\zeta=e^{i\phi}}$$

$$= -4\sin\frac{\phi}{2}\left|\cos\left(\frac{\phi}{2}-\alpha\right)\right|\frac{1}{v(\phi)}\, e^{i\left(Q+\frac{\phi}{2}\right)} \qquad (3\text{-}47)$$

Splitting this expression into its real and imaginary parts gives

$$\frac{dx}{d\phi} = - 4\sin \frac{\phi}{2} \left| \cos\left(\frac{\phi}{2} - \alpha\right) \right| \frac{1}{v(\phi)} \cos\left[\frac{\phi}{2} + Q(\phi)\right] \qquad (3\text{-}48)$$

$$\frac{dy}{d\phi} = - 4\sin \frac{\phi}{2} \left| \cos\left(\frac{\phi}{2} - \alpha\right) \right| \frac{1}{v(\phi)} \sin\left[\frac{\phi}{2} + Q(\phi)\right] \qquad (3\text{-}49)$$

Thus, once $Q(\phi)$ has been determined, the airfoil coordinates can be obtained by simple quadrature.

Up to now, the derivation has proceeded in such a way that a fixed angle of attack, α, is selected, as well as a velocity distribution, $v(\phi)$, which must satisfy the three integral constraints, equations (3-42)-(3-44). Then, using equations (3-48) and (3-49), a profile is determined whose velocity distribution, $v(\phi, \alpha)$, agrees with the prescribed $v(\phi)$ at the selected angle of attack. The method, however, is considerably more flexible. From equation (3-35), it is clear that the transformation, and therefore the airfoil shape, is fixed once the a_m's and b_m's have been determined. As a change in α has no effect on the coefficients, $P(\phi)$ is independent of α. Consequently, equation (3-41) can be written

$$P(\phi) = - \ln \left[\frac{v^*(\phi)}{2\left| \cos \left(\frac{\phi}{2} - \alpha^*\right)\right|} \right] \qquad (3\text{-}50)$$

where $v^*(\phi)$ is the velocity specified at a point on the profile corresponding to ϕ, and $\alpha^*(\phi)$ is the angle of attack at which that $v^*(\phi)$ is to be realized. Thus, the velocity distribution $v(\phi, \alpha)$, for any arbitrary α, is obtained from equation (3-50) as

$$\frac{v(\phi, \alpha)}{\left| \cos \left(\frac{\phi}{2} - \alpha\right)\right|} = \frac{v^*(\phi)}{\left| \cos \left(\frac{\phi}{2} - \alpha^*\right)\right|} = f(\phi) \qquad (3\text{-}51)$$

where $f(\phi)$ is invariant with respect to α. While $v(\phi, \alpha)$ must be continuous over the airfoil, it is possible for a discontinuity in α^* to be compensated by a discontinuity in $v^*(\phi)$. Thus, rather than specifying only a single α^* at which the velocity distribution $v^*(\phi)$ occurs, unlike other inverse methods, it is possible to select different values of α^*, as indicated by the notation $\alpha^*(\phi)$, for different segments of the airfoil. Consequently, different parts of the airfoil can be designed for different angles of attack. In this manner, an airfoil can be designed from the onset to have the desired aerodynamic characteristics over a chosen range of flight conditions, rather than being point-designed for a single angle of attack and modifying the result until acceptable off-design performance is achieved.

As mentioned, the numerical method is dependent on the convergence of the series contained in equation (3-34). This convergence is assured if the velocity distribution, $v^*(\phi)$, is specified such that it makes $P(\phi)$, equation (3-41), a piecewise continuous function containing, at most, points having finite jumps in the first derivative. In this case, as detailed in Reference [28], the a_m's and b_m's are $O(1/m^2)$. This not only allows successful numerical treatment, but also guarantees that the resulting profiles are smooth.

In order to implement the specification of the velocity distribution, the unit circle in the ζ-plane is divided into I_p segments over the interval $(0, 2\pi)$. Referring to Figure 23,

$$\phi_0 = 0 < \phi_1 < \phi_2 < \ldots < \phi_{I_p} \qquad (3-52)$$

and, in addition, $\phi_{1,le}$ denotes the arc limit containing the leading edge

stagnation point. To achieve the flexibility introduced by being able to specify different values of α^* for different segments of the airfoil, $\alpha^*(\phi)$ will be considered as constant over each of the defined intervals such that

$$\alpha^*(\phi) = \alpha_i = \text{constant} \qquad (\phi_{i-1} < \phi < \phi_i) \qquad (3\text{-}53)$$

The specification of the velocity $v^*(\phi)$ takes the form

$$v^*(\phi) = v_i w(\phi) \qquad (3\text{-}54)$$

where v_i is taken as constant within each circle segment, $\phi_{i-1} < \phi < \phi_i$, and $w(\phi)$ is a function which includes a term allowing for main pressure recovery on the airfoil, as well as a contribution to insure that the profile closes. On the upper surface, $0 < \phi < \phi_{i,le}$, the form of $w(\phi)$ is

$$w(\phi) = \left[1 + K\left\{\frac{\cos\phi - \cos\phi_w}{1 + \cos\phi_w}\right\}\right]^{-\mu} \left[1 - .36\left\{\frac{\cos\phi - \cos\phi_s}{1 - \cos\phi_s}\right\}^2\right]^{K_H} \qquad (3\text{-}55)$$

while on the lower surface, $\phi_{i,le} < \phi < 2\pi$, the parameters K_H, μ, ϕ_w, and ϕ_s are replaced by $\overline{K}_H$, $\overline{\mu}$, $\overline{\phi}_w$, and $\overline{\phi}_s$, respectively. The expressions within the braces, $\{f(\phi)\}$, are treated as special functions in that, if $f(\phi) < 0$ then $\{f(\phi)\} = 0$ and if $f(\phi) > 0$, $\{f(\phi)\} = f(\phi)$. For simplicity, equation (3-55) for the upper surface may be written

$$w(\phi) = W_w(\phi)^{-\mu} W_s(\phi)^{K_H} \qquad (3\text{-}56)$$

and, for the lower surface,

$$w(\phi) = \overline{W}_w(\phi)^{-\overline{\mu}} \, \overline{W}_s(\phi)^{\overline{K}_H} \qquad (3\text{-}57)$$

In both cases, the $W_w(\phi)$ term produces the main pressure recovery, the length of which is governed by the specification of ϕ_w. The total amount of recovery and its particular shape are established as part of the velocity specification, along with the ϕ_i's and α_i's, by the parameters K and μ. In the term generating closure of the airfoil, the quantity $h_s(\phi)$ is fixed by the specification of ϕ_s, while the exponents, K_H and $\overline{K}_H$ are left free to be determined by the solution procedure. A typical velocity distribution, $w(\phi(x))$, is sketched in Figure 24.

Substitution of equation (3-54) into equation (3-50) yields

$$P(\phi) = \ln\left|\cos\left(\frac{\phi}{2} - \alpha_i\right)\right| - \ln v_i - \ln w(\phi) + \ln 2 \qquad (3\text{-}58)$$

$$\left(\phi_{i-1} < \phi < \phi_i \ ; \quad i=1,2,3,\ldots,I_p\right)$$

Thus, at the trailing edge, continuity of $P(\phi)$ requires that

$$\ln\left|\cos\alpha_1\right| - \ln v_1 - \ln w(0) = \ln\left|\cos\alpha_{I_p}\right| - \ln v_{I_p} - \ln w(2\pi) \qquad (3\text{-}59)$$

whereas at all other segment boundaries,

$$\ln\left|\cos\left(\frac{\phi_i}{2} - \alpha_i\right)\right| - \ln v_i - \ln w(\phi) = \ln\left|\cos\left(\frac{\phi_i}{2} - \alpha_{i+1}\right)\right|$$

$$- \ln v_{i+1} - \ln w(\phi) \qquad (3-60)$$

$$\left(\phi_{i-1} < \phi < \phi_i \quad ; \qquad i=1,2,3,\ldots,I_{p-1} \right)$$

A problem arises with the velocity distribution at the leading edge stagnation point, given by $\phi = \pi + 2\alpha_i$, in that $P(\phi)$ is undefined at that point and no longer satisfies the conditions imposed on it. This problem can be avoided, however, by requiring $\phi_{i,le} - 2\alpha_{i,le} < \pi$ and $\phi_{i,le} - 2\alpha_{i,le+1} > \pi$, or, more simply, by requiring

$$\alpha_{i,le+1} < \alpha_{i,le} \qquad (3-61)$$

At this point, the method requires that the values of the pressure recovery and closure parameters, μ, $\overline{\mu}$, ϕ_w, $\overline{\phi}_w$, ϕ_s, and $\overline{\phi}_s$, be given, along with all of the ϕ_i, α_i pairs. The I_p constants, the v_i's, and the closure contribution exponents, K_H and $\overline{K}_H$, are solved for such that the I_p matching conditions, equations (3-59) and (3-60), as well as the three integral constraints, equations (3-42)-(3-44), are satisfied. Consequently, as given, the problem is over-specified and it is necessary to relax one of the given parameters so that all of the required conditions can be met. Because of its strong influence as the matching point of the upper and lower surface velocity distributions, the method uses the leading edge arc limit, $\phi_{i,le}$, as the necessary free variable.

By substituting equation (3-58), along with equation (3-56) or (3-57), into equations (3-42)-(3-44), it is found that the integral constraints can be

evaluated in closed form. With the substitutions indicated, equation (3-43)
becomes

$$\int_0^{2\pi} P(\phi)\cos\phi \, d\phi = \int_0^{2\pi} \left[\ln\left|\cos\left(\frac{\phi}{2} - \alpha_i\right)\right| - \ln v_i(\phi) \right.$$

$$\left. + \mu \ln W_w(\phi) - K_H \ln W_s(\phi) + \ln 2 \right] \cos\phi \, d\phi = \pi \qquad (3\text{-}62)$$

Now, defining

$$-\int_0^{2\pi} \ln W_s(\phi) \cos\phi \, d\phi = W_{c1} \qquad (3\text{-}63)$$

$$-\int_0^{2\pi} \ln \overline{W}_s(\phi) \cos\phi \, d\phi = W_{cI_p} \qquad (3\text{-}64)$$

and, introducing the notation

$$\ln(i,j) = \ln \left| \cos \left(\frac{\phi_i}{2} - \alpha_j\right)\right| \qquad (3\text{-}65)$$

The evaluation of equation (3-62) gives

$$\int_0^{2\pi} P(\phi) \cos\phi \, d\psi = K_H W_{c1} + \overline{K}_H W_{cI_p} + \sum_{i=1}^{I_p} \left\{ \sin 2\alpha_i \right.$$

$$\left[\ln(i,i) - \ln(i-1,i) \right] + \frac{1}{2} \left(\phi_i - \phi_{i-1} \right) \cos 2\alpha_i$$

$$+ \frac{1}{2} \left(\sin \phi_i - \sin \phi_{i-1} \right) + \sin \phi_i \left[\ln(i,i) - \ln v_i \right]$$

$$- \sin \phi_{i-1} \left[\ln(i-1,i) - \ln v_i \right] \}$$

$$+ \mu \int_0^{\phi_w} \ln W_w(\phi) \cos\phi \, d\phi + \bar{\mu} \int_{\bar{\phi}_w}^{2\pi} \ln \overline{W}_w(\phi) \cos\phi \, d\phi = \pi \qquad (3\text{-}66)$$

Using the matching condition, equation (3-60), it is found that a number of terms in this expression drop out such that, after simplification, it may be written

$$K_H W_{cI} + \overline{K}_H W_{cI_p} + J_c = 0 \qquad (3\text{-}67)$$

where J_c is defined as

$$J_c = \sum_{i=1}^{I_p} \left\{ \sin 2\alpha_i \left[\ln(i,i) - \ln(i-1,i) \right] \right.$$

$$\left. + \frac{1}{2} \left(\phi_i - \phi_{i-1} \right) \cos 2\alpha_i \right\} - \pi + \mu \int_0^{\phi_w} \ln W_w(\phi) \cos\phi \, d\phi$$

$$+ \bar{\mu} \int_{\bar{\phi}_w}^{2\pi} \ln \overline{W}_w(\phi) \cos\phi \, d\phi \qquad (3\text{-}68)$$

Now, after formally setting α_0 and α_{I_p} to zero, the terms containing ϕ_i are collected and the leading edge arc limit, $\phi_{i,le}$, is isolated such that equation (3-68) is rewritten as

$$J_c = a_c + b_c \ln(le,le) + c_c \ln(le, le + 1) + d_c \phi_{i,le} \qquad (3\text{-}69)$$

where the coefficients are given by

$$a_c = \sum_{i=0}^{i,le-1} \left\{ \sin 2\alpha_i \ln(i,i) - \sin 2\alpha_{i+1} \ln(i,i+1) \right.$$

$$\left. + \frac{1}{2} \phi_i \left(\cos 2\alpha_i - \cos 2\alpha_{i+1} \right) \right\} + \sum_{i=1,le+1}^{l_p} \left\{ \sin 2\alpha_i \ln(i,i) \right.$$

$$\left. - \sin 2\alpha_{i+1} \ln(i,i+1) + \frac{1}{2} \phi_i \left(\cos 2\alpha_i - \cos 2\alpha_{i+1} \right) \right\}$$

$$- \pi + \mu \int_0^{\phi_w} \ln W_w(\phi) \cos\phi \, d\phi + \bar{\mu} \int_{\bar{\phi}_w}^{2\pi} \ln \bar{W}_w(\phi) \cos\phi \, d\phi \qquad (3\text{-}70)$$

$$b_c = \sin 2\alpha_{le} \qquad (3\text{-}71)$$

$$c_c = - \sin 2\alpha_{le+1} \qquad (3\text{-}72)$$

$$d_c = \frac{1}{2} \left(\cos 2\alpha_{le} - \cos 2\alpha_{le+1} \right) \qquad (3\text{-}73)$$

Using the definitions given by

$$- \int_0^{\phi_s} \ln W_s(\phi) \sin\phi \, d\phi = W_{s1} \qquad (3\text{-}74)$$

$$- \int_{\bar{\phi}_s}^{2\pi} \ln \bar{W}_s(\phi) \sin\phi \, d\phi = W_{sI_p} \qquad (3\text{-}75)$$

the integral constraint of equation (3-44), in a manner similar to that

applied to equation (3-43), becomes

$$K_H W_{s1} + \bar{K}_H W_{sI_p} + J_s = 0 \qquad (3\text{-}76)$$

where J_s is ultimately expressed as

$$J_s = a_s + b_s \ln(le,le) + c_s \ln(le,le + 1) + d_s \phi_{le} \qquad (3-77)$$

and the coefficients are

$$a_s = \sum_{i=0}^{i,le-1} \{ -(1 + \cos 2\alpha_i) \ln(i,i) + (1 + \cos 2\alpha_{i+1})$$

$$\ln(i,i+1) + \frac{1}{2} \phi_i \left(\sin 2\alpha_i - \sin 2\alpha_{i+1} \right) \}$$

$$+ \sum_{i,le+1}^{I_p} \{ -(1 + \cos 2\alpha_i)\ln(i,i) + (1 + \cos 2\alpha_{i+1})$$

$$\ln(i,i+1) + \frac{1}{2} \phi_i \left(\sin 2\alpha_i - \sin 2\alpha_{i+1} \right) \}$$

$$+ \mu \int_0^{\phi_w} \ln W_w(\phi) \sin\phi \, d\phi + \bar{\mu} \int_{\phi_w}^{2\pi} \ln \overline{W}_w(\phi) \sin\phi \, d\phi \qquad (3-78)$$

$$b_s = - (1 + \cos 2\alpha_{le}) \qquad (3-79)$$

$$c_s = (1 + \cos 2\alpha_{le+1}) \qquad (3-80)$$

$$d_s = \frac{1}{2} \left(\sin 2\alpha_{le} - \sin 2\alpha_{le+1} \right) \qquad (3-81)$$

At this point, consider the trailing edge matching condition given by equation (3-59). By repeated applications of equation (3-60), the velocity terms v_1 and v_{I_p} can be eliminated and the resulting expression written as

$$- K_H \ln W_s(0) + \overline{K}_H \ln \overline{W}_s(2\pi) + J_t = 0 \tag{3-82}$$

in which

$$J_t = a_t + b_t \ln(le,le) + c_t \ln(le,le+1) \tag{3-83}$$

and

$$a_t = \sum_{i=0}^{i,le-1} \left\{ -\ln(i,i) + \ln(i,i+1) \right\}$$

$$+ \sum_{i=i,le+1}^{I_p} \left\{ -\ln(i,i) + \ln(i,i+1) \right\} - \mu \ln W_w(0)$$

$$+ \overline{\mu} \ln \overline{W}_w(2\pi) \tag{3-84}$$

$$b_t = -1 \tag{3-85}$$

$$c_t = 1 \tag{3-86}$$

Thus, equations (3-67), (3-76), and (3-82), can be used to solve for the three unknowns, K_H, $\overline{K}_H$, and $\phi_{1,le}$. In matrix notation, this system of equations may be represented

$$\begin{bmatrix} W_{cl} & W_{cI_p} & J_c \\ W_{sl} & W_{sI_p} & J_s \\ -\ln W_s(0) & \ln \overline{W}_s(2\pi) & J_t \end{bmatrix} \begin{Bmatrix} K_H \\ \overline{K}_H \\ \phi_{i,le} \end{Bmatrix} = 0 \qquad (3-87)$$

Solving for $\phi_{i,le}$ leads to a transcendental equation which can be expressed as

$$a + b \ln (le,le) + c \ln (le,le+1) + d\phi_{i,le} = 0 \qquad (3-88)$$

in which

$$a = D_1 a_c + D_2 a_s + D_3 a_t \qquad (3-89)$$

$$b = D_1 b_c + D_2 b_s + D_3 b_t \qquad (3-90)$$

$$c = D_1 c_c + D_2 c_s + D_3 c_t \qquad (3-91)$$

$$d = D_1 d_c + D_2 d_s \qquad (3-92)$$

and

$$D_1 = W_{sl} \ln \overline{W}_s(2\pi) + W_{sI_p} \ln W_s(0) \qquad (3-93)$$

$$D_2 = - W_{cl} \ln \overline{W}_s(2\pi) - W_{cI_p} \ln W_s(0) \qquad (3-94)$$

$$D_3 = W_{cl} W_{sI_p} - W_{cI_p} W_{sl} \qquad (3-95)$$

Equation (3-88) can now be solved numerically for $\phi_{i,le}$ using the technique of Regula falsi. Once $\phi_{i,le}$ has been obtained, $J_c-\pi$, J_s, and J_t can be calculated and used in a straightforward manner to solve for K_H and $\overline{K}_H$. In order to determine the v_i's, the first integral constraint, equation (3-42), is evoked along with the matching conditions given by equation (3-60). Thus,

$$\int_0^{2\pi} P(\phi)\,d\phi = \sum_{i=1}^{I_p} \left\{ \int_{\phi_{i-1}}^{\phi_i} \left[\ln|\cos\left(\tfrac{\phi}{2} - \alpha_i\right)| - \ln\frac{v_i}{v_1} \right. \right.$$

$$\left. \left. + \mu\,\ln W_w(\phi) - K_H \ln W_s(\phi)\right]\,d\phi + 2\pi(\ln 2 - \ln v_1) \right. \tag{3-96}$$

The velocity ratios, $\dfrac{v_i}{v_1}$, are found from sequential applications of equation (3-60) and the results used to determine v_i from equation (3-96). At this point, $P(\phi)$ and $Q(\phi)$ can be determined and the coordinates of the profile follow directly.

The closure requirements of the airfoil determine the values of K_H and $\overline{K}_H$ which, in turn, influence the trailing edge closure angle. In order that some control over the trailing edge shape is possible, the digital computer coding of the method allows a value of K_s, where $K_s = K_H + \overline{K}_H$, to be specified. Then, any one of a number of iteration schemes can be selected which vary particular combinations of the specified input parameters until the desired value of K_s is achieved. This procedure, along with a detailed discussion of the numerical implementation of the method, is contained in Reference [25].

Incorporation of the Conditions for Finite Trailing Edge Pressure Gradients into the Eppler Design Method

As developed previously, the condition on the transformation function

which results in a finite complex pressure gradient at the trailing edge of an
airfoil is given by equation (3-27). In order to incorporate this result into
the design method of Eppler, the representation of the derivative of the
transformation function, provided by equation (3-35), is differentiated to
yield

$$
z'' = e^{\sum\limits_{m=0}^{\infty} (a_m + ib_m)\zeta^{-m}} \left\{ \frac{1}{\zeta^2} - \left(1 - \frac{1}{\zeta}\right) \sum\limits_{m=0}^{\infty} m(a_m + ib_m)\zeta^{-(m+1)} \right\}
\tag{3-97}
$$

which, when evaluated at the trailing edge, $\zeta = 1$, becomes

$$
z_T'' = e^{\sum\limits_{m=0}^{\infty} (a_m + ib_m)}
\tag{3-98}
$$

Differentiating equation (3-97) yields

$$
z''' = e^{\sum\limits_{m=0}^{\infty} (a_m + ib_m)\zeta^{-m}} \left\{ -\frac{2}{\zeta} - \frac{2}{\zeta^2} \sum\limits_{m=0}^{\infty} m(a_m + ib_m)\zeta^{-(m+1)} \right.
$$

$$
+ \left(1 - \frac{1}{\zeta}\right) \sum\limits_{m=0}^{\infty} m(m+1)(a_m + ib_m)\zeta^{-(m+2)}
$$

$$
\left. + \left(1 - \frac{1}{\zeta}\right) \left[\sum\limits_{m=0}^{\infty} m(a_m + ib_m)\zeta^{-(m+1)} \right]^2 \right\}
\tag{3-99}
$$

For this expression to be evaluated at the trailing edge, it is necessary that

the last two terms drop out as occurs if the summation present in each term is finite. Noting that the a_m's and b_m's can be considered as the coefficients of the Fourier series representing $P(\phi)$, equation (3-41), and, considering the theorems concerning the differentiation and convergence of such a series, Reference [28] for example, it is found that the summations will be finite if $P'(\phi)$ is continuous at the trailing edge. Thus, it is required that

$$P'(0) = P'(2\pi) \qquad (3-100)$$

If this is the case, then equation (3-99) becomes

$$z_T''' = e^{\sum\limits_{m=0}^{\infty} (a_m + ib_m)} \left\{ -2 - 2 \sum\limits_{m=0}^{\infty} m(a_m + ib_m) \right\} \qquad (3-101)$$

Substitution of equations (3-98) and (3-101) into the condition for finite trailing edge pressure gradients, equation (3-27), yields

$$\frac{z_T'''}{z_T''} = -2 - 2 \sum\limits_{m=0}^{\infty} ma_m - 2i \sum\limits_{m=0}^{\infty} mb_m = -3 - i\tan\alpha \qquad (3-102)$$

To further resolve this expression, the series representations of $P(\phi)$ and $Q(\phi)$, given by equations (3-41) and (3-45), are differentiated to obtain

$$P'(\phi) = \sum\limits_{m=0}^{\infty} - ma_m \sin m\phi + mb_m \cos m\phi \qquad (3-103)$$

$$Q'(\phi) = \sum\limits_{m=0}^{\infty} - ma_m \cos m\phi - mb_m \sin m\phi \qquad (3-104)$$

which, when evaluated at the trailing edge, become

$$P'(0) = \sum_{m=0}^{\infty} mb_m \tag{3-105}$$

$$Q'(0) = \sum_{m=0}^{\infty} ma_m \tag{3-106}$$

Using these results, equation (3-102) yields the conditions that

$$P'(0) = \frac{1}{2} \tan \alpha \tag{3-107}$$

$$Q'(0) = -\frac{1}{2} \tag{3-108}$$

which must be satisfied in order for a airfoil to have finite trailing edge pressure gradients.

In order to consider equation (3-107) further, the expression for $P(\phi)$ of equation (3-58) is differentiated and evaluated at the trailing edge yielding

$$P'(0) = \frac{1}{2} \tan \alpha_1 - \frac{w'(0)}{w(0)} \tag{3-109}$$

In making the transition from $v(\phi)$ to $V(x)$, it is found that the velocity distribution on the airfoil, $V(x)$, has an infinite slope at the trailing edge unless $w'(0) = 0$. Because of this, it already a requirement in the method that $w'(0) = 0$ and, consequently, equation (3-109) becomes

$$P'(0) = \frac{1}{2} \tan \alpha_1 \tag{3-110}$$

Equating this result with equation (3-107), it is found that the condition imposed on $P'(0)$ is satisfied when

$$\alpha = \alpha_1 \qquad\qquad (3\text{-}111)$$

Thus, the complex trailing edge pressure gradient on an airfoil can only be finite when the airfoil is operating at an angle of attack corresponding to that specified in the design process for the first arc segment.

To satisfy the second condition required for bounded trailing edge pressure gradients, equation (3-108), the integral expression for $Q(\phi)$, equation (3-45), is differentiated and calculated at the trailing edge giving

$$Q'(0) = \frac{1}{4\pi} \int_0^{2\pi} P(\psi) \, csc^2\left(\frac{\psi}{2}\right) d\psi \qquad\qquad (3\text{-}112)$$

Substituting this result into equation (3-108) introduces an additional integral constraint which is given by

$$\int_0^{2\pi} P(\psi) \, csc^2 \frac{\psi}{2} \, d\psi = -2\pi \qquad\qquad (3\text{-}113)$$

In addition to the conditions of equations (3-111) and (3-113), examination of equation (3-22) reveals that in order for R_T to be finite, the fourth derivative of the transformation evaluated at the trailing edge, z_T^{iv}, must also be finite. Evoking the same arguments used for insuring the finiteness of z_T''', it is found that z_T^{iv} will be bounded provided that $P''(\phi)$ is continuous at the trailing edge. To insure this, consider the result of differentiating equation (3-58) twice, giving

$$P''(\phi) = -\frac{1}{4} \sec^2 \left(\frac{\phi}{2} - \alpha_i\right) - \frac{w''(\phi)}{w(\phi)} + \left[\frac{w'(\phi)}{w(\phi)}\right]^2 \qquad (3\text{-}114)$$

$$\left(\phi_{i-1} \leqslant \phi \leqslant \phi_i \; ; \quad i=1,2,3,\ldots,I_p\right)$$

Because $w'(0) = w'(2\pi) = 0$, it is evident that the continuity of $P''(\phi)$ at the trailing edge requires

$$\frac{w''(0)}{w(0)} = \frac{w''(2\pi)}{w(2\pi)} \qquad (3\text{-}115)$$

After performing the necessary manipulations, making use of equation (3-55), it is found that this condition can be written more specifically as

$$\frac{\mu K}{1 + K + (1-K)\cos\phi_w} + 1.125 \left(\frac{K_H}{1 - \cos\phi_s}\right)$$

$$= \frac{\bar{\mu}\,\bar{K}}{1 + \bar{K} + (1-\bar{K})\cos\bar{\phi}_w} + 1.125 \left(\frac{\bar{K}_H}{1 - \cos\bar{\phi}_s}\right) \qquad (3\text{-}116)$$

It should be noted that satisfying this condition also guarantees that the last two terms in equation (3-99) drop out.

As presented thus far, the development has shown that an airfoil which satisfies equations (3-111), (3-113), and (3-116) will have finite trailing edge pressure gradients; however, in order to incorporate these conditions into the design process it remains to evaluate the integral constraint, given by equation (3-113) in terms of the appropriate design parameters. To begin, although the integrand of equation (3-113) is singular, the integral can be shown to exist in the Cauchy Principal Value sense by differentiating the

expression for $Q(\phi)$, equation (3-45), to obtain

$$Q'(\phi) = \frac{1}{4\pi} \int_0^{2\pi} P(\psi) \csc^2 \left(\frac{\psi-\phi}{2}\right) d\psi \qquad (3-117)$$

and, integrating oy parts, yields

$$Q'(\phi) = -\frac{1}{2\pi} P(2\pi) \operatorname{ctn} \left(\pi - \frac{\phi}{2}\right) + \frac{1}{2\pi} P(0) \operatorname{ctn} \left(-\frac{\phi}{2}\right)$$

$$+ \frac{1}{2\pi} \int_0^{2\pi} P'(\psi) \operatorname{ctn} \left(\frac{\psi-\phi}{2}\right) d\psi \qquad (3-118)$$

Because the required continuity of $P(\phi)$ gives $P(0) = P(2\pi)$, the leading terms of this expression cancel leaving

$$Q'(\phi) = \frac{1}{2\pi} \int_0^{2\pi} P'(\psi) \operatorname{ctn} \left(\frac{\psi-\phi}{2}\right) d\psi \qquad (3-119)$$

and the fou :h ntegral constraint then becomes

$$Q'(0) = \frac{1}{2\pi} \int_0^{2\pi} P'(\psi) \operatorname{ctn} \frac{\psi}{2} d\psi = -\frac{1}{2} \qquad (3-120)$$

After renaming the variable of integration, this result is used to define I_4 as

$$I_4 = 2 \int_0^{2\pi} P'(\phi) \operatorname{ctn} \frac{\phi}{2} d\phi = -2\pi \qquad (3-121)$$

Now, differentiating equation (3-58) gives

$$P'(\phi) = -\frac{1}{2} \tan\left(\frac{\phi}{2} - \alpha_i\right) - \frac{w'(\phi)}{w(\phi)} \qquad (3\text{-}122)$$

$$\left(\phi_{i-1} < \phi < \phi_i ; \quad i=1,2,3,\ldots,I_p\right)$$

Substituting this expression into equation (3-121) ultimately yields a result which is denoted as

$$I_4 = I_a + I_b = -2\pi \qquad (3\text{-}123)$$

where

$$I_a = -\sum_{i=1}^{I_p} \int_{\phi_{i-1}}^{\phi_i} \tan\left(\frac{\phi}{2} - \alpha_i\right) \operatorname{ctn} \frac{\phi}{2}\, d\phi \qquad (3\text{-}124)$$

$$\left(\phi_{i-1} < \phi < \phi_i ; \quad i=1,2,3,\ldots,I_p\right)$$

and

$$I_b = -2 \int_0^{2\pi} \frac{w'(\phi)}{w(\phi)} \operatorname{ctn} \frac{\phi}{2}\, d\phi \qquad (3\text{-}125)$$

The analytical evaluation of I_a is now undertaken, beginning with consideration of the indefinite integral

$$I_{a1} = \int \tan\left(\frac{\phi}{2} - \alpha_i\right) \operatorname{ctn} \frac{\phi}{2}\, d\phi \qquad (3\text{-}126)$$

for which, after some manipulation, it is found that

$$I_{al} = \phi - 2 \tan\alpha_i \ln \left| \frac{\sin\frac{\phi}{2}}{\cos(\frac{\phi}{2} - \alpha_i)} \right| \tag{3-127}$$

Using this expression in equation (3-124) gives

$$I_a = \sum_{i=1}^{I_p} \left\{ -\phi + 2\tan\alpha_i \ln \left| \frac{\sin\frac{\phi}{2}}{\cos(\frac{\phi}{2} - \alpha_i)} \right| \Big|_{\phi_{i-1}}^{\phi_i} \right\} \tag{3-128}$$

which becomes

$$I_a = \sum_{i=1}^{I_p} \left\{ -\phi_i + \phi_{i-1} + 2\tan\alpha_i \left[\ln\left|\sin\frac{\phi_i}{2}\right| - \ln\left|\sin\frac{\phi_{i-1}}{2}\right| \right] \right.$$

$$\left. - 2\tan\alpha_i \left[\ln\left|\cos\left(\frac{\phi_i}{2} - \alpha_i\right)\right| - \ln\left|\cos\left(\frac{\phi_{i-1}}{2} - \alpha_i\right)\right| \right] \right\} \tag{3-129}$$

Performing the indicated summation with $\phi_0 = \epsilon \to 0$ and $\phi_{I_p} = 2\pi$ yields,

$$I_a = 2\tan\alpha_1 \left[\ln\left|\sin\frac{\phi_i}{2}\right| - \ln\left|\sin\frac{\epsilon}{2}\right| \right]$$

$$- 2\tan\alpha_1 \left[\ln\left|\cos\left(\frac{\phi_i}{2} - \alpha_1\right) - \ln\left|\cos(-\alpha_1)\right| \right] \right]$$

$$- 2\pi + 2\tan\alpha_{I_p} \left[\ln\left|\sin\left(\pi - \frac{\epsilon}{2}\right) - \ln\left|\sin\frac{\phi_{I_{p-1}}}{2}\right| \right] \right]$$

$$- 2\tan\alpha_{I_p} \left[\ln\left|\cos(\pi - \alpha_{I_p})\right| - \ln\left|\cos\left(\frac{\phi_{I_{p-1}}}{2} - \alpha_{I_p}\right)\right| \right]$$

$$+ \sum_{i=2}^{I_p} \left\{ 2\tan\alpha_i \left[\ln\left|\sin\frac{\phi_i}{2}\right| - \ln\left|\sin\frac{\phi_{i-1}}{2}\right| \right] \right.$$

$$- 2\tan\alpha_i \left[\ln\left|\cos\left(\frac{\phi_i}{2} - \alpha_i\right)\right| - \ln\left|\cos\left(\frac{\phi_{i-1}}{2} - \alpha_i\right)\right|\right]\} \qquad (3\text{-}130)$$

Extracting the singular terms in the above expression and combining them as S_{Ia} gives

$$S_{Ia} = - 2\tan\alpha_1 \ln\left|\sin\frac{\epsilon}{2}\right| + 2\tan\alpha_{I_p} \ln\left|\sin\left(\pi - \frac{\epsilon}{2}\right)\right| \qquad (3\text{-}131)$$

Because $\left|\sin\left(\pi - \frac{\epsilon}{2}\right)\right| = \left|\sin\frac{\epsilon}{2}\right|$, the singular terms can be eliminated by requiring that

$$\alpha_{I_p} = \alpha_1 \qquad (3\text{-}132)$$

The expression for I_a that remains is then simplified by incorporating additional terms under the summation such that

$$I_a = - 2\pi + \sum_{i=1}^{I_p-1} \{2\tan\alpha_i\left[\ln\left|\sin\frac{\phi_i}{2}\right| - \ln\left|\cos\left(\frac{\phi_i}{2} - \alpha_i\right)\right|\right]$$

$$+ 2\tan\alpha_{i+1}\left[\ln\left|\cos\left(\frac{\phi_i}{2} - \alpha_{i+1}\right)\right| - \ln\left|\sin\frac{\phi_i}{2}\right|\right] \qquad (3\text{-}133)$$

To begin the evaluation of I_b, equation (3-125), recall that $w'(\phi)/w(\phi)$ varies in a piecewise fashion with ϕ. Using the form of equation (3-56) to describe $w(\phi)$, and comparing that with equation (3-55), it is found that, on the upper surface,

$$W_w(\phi) = 1 + K\left(\frac{\cos\phi - \cos\phi_w}{1 + \cos\phi_w}\right) \qquad (3\text{-}134)$$

$$W_s(\phi) = 1 - m \left(\frac{\cos\phi - \cos\phi_s}{1 - \cos\phi_s}\right)^2 \tag{3-135}$$

while, on the lower surface,

$$\overline{W}_w(\phi) = 1 + \overline{K} \left(\frac{\cos\phi - \cos\overline{\phi}_w}{1 + \cos\overline{\phi}_w}\right) \tag{3-136}$$

$$\overline{W}_s(\phi) = 1 - m \left(\frac{\cos\phi - \cos\overline{\phi}_s}{1 - \cos\overline{\phi}_s}\right) \tag{3-137}$$

With regard to the earlier discussion concerning the piecewise treatment given to the function described by equation (3-55), I_b is evaluated over the piecewise segments defined as follows:

$$\frac{w'(\phi)}{w(\phi)} = - \mu \frac{W_w'(\phi)}{W_w(\phi)} + K_H \frac{W_s'(\phi)}{W_s(\phi)} \qquad 0 < \phi < \phi_s \tag{3-138}$$

$$\frac{w'(\phi)}{w(\phi)} = - \mu \frac{W_w'(\phi)}{W_w(\phi)} \qquad \phi_s < \phi < \phi_w \tag{3-139}$$

$$\frac{w'(\phi)}{w(\phi)} = 0 \qquad \phi_w < \phi < \overline{\phi}_w \tag{3-140}$$

$$\frac{w'(\phi)}{w(\phi)} = \overline{\mu} \frac{\overline{W}_w'(\phi)}{\overline{W}_w(\phi)} \qquad \overline{\phi}_w < \phi < \overline{\phi}_s \tag{3-141}$$

$$\frac{w'(\phi)}{w(\phi)} = - \overline{\mu} \frac{\overline{W}_w'(\phi)}{\overline{W}_w(\phi)} + \overline{K}_H \frac{\overline{W}_s'(\phi)}{\overline{W}_s(\phi)} \qquad \overline{\phi}_s < \phi < 2\pi \tag{3-142}$$

Thus, for the most general case, the indefinite integral is given by

$$I_b = I_{b1} + I_{b2} \tag{3-143}$$

where

$$I_{b1} = 2\mu \int \frac{W_w'(\phi)}{W_w(\phi)} \, \text{ctn} \, \frac{\phi}{2} \, d\phi \tag{3-144}$$

and

$$I_{b2} = -2 K_H \int \frac{W_s'(\phi)}{W_s(\phi)} \, \text{ctn} \, \frac{\phi}{2} \, d\phi \tag{3-145}$$

In the following evaluation of I_b, only the notation for the upper surface will be used; however, the results are valid for the lower surface as well, if the upper surface quantities are replaced by their appropriate lower surface counterparts. In order to evaluate I_{b1}, let

$$g = \frac{K}{1 + \cos\phi_w} \tag{3-146}$$

$$f = 1 - g \cos \phi_w \tag{3-147}$$

so that

$$W_w(\phi) = f + g \cos\phi \tag{3-148}$$

Thus, the integral becomes

$$I_{b1} = -2\mu \int \left(\frac{g \, \sin\phi}{f + g \, \cos\phi} \right) \text{ctn} \, \frac{\phi}{2} \, d\phi \tag{3-149}$$

After some manipulation, it is found that

$$I_{b1} = -2\mu\phi + \mu F\left(\phi, f, g\right) \tag{3-150}$$

where

$$F = -\frac{2(g-f)}{\left(g^2 - f^2\right)^{1/2}} \ln\left|\frac{(g-f)\tan\frac{\phi}{2} + \left(g^2 - f^2\right)^{1/2}}{(g-f)\tan\frac{\phi}{2} - \left(g^2 - f^2\right)^{1/2}}\right| \qquad g^2 > f^2 \tag{3-151}$$

$$F = -\frac{4(g-f)}{\left(f^2 - g^2\right)^{1/2}} \tan^{-1}\left[\frac{(f-g)\tan\frac{\phi}{2}}{\left(f^2 - g^2\right)^{1/2}}\right] \qquad f^2 > g^2 \tag{3-152}$$

In order to evaluate I_{b2}, let

$$N_1 = \frac{\sqrt{m}}{1 - \cos\phi_s} \tag{3-153}$$

$$a = 1 - \sqrt{m} \tag{3-154}$$

$$b = 1 + \sqrt{m} \tag{3-155}$$

so that

$$W_s(\phi) = \left[a + N_1\left(1 - \cos\phi\right)\right]\left[b - N_1\left(1 - \cos\phi\right)\right] \tag{3-156}$$

and

$$W_s{}'(\phi) = N_1\sin\phi\left[b - N_1(1 - \cos\phi)\right] - N_1\sin\phi\left[a + N_1(1 - \cos\phi)\right]$$

$$\tag{3-157}$$

The expression for I_{b2} may then be written as

$$I_{b2} = I_{b2a} + I_{b2b} \tag{3-158}$$

where

$$I_{b2a} = -2K_H N_1 \int \frac{\sin \phi}{[a + N_1(1 - \cos\phi)]} \, ctn \, \frac{\phi}{2} \, d\phi \tag{3-159}$$

$$I_{b2b} = 2K_H N_1 \int \frac{\sin \phi}{[b - N_1(1 - \cos\phi)]} \, ctn \, \frac{\phi}{2} \, d\phi \tag{3-160}$$

After performing the integration indicated in equation (3-159), I_{b2a} becomes

$$I_{b2a} = 2K_H\phi - 4K_H \left(\frac{a + 2N_1}{a}\right)^{1/2} \tan^{-1}\left[\left(\frac{a + 2N_1}{a}\right)^{1/2} \tan \frac{\phi}{2}\right] \tag{3-161}$$

Evaluation of the expression for I_{b2b}, equation (3-160), after some manipulation, gives

$$I_{b2b} = 2K_H\phi + 4K_H K_F(\phi, N_1, b) \tag{3-162}$$

where

$$K_F = \frac{(2N_1 - b)}{(b^2 - 2N_1 b)^{1/2}} \tan^{-1} \frac{(b - 2N_1)\tan \frac{\phi}{2}}{(b^2 - 2N_1 b)^{1/2}} \qquad b > 2N_1 \tag{3-163}$$

$$K_F = \frac{(2N_1 - b)}{2(2bN_1 - b^2)^{1/2}} \ln \left| \frac{(2N_1 - b)\tan \frac{\phi}{2} + (2N_1 b - b^2)^{1/2}}{(2N_1 - b)\tan \frac{\phi}{2} - (2N_1 b - b^2)^{1/2}} \right| \qquad b < 2N_1$$

$$\tag{3-164}$$

Combining equations (3-150), (3-158), (3-161), and (3-162) into the expression for I_b, equation (3-143), yields

$$I_b = - 2\mu\phi + \mu\, F(\phi,f,g) + 4K_H\phi + 4K_H\, K_F(\phi,N_1,b)$$

$$- 4K_H \left(\frac{a + 2N_1}{a}\right)^{1/2} \tan^{-1}\left[\left(\frac{a + 2N_1}{a}\right)^{1/2} \tan\frac{\phi}{2}\right] \qquad (3\text{-}165)$$

Using this result, I_b can be evaluated at the appropriate integration limits for the given intervals so that

$$I_b = 4K_H\, \phi_s - 4K_H \left(\frac{a + 2N_1}{a}\right)^{1/2} \tan^{-1}\left[\left(\frac{a + 2N_1}{a}\right)^{1/2} \tan\frac{\phi_s}{2}\right]$$

$$+ 4K_H\, K_F\left(\phi_s,N_1,b\right) - 2\mu\phi_w + \mu F\left(\phi_w,f,g\right) + 2\,\bar{\mu}\,\bar{\phi}_w$$

$$- \bar{\mu}\,\bar{F}\left(\bar{\phi}_w,\, \bar{f},\, \bar{g}\right) - 4\pi\,\bar{\mu} + 8\pi\,\bar{K}_H - 4\,\bar{K}_H\,\bar{\phi}_s - 4\,\bar{K}_H\,\bar{K}_F(\bar{\phi}_s,\,\bar{N}_1,\, b)$$

$$+ 4\bar{K}_H \left(\frac{a + 2\bar{N}_1}{a}\right)^{1/2} \tan^{-1}\left[\left(\frac{a + 2\bar{N}_1}{a}\right)^{1/2} \tan\frac{\bar{\phi}_s}{2}\right] \qquad (3\text{-}166)$$

This result, combined with that obtained for I_a, equation (3-133), provides an analytical representation of the integral constraint, I_4, which must be satisfied in order to insure that the trailing edge pressure gradients of an airfoil are bounded.

At this point, there are four integral constraints and I_p matching conditions which must be solved for $\phi_{i,le}$, K_H, $\bar{K}_H$, and the I_p unknown constants, the v_i's. Thus, in order to satisfy a fourth constraint, an additional parameter must be relaxed. Because for most applications of

interest, the specification of the upper surface velocity distribution is of greater consequence than the specification of the lower, both $\bar{\mu}$, and $\bar{K}$, which control the shape of the lower surface recovery, are candidates; however, as freeing $\bar{\mu}$ results in a more direct method of solution, it is chosen as the additional parameter to relax.

At this point, it is necessary to isolate $\phi_{i,le}$ for solution in the expression for I_a, equation (3-133). To facilitate this, the terms not containing $\phi_{i,le}$ are combined in a parameter, K_{Ia}, such that I_a becomes

$$I_a = -2\pi + K_{Ia} + 2\tan \alpha_{le}\left[\ln\left|\sin \frac{\phi_{i,le}}{2}\right| - \ln\left|\cos\left(\frac{\phi_{i,le}}{2} - \alpha_{le}\right)\right|\right]$$

$$- 2\tan \alpha_{le+1}\left[\ln\left|\sin \frac{\phi_{i,le}}{2}\right| - \ln\left|\cos\left(\frac{\phi_{i,le}}{2} - \alpha_{le+1}\right)\right|\right] \qquad (3-167)$$

where K_{Ia} is given by

$$K_{Ia} = \sum_{i=1}^{le-1} \left\{2\tan \alpha_i\left[\ln\left|\sin \frac{\phi_i}{2}\right| - \ln\left|\cos \left(\frac{\phi_i}{2} - \alpha_i\right)\right|\right]\right.$$

$$+ 2\tan \alpha_{i+1}\left[\ln\left|\cos \left(\frac{\phi_i}{2} - \alpha_{i+1}\right)\right| - \ln\left|\sin \frac{\phi_i}{2}\right|\right]\right\}$$

$$+ \sum_{i=le+1}^{I_p-1} \left\{2\tan \alpha_i\left[\ln\left|\sin \frac{\phi_i}{2}\right| - \ln\left|\cos\left(\frac{\phi_i}{2} - \alpha_i\right)\right|\right]\right.$$

$$+ 2\tan \alpha_{i+1} \left[\ln\left|\cos \left(\frac{\phi_i}{2} - \alpha_{i+1}\right)\right| - \ln\left| \sin \frac{\phi_i}{2}\right|\right]\right\} \qquad (3-168)$$

Similarly, the expression for I_b, equation (3-165), is rewritten to isolate the unknowns K_H, $\bar{K}_H$, and $\bar{\mu}$ for solution. Thus,

$$I_b = K_H c_1 + \overline{K}_H c_2 + \overline{\mu} c_3 + K_{Ib} \qquad (3-169)$$

where the constant terms are:

$$c_1 = 4\phi_s - 4 \left(\frac{a + 2N_1}{a}\right)^{1/2} \tan^{-1}\left[\left(\frac{a + 2N_1}{a}\right)^{1/2} \tan^{-1} \frac{\phi_s}{2}\right] + 4K_F(\phi_s, N_1, b)$$

$$\qquad (3-170)$$

$$c_2 = 8\pi - 4\overline{\phi}_s + 4\left(\frac{a + 2\overline{N}_1}{a}\right)^{1/2} \tan^{-1}\left[\left(\frac{a + 2\overline{N}_1}{a}\right)^{1/2} \tan \frac{\overline{\phi}_s}{2}\right]$$

$$- 4\overline{K}_F(\overline{\phi}_s, \overline{N}_1, b) \qquad (3-171)$$

$$c_3 = 2\overline{\phi}_w - \overline{F}(\overline{\phi}_w, \overline{f}, \overline{g}) - 4\pi \qquad (3-172)$$

$$K_{Ib} = -2\mu\phi_w + \mu F(\phi_w, f, g) \qquad (3-173)$$

Using equations (3-123), (3-167), and (3-169), I_4 can be expressed as

$$I_4 = K_H c_1 + \overline{K}_H c_2 + \overline{\mu} c_3 + J_4 = 0 \qquad (3-174)$$

in which J_4 is defined, using the notation of equation (3-65), as

$$J_4 = a_J + b_J \ln(1e,1e) + c_J \ln(1e,1e+1) + e_J \ln\left|\sin \frac{\phi_{1,1e}}{2}\right| \qquad (3-175)$$

where the coefficients are given by

$$a_J = K_{Ia} + K_{Ib} \qquad (3-176)$$

$$b_J = -2 \tan \alpha_{le} \tag{3-177}$$

$$c_J = 2 \tan \alpha_{le+1} \tag{3-178}$$

$$e_J = 2 \left(\tan \alpha_{le} - \tan \alpha_{le+1} \right) \tag{3-179}$$

At this point, the integral constraint required for finite pressure gradients at the trailing edge has been written with the unknowns isolated appropriately for solution. It remains to rewrite the previously given constraint equations of the Eppler method to include $\bar{\mu}$ as an unknown parameter. To aid in this, the quantity W_{wcI_p} is defined by

$$W_{wcI_p} = \int_{\bar{\phi}_w}^{2\pi} \ln \bar{W}_w(\phi) \cos\phi \, d\phi \tag{3-180}$$

and the equation resulting from the first closure constraint, equation (3-67), is written as

$$K_H W_{cl} + \bar{K}_H W_{cI_p} + \bar{\mu} W_{wcI_p} + J_c = 0 \tag{3-181}$$

where J_c is defined as before, equations (3-69)-(3-73), except that the expression given for a_c, equation (3-70), no longer includes the term involving $\bar{\mu}$. Similarly, the equation resulting from the second closure constraint, equation (3-76), becomes

$$K_H W_{sl} + \bar{K}_H W_{sI_p} + \bar{\mu} W_{wsI_p} + J_s = 0 \tag{3-182}$$

where

$$W_{wsI_p} = J_{\overline{\phi}_w}^{2\pi} \ln \overline{W}_w(\phi) \sin\phi \, d\phi \tag{3-183}$$

and the $\overline{\mu}$ term is no longer included in the expression for a_s, equation
(3-78), which is used in defining J_s, equation (3-77). Finally, equation
(3-82), obtained using the matching condition at the trailing edge, is
rewritten as

$$- K_H \ln W_s(0) + \overline{K}_H \ln \overline{W}_s(2\pi) - \overline{\mu} \ln \overline{W}_w(2\pi) + J_t = 0 \tag{3-184}$$

and, as before, the $\overline{\mu}$ term is eliminated from the definition of a_t, equation
(3-84), used in the expression for J_t, equation (3-82).

Equations (3-174), (3-181), (3-182), and (3-184) can be used to solve the
four unspecified parameters of the design problem. In matrix notation, this
system of equations is represented by

$$\begin{bmatrix} W_{c1} & W_{cI_p} & W_{wcI_p} & J_c \\ W_{s1} & W_{sI_p} & W_{wsI_p} & J_s \\ -\ln W_s(0) & \ln\overline{W}_s(2\pi) & -\ln\overline{W}_w(2\pi) & J_t \\ c_1 & c_2 & c_3 & J_4 \end{bmatrix} \begin{Bmatrix} K_H \\ \overline{K}_H \\ \overline{\mu} \\ \phi_{1,le} \end{Bmatrix} = 0 \tag{3-185}$$

Expanding this system results in a transcendental equation for $\phi_{1,le}$ which is
£ the form

$$a + b \ln(le,le) + c \ln(le,le) + d\phi_{1,le}$$

$$+ e \ln\left|\sin -\frac{\phi_{1,1e}}{2}\right| = 0 \qquad (3\text{-}186)$$

As in the unmodified scheme, this equation is solved by Regula falsi, after which, J_c, J_s, and J_t are calculated and K_H, $\overline{K}_H$, and $\overline{\mu}$ obtained by back substitution. At this point, it is still necessary to satisfy equation (3-116) in order for the resulting airfoil to have a finite complex trailing edge pressure gradient. In order to achieve this, the computational procedure allows the designer to choose one of several possible iteration schemes which varies one of the parameters, K, $\overline{K}$, μ, or $\overline{\psi}_s$, until the condition of equation (3-116) is met.

Calculation of Trailing Edge Pressure Gradients in the Modified Eppler Method

Once an airfoil has been designed having bounded trailing edge pressure gradients, it is of interest to know the values of those gradients. As z_T'' is obtained in connection with the design process from equation (3-98), then, in reference to equation (3-28), the calculation of R_T further requires that z_T^{iv} be determined. While z_T^{iv} is made finite by requiring continuity of $P''(\phi)$ at the trailing edge, the actual calculation of the value of z_T^{iv} by further differentiating the series representations of $P(\phi)$ and $Q(\phi)$, in a manner similar to that used in obtaining z_T''', would necessitate that $P'(\phi)$ be continuous everywhere and that $P''(\phi)$ be piecewise continuous. As this would place severe restrictions on the velocity distributions allowable simply to facilitate the calculation of R_T, an alternative method was developed to approximate the value of z_T^{iv}. The scheme employed centers on expanding the transformation, $z(\zeta)$, in a Taylor series about the trailing edge to obtain

$$z(\zeta) = z_T + z_T{}'(\zeta-\zeta_T) + \frac{1}{2!} z_T{}''(\zeta-\zeta_T)^2 + \frac{1}{3!} z_T{}'''(\zeta-\zeta_T)^3$$

$$+ \frac{1}{4!} z_T{}^{iv} (\zeta-\zeta_T)^4 + \ldots \tag{3-187}$$

in which, as determined previously,

$$z_T{}' = 0 \tag{3-188}$$

$$\zeta_T = 1 \tag{3-189}$$

and, as just noted, $z_T{}''$ is given by equation (3-98). In addition, because the airfoil satisfies the conditions for a finite complex trailing edge pressure gradient, the value of $z_T{}''$ can be used in equation (3-27) to solve for $z_T{}'''$. By substituting a coordinate from near the trailing edge on the airfoil and the corresponding coordinate on the unit circle into equation (3-187), is possible to approximate $z_T{}^{iv}$ using the Taylor series representation truncated to fourth-order terms.

In actual applications, by comparison with exact values obtained using airfoils from the von Mises family, it was found that the most reliable values of $z_T{}^{iv}$ from the approximate method were obtained when the upper surface coordinate nearest the trailing edge was substituted into the truncated series and this result averaged with one obtained using a similar point on the lower surface. A value of R_T resulting from a $z_T{}^{iv}$ obtained in this manner, however, must be viewed with some caution. The primary difficulty is that the calculation is very sensitive to the detailed geometry of the trailing edge region. For example, while it might be expected that the shape of the

trailing edge should not be altered significantly by increasing the number of points used to generate the airfoil, it can happen that when the resolution is improved by increasing the number of points, what appeared to be a reasonable trailing edge shape is actually overlapped. While this geometrical alteration might be so slight that it is not evident in plotted results, the influence on R_T is very significant. Although better accuracy can be achieved by greatly increasing the number of points used to generate an airfoil, this is entirely un necessary with regard to the basic design problem. Thus, in light of the large number of computer runs dictated by the iterative nature of design, and because the need for higher accuracy has yet to be established, the maintenance of low-cost and minimal run time were considered more important than obtaining R_T to higher accuracy.

Finally, it should be noted that once the non-dimensional values of the trailing edge pressure gradients have been determined, they are resolved into components and denoted as C_{pST} and C_{pNT} in the output from the modified design code. The streamline flowing from the trailing edge is considered to be directed along the bisector of the trailing edge closure angle and C_{pST} is the non-dimensional pressure gradient with respect to that direction. The non-dimensional pressure gradient normal to the trailing edge streamline is given by C_{pNT}.

Influence of the Conditions for Finite Trailing Edge Pressure Gradients on Airfoils Designed Using the Eppler Method

In order to better understand the impact of the finite complex trailing edge pressure gradient conditions on the design of airfoils using the Eppler and Somers code [25], it is instructive to compare results obtained using the original code with examples generated using a version of the code which

incorporates the additional constraints. The airfoils to be considered in this comparison are only to aid in the understanding of the influence of the additional conditions on the designs generated by the code and are not necessarily intended as viable design possibilities.

The airfoil and velocity distribution shown in Figure 25 were obtained using the unmodified Eppler and Somers code. In this extreme case, none of the iteration schemes for achieving a particular trailing edge angle are implemented and the trailing edge geometry resulting from the specified input produces very steep velocity gradients in the trailing edge region, as well as a very low trailing edge velocity ratio. Using the same input design parameters in the modified version of the code, the value of $\bar{u}$ is determined by the method such that the integral constraint required for finite trailing edge pressure gradients, equation (3-113), is satisfied. As seen in Figure 26, imposing this constraint causes the flow in the recovery region and in the vicinity of the trailing edge to be modified considerably. In particular, note that the extent of the steepened gradients due to the closure contribution has been lessened and that the trailing edge velocity ratio increased significantly. This airfoil does not satisfy all of the conditions for finite trailing pressure gradients, however, in that the requirement of equation (3-116) has not been met. Next, the unmodified code is used with the same input as before, except now the value of K is iterated to achieve $K_s = K_H + \bar{K}_H = 0$. The results of this case are shown in Figure 27. Clearly the final iterated value of K has produced an airfoil very dissimilar to that obtained using the value initially specified. Last in this series of comparisons, Figure 28 presents the airfoil obtained by iterating the value of K from that used for the design of Figure 26 in order to satisfy equation (3-116). The

global influence, in particular the reduction in aft loading, which results from imposing the conditions for finite trailing edge pressure gradients should be noted.

It must be emphasized that the class of airfoils having finite trailing edge pressure gradients is a subset of the family of airfoils designable using the Eppler code. Thus, the utility of the modified method is to facilitate the determination of the appropriate parameters which allow the conditions for finite trailing edge pressure gradients to be satisfied. If after these values have been found they are input into the unmodified code, then the resulting airfoil would be the same as that generated by the modified scheme.

As the airfoils considered in the preceding examples are somewhat extreme, Figures 29 and 30 provide a comparison of designs which are more reasonable. The airfoil shown in Figure 29 is obtained using the unaltered code while that of Figure 30 is a result of the modified version. As before, the reduction in aft loading and the increase in trailing edge velocity ratio occurring in the case of the airfoil generated with the additional constraints in force should be noted.

Further appreciation of the behavior of the modified code is obtained by comparing the differences in the manner that the modified and unmodified codes are used to design symmetrical airfoils. A symmetrical profile using the original Eppler and Somers code is obtained by setting corresponding upper and lower surface design parameters equal to one another. If iteration to a particular trailing edge closure angle is desired, a mode is chosen in which the selected upper and lower surface interating parameters are incremented in a manner that maintains the equality. Because the modified code solves for the value of $\bar{u}$ that allows the additional integral constraint to be satisfied,

its value cannot be specified equal to μ. A symmetrial airfoil will result, however, if the other corresponding upper and lower surface inputs are set equal, and the iteration mode selected to satisfy equation ((3-116) iterates on μ. Fulfilling the requirement that $w''(0) = w''(2\pi)$ in this way forces μ to be equal to $\bar{\mu}$. As demonstrated, for example, by the result shown in Figure 31, this procedure yields a symmetrical airfoil having finite trailing edge pressure gradients.

CHAPTER IV

DESIGN EXAMPLES AND APPLICATIONS

To explore the characteristics and capabilities of the modified version
of the Eppler code, the usage of which is described in Appendix C, the
velocity distributions of several airfoils appearing in the literature were
adjusted as necessary and used to generate comparative airfoils having finite
trailing edge pressure gradients. The first airfoil to be considered in this
manner is the design of Strand presented in Reference [34]. The inverse
method developed by Strand, used to generate this airfoil, is a development of
Arlinger's procedure [10] which, in turn, grew out of that of Lighthill [9].
In the formulation of this procedure, the constraints imposed by the inverse
problem on the velocity distribution are satisfied by making adjustments to
the portion of the desired velocity distribution which occurs on the lower
surface of the airfoil. The differences between the desired distribution and
that achieved are minimized by making the required adjustments as small, in a
least-squares sense, as possible. The design point potential flow velocity
distribution for this airfoil, shown in Figure 32, is calculated using the
coordinates given by Strand [34] in the panel-method analysis procedure of the
Eppler and Somers code [25]. At this angle of attack, the velocity
distribution is intended to have a constant velocity rooftop followed by the
appropriate Stratford recovery. The non-smooth appearance of the points on
this calculated velocity distribution is largely a result of having an
insufficient number of coordinates to describe the airfoil. Also shown in
Figure 32 are the airfoil and velocity distribution obtained when the airfoil

is modified to have finite trailing edge pressure gradients. The two
distributions are seen to be very similar except near the trailing edge. In
fact, it was found that these aifferences could be largely eliminated by
splining in additional coordinates. A comparison of the original Strand
airfoil with the modified one is not presented as the geometrical differences
between them are almost imperceptible. In comparing the analysis results for
the two airfoils at the design angle of attack and Reynolds number of 3×10^6, a
lift coefficient of 1.32 is calculated for both airfoils. With natural
transition determined by the program, the lift-to-drag ratio of the original
airfoil at the design point is found to be 197, while that of the modified
profile is slightly better at 207.

Another example of a airfoil redesigned such that the trailing edge
pressure gradients are bounded is that shown in Figure 33. The parent airfoil
in this case is one developed by Liebeck and given the designation L1004 in
Reference [12]. It is intended that this airfoil have a fully turbulent
rooftop at the design Reynolds number of 3×10^6. Although details of the
velocity distribution and airfoil coordinates are unavailable, points taken
from the velocity distribution presented in Reference [12] are noted in Figure
33 for comparison with the distribution obtained for the modified version
having finite trailing edge pressure gradients. While the design lift
coefficients of 1.31, as calculated using the code of Eppler and Somers [25],
is slightly less than the value given of 1.35 given for the L1004 by Liebeck
[12], the calculated lift-to-drag ratio of 184 for the modified airfoil is a
slight improvement over the value of 181 for the L1004.

Another example, from the same family as the preceding airfoil, is the
Liebeck L1003, designed to have a fully laminar rooftop at a Reynolds number

of 2×10^6. As evident in Figure 34, the redesigned velocity distribution is close to that plotted in Reference [12]. In this case, however, even after fixing transition at the appropriate location, the Eppler and Somers analysis indicates that the entire recovery region is separated. As noted by Liebeck [34], obtaining an unseparated recovery for this section is extremely dependent upon having particular flow conditions at the beginning of the pressure rise. Thus, it is likely that the separation problems result because of small differences in the flow conditions between the two airfoils at the initiation of recovery.

In addition to resulting in abrupt stalling behavior, the use of a Stratford pressure recovery for practical airfoils is often criticized in that, with regard to the normal flowfield variations that occur in realistic applications, the attainment of the precise flow conditions required at the beginning of the pressure rise cannot be assured. Consequently, the consideration of designs incorporating Stratford distributions is often of an academic nature, as is the case of studies directed toward exploring ultimate possibilities in airfoil performance. Thus, an example of a more practical candidate for adaptation to an airfoil having finite trailing edge pressure gradients is provided by the well-proven and documented Wortmann FX 67-K-150, Reference [36]. The actual airfoil considered here, shown in Figure 35, is defined by the aerodynamically smoothed coordinates given by Somers [37]. Although this section is optimized for use with flaps, only the configuration having a neutral flap setting will be treated. The lack of steep gradients near the trailing edge in the velocity distribution examples considered up to now has permitted the conditions for a finite complex trailing edge pressure gradient to be applied to the existing designs with only minor alterations

necessary. Hence, the goal has been to obtain an airfoil with bounded trailing edge pressure gradients that has a velocity distribution as close as possible to that of the parent section. The Wortmann section, however, is unlike those already considered in that, due to the significant differential between velocities on the upper and lower surfaces near the trailing edge, a steep adverse pressure gradient is present over the aft portion of the velocity distribution. Consequently, the concern in this case is to obtain an airfoil with finite trailing edge pressure gradients which, although having a somewhat altered velocity distribution, embodies the same design philosophy and achieves comparable performance. With this in mind, consider the result shown in Figure 37 and note that the use of the modified code has changed the velocity distribution such that the upper surface aft loading present on the Wortmann section, causing the steep adverse pressure gradient near the trailing edge, has been eliminated. It should be pointed out that there is a drag penalty associated with the steep lower surface favorable pressure gradient that is a result of the closure contribution on the newly designed airfoil. While it was found that the drag could be reduced considerably by beginning the lower surface closure contribution sooner, and thereby lessen the gradient, the distribution shown was retained as it is more like that of the Wortmann section. In addition, in order to control separation problems that were introduced by the velocity distribution changes at the trailing edge, some modifications were made to the shape of the upper surface recovery distribution. Although the elimination of the upper surface aft loading results in a loss of lift as calculated by potential flow methods, this is more than offset by the increased value of V_{TE}/U which allows the lower surface to carry a greater amount of aft loading. A comparison of the overall

aerodynamic performance of the two airfoils is provided by the viscous analysis results obtained using the Eppler and Somers code and presented in Figures 36 and 38. The finite trailing edge pressure gradients airfoil has been designed such that the maximum lift-to-drag ratio occurs near the design angle of attack dictated by equation (3-111). Both airfoils exhibit best lift-to-drag ratios at a lift coefficient near unity. A more detailed comparison reveals that the drag polars of the new profile are roughly equivalent to those of the original section over most of the usable performance range; however, the performance of the section generated with the modified code is extended considerably in the direction of higher lift coefficients.

While the imaginary part of the condition necessary for an airfoil to have finite trailing edge pressure gradients can only be satisfied at a single angle of attack, as equation (3-27) reveals, the results of the Eppler and Somers code viscous analysis of such airfoils indicates nothing particularly special about the aerodynamic characteristics at that angle of attack. This fact, however, should be to some degree expected in that the analysis makes use of conventional boundary layer theory in which normal pressure gradients through the boundary layer, as well as all wake influences, are assumed to be unimportant. As has been discussed, this assumption breaks down near the trailing edge where the inviscid pressure gradients are generally unbounded. It should be no surprise, then, that the results of a calculation based on conventional boundary layer theory do not indicate any characteristics attributable to the presence of finite trailing edge pressure gradients. Thus, a thorough evaluation of the effect of such factors on airfoil performance would require a fairly extensive investigation that makes use of a

theoretical model having a more detailed description of the flow in the
vicinity of the trailing edge. To demonstrate what such a model might
indicate, consider the application of the GRUMFOIL code [21] to the two
airfoils just presented. The results of this analysis for the FX 67-K-150 are
given in Figures 39-41, and those for the corresponding finite trailing edge
pressure gradient airfoil in Figures 42-44. The analysis of the latter
section was performed at its design angle of attack and that of the Wortmann
at an angle of attack which resulted in the lift coefficients matching. The
Reynolds number used was $2x10^6$ and the Mach number was set to zero. The
aerodynamic characteristics calculated using GRUMFOIL are somewhat different
from those obtained with the Eppler and Somers code. In general, the lift
coefficients calculated by GRUMFOIL are slightly greater than those of the
Eppler and Somers code, while the drag coefficients, even though transition
predictions agree fairly well, are notably less.

The fully viscous GRUMFOIL pressure distributions for the two airfoils
are given in Figure 39 and 42. In considering the viscous pressure
distribution for the Wortmann section, Figure 39, the pressure spike near the
leading edge which is not present in the Eppler and Somers potential flow
results warrants explanation. Based on distributions obtained at lower angles
of attack, it was concluded that the peak is due to a lack of smoothness in
one of the coordinates rather than from the angle of attack under
consideration being too large. It has been found that only a very small
inconsistency in the given coordinates can be responsible for such a result.
In further considering the viscous pressure distribution of the Wortmann
design, it should be observed that the steep upper surface gradients near the
trailing edge present in the potential flow results are largely elimi ed by

the smoothing action of viscous influences. As seen in Figure 42 for the airfoil having finite trailing edge pressure gradients, on the other hand, the inviscid calculations are little impacted by the inclusion of viscid-inviscid iterations.

Further differences in the trailing edge region flow behavior are well demonstrated by comparing the boundary layer characteristics of the two airfoils. In the case of the Wortmann profile, Figures 40 and 41 readily demonstrate the singular behavior at the trailing edge of the displacement thickness, form factor, and the equivalent surface source velocity. It should be noted that these results conform very well to those found experimentally, such as in the work of Preston, et. al., [29]-[31]. In remarkable contrast, as seen in Figures 43 and 44, the slope discontinuities are eliminated for the airfoil with bounded trailing edge pressure gradients. The ramifications of these results are significant. In addition to any performance benefits arising from smooth flow off the airfoil and into the wake, the application of the condition for finite trailing edge pressure gradients has produced a class of airfoils for which the strong viscid-inviscid interactions, beyond that of the displacement thickness, can be neglected. That is, convenal boundary layer theory remains valid in the region of the trailing e uch airfoils and is sufficient for the prediction of their aerud/ characteristics. Furthermore, as the influences due to viscos!'v minimized, the results calculated using potential flow design should be more reliable than those generally obtained.

Because the imaginary part of the condition required for achieving finite trailing edge pressure gradients can only be satisfied at a single angle of attack, equation (3-27), it is of interest to examine the importance of this

limitation by considering the off-design boundary layer behavior as calculated

using GRUMFOIL. First, however, it should be noted that because of

differences in the zero-lift angle of attack prediction, it is likely that the

correspondence between the angles of attack calculated by the Eppler and

Somers code and those used in GRUMFOIL is not exact. Thus, in all

probability, the case already presented represents a slightly off-design

situation. In any event, to further consider the flowfield behavior off-

design, Figures 45 to 47 summarize the GRUMFOIL output for the Wortmann based

finite trailing edge pressure gradients airfoil at an angle of attack of

approximately four degrees less than the design value. From these results, it

is apparent that strong singular boundary layer characteristics at the

trailing edge do not dramatically appear when the airfoil is operated at

conditions other than those of the design point. It is evident from Figure

45, however, that the streamwise change of pressure along the wake centerline

in the vicinity of the trailing edge, and consequently its effect on the

inviscid flow, has increased over than seen in Figure 42. In addition,

although certainly not discontinuous, the slopes in the immediate vicinity of

the trailing edge on the boundary layer property distributions do appear

slightly steeper than those present at the design angle of attack. Although

additional verification is warranted, on the basis of these off-design

GRUMFOIL results, it can be concluded that if any aerodynamic benefits are

realized by the presence of finite trailing edge pressure gradients, then

these benefits are not limited to the design angle of attack but are present

to some extent over an operational range of angles. Thus, in addition to

being of academic interest, this allows airfoils designed with finite trailing

edge pressure gradients to merit consideration for practical application.

CHAPTER V

CONCLUDING REMARKS

The potential flow solution for any airfoil having non-zero trailing edge
loading is characterized by the presence of unbounded pressure gradients at
the trailing edge. Although in a real fluid the pressure gradients are
somewhat softened by viscous effects, those in the trailing edge region do
indeed become extremely steep resulting in, among other things, the slope of
the displacement thickness distribution being discontinuous at the trailing
edge. Considering the near critical nature of many of the velocity
distributions prescribed for maximum lift or minimum drag, the encounter of
such a disturbance could be sufficient to cause severe upstream separation
problems. Thus, the goal of separation free flow should benefit by the
removal of this disturbance to allow the fluid on the airfoil to flow into the
wake as smoothly as possible. Of additional concern in this regard, the
presence of strong adverse pressure gradients in the vicinity of the trailing
edge, as seen in many maximum performance design efforts, may result in
upstream separation problems. Thus, to help ensure that the high performance
levels promised by potential flow methods are realized in practice, a
procedure has been developed to design airfoils for which the trailing edge
pressure gradients are finite and the flows on the upper and lower surfaces
approach the trailing edge free of strong adverse pressure gradients.

The ability to specifically configure the trailing edge region of an
airfoil to achieve finite pressure gradients has been made possible by the
unique capability of the Eppler method which allows different segments of an

airfoil to be designed for different angles of attack. As the removal of the trailing edge pressure gradient singularities requires that no load be carried by the trailing edge, the method is able to adapt the aft portions of the airfoil such that this no-load requirement is met. To some extent, the resulting airfoil can be thought of as one in which the trailing edge region behaves locally like a flat plate at zero angle of attack although, in the flat plate case, the gradients are not only finite but zero. By eliminating the unbounded trailing edge pressure gradients, it is possible to specify a velocity distribution on an airfoil which pushes boundary layer performance to its critical limits as is the case, for example, in specifying a Stratford recovery, or in choosing a distribution for which the trailing edge velocity ratio is maximized.

In the formulation of conventional boundary layer theory, normal pressure gradients through the boundary layer are ignored and only the influence of the displacement thickness on the inviscid results is considered. Thus, because of the unbounded pressure gradients that generally occur at the trailing edge in the potential flow solution, conventional boundary layer theory is invalid in the vicinity of the trailing edge. In regard to this limitation, Melnik, et. al. [33] demonstrated that the potential flow solution singularities give rise to additional viscid-inviscid interactions, each having an effect as important as that of the displacement thickness. Thus, by allowing for the influences caused by the normal pressure gradients in the trailing edge region, wake thickness, and wake curvature, Melnik and his coworkers developed a self-consistent boundary layer theory able to account for the strong viscous interactions due to the singularities in the inviscid flow solution. Although the formulation is distinctly different, the removal of the trailing edge

singularities can be considered an alternative approach to the same problem. In this light, airfoils having finite trailing edge pressure gradients represent a class for which the strong viscid-inviscid interactions in the trailing edge region have been minimized. Consequently, conventional boundary layer theory is sufficient for the viscous analysis of such airfoils. Furthermore, because the corrections necessary to the inviscid solution due to viscous effects are minimal, potential flow design methods are likely to yield more reliable results than they otherwise would.

Considering the nature of the flow behavior in the region of the trailing edge, airfoils designed to have finite trailing edge pressure gradients may be ideally suited to aid in the development and calibration of improved aerodynamic prediction methods for airfoils. For example, in the theoretical formulation used in the GRUMFOIL code [33], the local trailing edge region is modeled as unseparated flow over a flat plate at angle of attack. Thus, the class of airfoils having bounded pressure gradients at the trailing edge are much more consistent with this model than is generally the case. Such airfoils should, therefore, provide useful development tools and calibration cases. In a similar application, because the rapid growth of the displacement thickness at the trailing edge that generally occurs leads to numerical divergence problems, the development of viscous analysis methods in which potential flow-boundary layer iteration is employed should benefit from the well-behaved growth in displacement thickness at the trailing edge on airfoils having finite trailing edge pressure gradients.

Finally, if imposing the requirement for finite trailing edge pressure gradients does indeed minimize the viscous interactions and allow potential flow predictions to be more fully realized, then this situation clearly

suggests that an improvement in airfoil performance is possible. In the examples that were considered, the design effort was directed at matching the characteristics of previously defined velocity distributions. Consequently, it remains to explore the potential of exploiting the use of finite trailing edge pressure gradients to enhance airfoil aerodynamics. Encouragement that gains might be made, however, is provided by the results of the GRUMFOIL analysis from which, for example, the employment of the finite trailing edge pressure gradients condition yields an airfoil having a thinner displacement thickness and wake than otherwise occurs. If such performance benefits are indeed found to exist then, as the GRUMFOIL results indicate that reasonable off-design capability is present, airfoils having finite trailing edge pressure gradients become candidates for practical application.

APPENDIX A

LIMITING COEFFICIENT VALUES OF THE GENERAL TRANSFORMATION

FOR MAPPING A CIRCLE TO AN AIRFOIL

Consider the general transformation which maps a circle centered at the origin of the ζ-plane into an airfoil in the z-plane as given by

$$z = \zeta + \sum_{n=1}^{\infty} \frac{c_n}{\zeta^n} \tag{A-1}$$

where $c_n = a_n + ib_n$. In this transformation, depicted in Figure 48, it is assumed that $|\zeta| \geqslant r$ and $r \geqslant 1$. Given that the origin of the z-plane lies within the profile, the area enclosed by the boundary of the airfoil is

$$A = \frac{1}{2} \int_c R^2 d\theta = \frac{1}{2} \int_0^{2\pi} R^2 \frac{\partial \theta}{\partial \phi} d\phi \tag{A-2}$$

and, from the Cauchy-Riemann equations,

$$\frac{\partial \theta}{\partial \phi} = \frac{r}{R} \frac{\partial R}{\partial r} \tag{A-3}$$

Substitution of equation (A-3) into (A-2) yields

$$A = \frac{r}{2} \int_0^{2\pi} R \frac{\partial R}{\partial r} d\phi = \frac{r}{4} \frac{\partial}{\partial r} \left\{ \int_0^{2\pi} R^2 d\phi \right\}$$

$$= \frac{r}{4} \frac{\partial}{\partial r} \left\{ \int_0^{2\pi} |z(re^{i\phi})|^2 d\phi \right\} \tag{A-4}$$

Noting that

$$z(re^{i\phi}) = re^{i\phi} + \sum_{n=1}^{\infty} \frac{c_n}{r^n e^{in\phi}} \tag{A-5}$$

$$\overline{z(re^{i\phi})} = re^{-i\phi} + \sum_{n=1}^{\infty} \frac{\overline{c_n}}{r^n e^{-in\phi}} \tag{A-6}$$

the integral in equation (A-4) yields

$$\int_0^{2\pi} |z(re^{i\phi})|^2 \, d\phi = \int_0^{2\pi} z(re^{i\phi}) \, \overline{z(re^{i\phi})} \, d\phi$$

$$= \int_0^{2\pi} \left[re^{i\phi} + \sum_{n=1}^{\infty} \frac{c_n}{r^n e^{in\phi}} \right] \left[re^{-i\phi} + \sum_{n=1}^{\infty} \frac{\overline{c_n}}{r^n e^{-in\phi}} \right] d\phi$$

$$= 2\pi \left[r^2 + \sum_{n=1}^{\infty} \frac{|c_n|^2}{r^{2n}} \right] \tag{A-7}$$

Thus, equation (A-4) becomes

$$A = \frac{\pi r}{2} \frac{\partial}{\partial r} \left[r^2 + \sum_{n=1}^{\infty} \frac{|c_n|^2}{r^{2n}} \right] = \frac{\pi r}{2} \left[2r - \sum_{n=1}^{\infty} \frac{2n|c_n|^2}{r^{2n+1}} \right]$$

which can be rearranged to give

$$\frac{A}{\pi} = r^2 - \sum_{n=1}^{\infty} \frac{n|c_n|^2}{r^{2n}} \tag{A-8}$$

Since the area of the airfoil cannot be negative, it follows that

$$r^2 > \sum_{n=1}^{\infty} \frac{n|c_n|^2}{r^{2n}} \qquad (A-9)$$

As the expression is valid for all values of r between one and infinity, it must hold for r equal to one. Thus,

$$\sum_{n=1}^{\infty} n|c_n|^2 = \sum_{n=1}^{\infty} n(a_n^2 + b_n^2) < 1 \qquad (A-10)$$

An immediate consequence of this result is that

$$|c_1| = (a_1^2 + b_1^2)^{1/2} < 1 \qquad (A-11)$$

To examine these results further, consider the case for which the equality in equation (A-11) holds, i.e., when $|c_1|$ is unity. Observe from equation (A-10), that for this to be true all of the other transformation coefficients must be zero. Thus, for this case, the transformation becomes

$$z = \zeta + \frac{c_1}{\zeta} \qquad (A-12)$$

where $|c_1| = 1$. Writing the transformation coefficient as

$$c_1 = e^{2i\gamma}$$

where $0 < \gamma < 2\pi$, the mapping function becomes

$$z(\zeta) = \zeta + \frac{e^{2i\gamma}}{\zeta} \qquad (A-13)$$

For the case of mapping the unit circle, this gives

$$z(e^{i\phi}) = e^{i\phi} + e^{2i\gamma}e^{-i\phi} = e^{i\gamma}[e^{i\phi}e^{-i\gamma} + e^{-i\phi}e^{+i\gamma}]$$

$$= e^{i\gamma}[e^{i(\phi-\gamma)} + e^{i(-\phi+\gamma)}] = e^{i\gamma}[2\cos(\phi-\gamma)]$$

$$= 2e^{i\gamma}\cos(\phi-\gamma) \qquad\qquad (A-14)$$

Hence, as shown in Figure 49, if ζ describes the unit circle chen its conformal image, z, describes both sides of a flat plate oriented to the positive real axis at the angle γ. Thus, $|c_1|$ can be equal to unity only for functions mapping the unit circle to a flat plate. Note that without loss of generality, the trailing edge of the profile generated can be assumed to be located on the real axis. For the example given, this results in the orientation of the flat plate being along the real axis with $\gamma = 0$. Thus, a_1 is unity and all the other a_n's and b_n's must be zero. This case is equivalent to that of the Joukowsky flat plate at zero angle of attack.

To examine the relationship of the transformation coefficients to the maximum possible trailing edge velocity, VTE, consider the expression for the trailing edge velocity for an airfoil obtained from a mapping of the unit circle as given by

$$VTE = \frac{2U \cos\alpha}{|z_T''|} \qquad\qquad (A-15)$$

where, for the case of the trailing edge fixed on the real axis,

$$|z_T{''}| = \left[\left(\sum_{n=1}^{\infty} n(n+1)a_n\right)^2 + \left(\sum_{n=1}^{\infty} n(n+1)b_n\right)^2\right]^{1/2} \qquad \text{(A-16)}$$

Clearly, the maximum value of VTE/U is obtained when $|z_T{''}|$ is minimized. This occurs when the second term on the right is zero as accomplished when all of the b_n's are zero. Although there are non-zero values of the b_n's which can achieve the same result, there are none which can result in a higher value of VTE/U. Consequently, the symmetrical airfoil that results when the b_n's are zero has a trailing edge velocity ratio which is at least as great as any non-symmetrical airfoil generated using the same set of a_n's.

APPENDIX B

COEFFICIENTS OF THE INEQUALITY EXPRESSION FOR POSITIVE THICKNESS

The expression which is developed to insure that physically realizable airfoils will result from a six term von Mises transformation, equation (2-58), is

$$Af^4 + Bf^3 + Cf^2 + Df + E > 0 \qquad (B-1)$$

the coefficients terms for this expression are given by

$$A = 16r^4(r-1)^5 \qquad (B-2)$$

$$B = 8r^3[5(r-1)^4 - a_1(r-1)^4 + a_2(r-1)^3 - a_3(r-1)^2$$

$$+ a_4(r-1) - a_5] \qquad (B-3)$$

$$C = 4r^2[(10 - 4a_1 - 2a_2)(r-1)^3 + (3a_2 + 3a_3 + a_3r)(r-1)^2$$

$$- (2a_3 + 4a_4 + 2a_4r)(r-1) + (a_4 + 5a_5 + 3a_5r)] \qquad (B-4)$$

$$D = 2r[(10 - 6a_1 - 6a_2 - 3a_3)(r-1)^2 + (3a_2 + 6a_3 + 6a_4$$

$$+ 2a_3r + 4a_4r)(r-1) - (a_3 + 4a_4 + 10a_5 + 2a_4r$$

$$+ 10a_5r + a_5r^2)] \qquad (B-5)$$

$$E = \left(5 - 4a_1 - 6a_2 - 6a_3 - 4a_4\right)\left(r-1\right) + \left(a_2 + 3a_3\right.$$

$$\left. + 6a_4 + 10a_5 + a_3 r + 4a_4 r + 10a_5 r\right) \tag{B-6}$$

APPENDIX C

USAGE OF THE EPPLER CODE INCORPORATING THE CONDITIONS FOR FINITE TRAILING

EDGE PRESSURE GRADIENTS AND LISTING OF PROGRAM MODIFICATIONS

In making modifications to the Eppler and Somers code [25] in order to
facilitate the design of airfoils having finite trailing edge pressure
gradients, the effort was made to leave as much of the existing code and its
data input as unchanged as possible. Thus, the discussion included in this
appendix should be considered in conjunction with the code description and
operating instructions presented in Reference [25].

While the primary purpose of the modified code is the design of airfoils
having finite trailing edge pressure gradients, it might also be of use in the
design of airfoils in which the upper and lower velocity distributions merge
smoothly at the trailing edge without the nearby presence of steep gradients.
In either case, the integral constraint of equation (3-113) is satisfied.
Because this condition eliminates the pressure loading at the trailing edge,
the shape of the aft portion the airfoil is largely governed by the zero
closure angle which results. Thus, although control remains over the extent
that this zero closure angle is allowed to influence the overall shape of the
rear of the profile, much of the ability to iterate to a desired closure angle
that is present in the original code is lost.

With reference to Eppler and Somers [25], the input to the modified code
differs from that of the original as follows:

1. On the TRA1 card, although assumed internally by the modified code,
    α_{I_p} should be set equal to α_1 as required by equation (3-132).

2. The value of $\bar{\mu}$ is no longer specified by the F_{10} word on the TRA2 card, but determined by the program such that the fourth integral constraint is satisfied. In its place, however, the quantity IWPPM is designated to select the mode of iteration used to achieve the requirement that $P''(0) = P''(2\pi)$, equation (3-116). The iteration mode possibilities are as follows:

IWPPM = 0   –   No iteration is performed and $P''(0)$ will, in general, not be equal to $P''(\cdot\cdot)$.

IWPPM = 1   –   K is replaced by $K + \Delta K$

IWPPM = 2   – $\bar{K}$ is replaced by $\bar{K} + \Delta K$

IWPPM = 3   – μ is replaced by $\mu + \Delta\mu$

IWPPM = 4   – $\vec{\lambda}^*$ is replaced by $\vec{\lambda}^* + \Delta\lambda$, unless that result is calculated to be less than zero or greater than $\bar{\lambda}$. In that case, the program switches to IWPPM = 1.

3. Also on the TRA2 card, $F_8 = RMS_{1s}$, which determines the interpretation of F_9 and F_{10}, must be set to zero. Consequently, .1 F_9 is always interpreted as $\bar{K}$.

4. While still active in the code, it should be noted that the specification of ITMOD equal to 5 or 6, F_{11} on the TRA2 card, will generally not result in convergence to the specified value of K_s. This is because in these modes, $\bar{K}$ is iterated and the calculated iteration increment, $\Delta\bar{K}$, is superseded by the code determination of $\bar{\mu}$ which, in turn, alters the value of $\bar{K}$.

A sample input set for the modified code is presented in Figure 50. The result of this input is the airfoil having finite trailing edge pressure gradients shown in Figure 37.

It should be noted that that it is not intended that the modified code be run with ITMOD ≠ 0 and IWPPM ≠ 0 simultaneously. The design of airfoils having finite trailing edge pressure gradients is carried out with ITMOD = 0 and IWPPM ≠ 0. The design of airfoils in which it is only desired that velocity distribution be free of steep adverse gradients in the vicinity of the trailing edge can be accomplished with ITMOD ≠ 0 and IWPPM = 0. In designing airfoils having finite pressure gradients, it is sometimes advantageous to begin the process with one of the ITMOD modes and switching to one of the IWPPM options when close to the desired velocity distribution. For example, a symmetrical airfoil can be obtained by first setting ITMOD = 6 or 9, IWPPM = 0, and specifying the additional inputs as described '· Eppler and Somers [25] such that the upper and lower surface velocity distribution specification quantities are equivalent. In the case of using the modified code, however, the program will solve for a value of $\bar{\mu}$ which is different from that specified for μ. Now, inputting the results from this run and changing to ITMOD = 0 and IWPPM = 3, μ will be iterated until it agrees with $\bar{\mu}$ and a symmetrical profile having finite trailing edge pressure gradients will result.

A listing of the modifications made to the Eppler and Somers code [25] will follow. Only the main program and modified subroutines, in addition to several newly added subroutines, will be presented. The reader is again referred to Reference [25] for a listing of the original code.

```
      PROGRAM EPPLER3 (INPUT,OUTPUT,TAPE4,TAPE5=INPUT,TAPE6=OUTPUT)
      DIMENSION XF(121),YF(121),BETAF(121)
      DIMENSION AM(7,7),AV(7)
      DIMENSION V(14),MARKEN(20),ALCA(14),CAE(2)
      DIMENSION RE(5),MA(5),MU(5),T(42)
      DIMENSION TM(5),ALS(5),RER(5),MUR(5)
      DIMENSION TST(5),BANT(5),CW(5,2,14),SU(5,2,14),SA(5,2,14)
      COMMON P1(121),P(121),XP(121),YP(121),PUFF(14),AGAM(14),X(121),
     1Y(121),DS(122),VF(121),ARG(121),ANI(28),ALFA(29),IZZ,KFU,NQ,NUPRO,
     2JAB,JST,CM,ETA,ABFA,PI,BOGEN,DARG,PURES(13),FUW(60,7),RS(60)
      COMMON XTF,SMA,XFL(10),GAMMA(121,2),AMAT(120,120)
      COMMON /GRZK/CDK,AA(7),BB(7)
      COMMON/PRAL/DLT,DLTU,ALN,ALV(14),NAL,ITP,NAMP(12),CML(14),CRL(14)
     1 ,CPV(2),ALTX(4,2),DARF,ITIT1,ITIT2
      COMMON/PLTM/MPL,MGC,XZEH,YZEH,MSPLI
      COMMON/EA/ILES,IDRU,ISTA,NNESE
      COMMON/TRIT/DLV,SUMP,XTRI(4),NU,ND
      COMMON /LINING/BROKL(12),NLINE(5),NPAR(5),JNEW
      EQUIVALENCE(XF(1),FUW(1,1)),(YF(1),FUW(3,3)),(BETAF(1),FUW(5,5))
      EQUIVALENCE (CW(1,1,1),P1(1)),(SA(1,1,1),P(20)),
     1 (SU(1,1,1),XP(39))
      DATA ILES,IDRU,ISTA,NNESE/5,6,4,1H1/
      DATA MARKEN/4HTRA1,4HTRA2,4HALFA,4HAGAM,4HABSZ,4HSTRK,4HENDE,
     14HDIAG,4HRE  ,4HSTRD,4HFLZW,4HPLWA,4HPLW ,4HTRF ,4HAPPR,4HCDCL,
     24HPAN ,4HFXPR,4HFLAP,4HPUXY/
      DATA CPV/9HVELOCITY ,9HPRESSURE /,ALTX/4H ZER,4HO-LI,4HFT L,
     *4HINE ,4H CHO,4HRD L,4HINE ,4H    /,KBLT/1H /
      DATA MGC,ISTIFT,MXZ,CDK/0,1,-1,.01/
      DATA ZAEH,DICHTE/13.6E-6,.12533/
      MPL=0
      PI = 3.141592654
      BOGEN = 0.0174532925199
      ABFA = 1.0
      AGAM(2)=1.
      AGAM(3)=1.
      AGAM(6)=1.
      AGAM(8)=0.
      AGAM(10)=1.
    9 MTR=0
   11 READ(ILES,2)MARKE,NUPA,NUPE,NUPI,NUPU,PUFF
    2 FORMAT(A4,3I1,I3,14F5.2)
      DO 12 I=1,20
      IF (MARKE.EQ.MARKEN(I)) GO TO 13
   12 CONTINUE
   14 WRITE(IDRU,3) MARKE
    3 FORMAT (11H INCORRECT ,A4,5H CARD)
      GO TO 11
C   TRA1TRA2ALFAAGAMABSZSTRKENDEDIAGRE  STRDFLZWPLWAPLW TRF APPRCDCL
C   PAN FXPRFLAPPUXY
   13 GO TO(15,22,333,14,142,90,150,104,30,112,30,71,60,14,14,160,
     *170,180,190,106),I
```

```
C    TRA1 CARD
   15 NUPRO=NUPU+1000*NUPI
      IF(MTR.EQ.0)JST=0
      I=0
   18 I=I+1
      ANRI=RUND(PUFF(I)*ABFA,1000.)
      IF(ANRI.NE.0.)GO TO 20
      IF(JST.NE.0)GO TO 21
      JST=MTR+1
   20 MTR=MTR+1
      ANI(MTR)=ANRI
      I=I+1
      ALFA(MTR)=PUFF(I)
      IF(I.NE.14)GO TO 18
   21 JAB=MTR
      GOTO 11
C    TRA2 CARD
   22 DO 23 I=1,13
   23 PURES(I)=RUND(PUFF(I),1000.)
      MSPLI=0
      ITP=0
      IZZ=INT(PUFF(14))
      CALL TRAPRO
      XDA=0.
      YDA=0.
      DEFLG=0.
      GO TO 9
C    RE   CARD
   25 IF(PUFF(2).EQ.0.) GO TO 28
      DO 27 J=1,5
      RERX= PUFF(2*J)
      IF(RERX.EQ.0.)GO TO 26
      RE(J)=1.E5*RERX
      IPU = INT(PUFF(2*J-1))
      MA(J) = IPU/100
      MU(J) = IPU/10 - 10*MA(J)
   27 JR  = J
   26 DO 29 J=1,4
   29 XTRI(J)=PUFF(J+10)*.01
   28 CALL GRP(NAL,RE,MU,JR,ISTIFT)
      MSPLI=0
      JP=JR
      GOTO 11
C    FLZW CARD
   30 IF(NUPA.EQ.0) GO TO 31
      AGAM(6)=FLOAT(NUPE)
      AGAM(8)=FLOAT(NUPI)
   31 IF(I.EQ.9) GO TO 25
      IF(PUFF(2).EQ.0.) GO TO 36
      GDF = PUFF(1)
      VMAX = PUFF(2)
      IF(PUFF(3).NE.0.) DICHTE = .1*PUFF(3)/9.806
```

```
      IF(PUFF(4).NE.0.)ZAEH = PUFF(4)*1.E-6
      IF(PUFF(5).EQ.0.) GO TO 50
      D = 0.
      DO 34 J = 1,5
      JZ = 2*J + 3
      IF(PUFF(JZ).EQ.0.) GO TO 36
      TM(J)=PUFF(JZ)
      ALS(J)=PUFF(JZ+1)
      MUR(J) = NUPU
   34 JT = J
   36 IZT=NZPZ(2,6*NAL+2)
      JP=JT
      WRITE(IDRU,37)IZT,NAMP,(ALTX(J,ITIT2),J=1,4)
   37 FORMAT (A1,36HAIRCRAFT-ORIENTED SUMMARY   AIRFOIL ,12A1,3X,
     *31HANGLE OF ATTACK RELATIVE TO THE,4A4)
      IVMAX=INT(VMAX*3.6)+1
      IZT=NZPZ(2,0)
      WRITE(IDRU,38)IZT,GDF,IVMAX,DICHTE,ZAEH
   38 FORMAT (A1,6H W/S =,F6.2,8H KG/SQ.M,3X,7HV MAX =,I4,5H KM/H,3X,
     *5HRHO =,F5.3,13H KG*S E2/M E4,3X,4HNU =,F10.8,7H SQ.M/S)
      IZT=NZPZ(2,0)
      WRITE(IDRU,40)IZT,(KBLT,TM(J),ALS(J),J=1,JT)
   40 FORMAT (A1,5X,5(A1,4X,3HC =,F5.2,8H THETA =,F5.2))
   41 V1 = SQRT(2.*GDF/DICHTE)
      DO 48 I=1,NAL
      IVS = -I
      DO 46 J = 1,JT
      IF(ALV(I)-ALS(J))42,44,42
   42 VALF = V1/SQRT(.11*ABS(ALV(I)-ALS(J)))
      IF(VALF - VMAX)46,46,44
   44 VALF = VMAX
   46 RER(J) = VALF*TM(J)/ZAEH
   48 CALL GRP(IVS,RER,MUR,JT,ISTIFT)
      MSPLI=0
   49 IF(D)72,50,72
   50 GO TO 11
C     PLW  CARD
   60 IF(PUFF(1))62,68,62
   62 DST = PUFF(1)*.01
      GST = PUFF(2)
      DGF = PUFF(3)
      CWSF = PUFF(4)*.001
      DO 66 J = 1,5
      JZ = 2*J+3
      IF(PUFF(JZ))64,68,64
   64 TST(J) = PUFF(JZ)
      BANT(J) = PUFF(JZ+1)
      MUR(J) = NUPU
   66 JT = J
   68 BF = 0.
      FST = 0.
      NF = 0
```

```
      CALL DIA(X,Y,NQ,D)
      IF(DST.LT.0.) DST = D
      DO 70 J = 1,JT
      TM(J) = TST(J)*DST/D
      ALS(J) = 0.
      BF = BF + BANT(J)
70 FST = FST + BANT(J)*TST(J)
      FF = FST*DST/D
      GEW = GST + (FF-FST)*DGF
      GDF = GEW/FF
      GO TO 36
C   PLWA CARD
71 NAN = NUPU
      CWSFU=CWSF
      FAU = FF
      GAU = GEW
      DO 88 NF = 1,NAN
      FF = FF+PUFF(1)
      GEW = GEW+PUFF(2)
      CWSF=CWSF+.001*PUFF(3)
      V1 = SQRT(2.*GEW/(DICHTE*FF))
72 IZT=NZPZ(3,NAL+10)
      WRITE(IDRU,74)IZT,NAMP
74 FORMAT (A1,25HAIRCRAFT POLAR   AIRFOIL ,12A1)
      CWS = CWSF/FF
      IZT=NZPZ(2,0)
      WRITE(IDRU,76)IZT
76 FORMAT (A1,39H  B(M)   S(SQ.M) S*(SQ.M) W(KG)    W*(KG),
     *3X,3HT/C,3X,6H(T/C)*,2X,8HAP(SQ.M),2X,3HCDP)
      IZT=NZPZ(1,0)
      WRITE(IDRU,78)IZT,BF,FF,FST,GEW,GST,D,DST,CWSF,CWS
78 FORMAT (A1,F6.2,2F8.2,2F8.0,4F8.4)
      IZT=NZPZ(2,0)
      WRITE(IDRU,80)IZT
80 FORMAT (A1,54H ALPHA      CL      CDP     CDT   V(KM/H)  VS(M/S)   L
     */D)
      DO 84 I = 1,NAL
      CA = 0.
      CWP = 0.
      DO 82 J = 1,JT
      BATF=BANT(J)*TST(J)/FST
      CALL VISC(I.J,CANT,CWNT,CMDU)
      CA=CA+CANT*BATF
82 CWP=CWP+CWNT*BATF
      CWGES = CWP + CWS + 1.03*CA*CA*FF/(PI*BF*BF)
      IF(ABS(CA).LT..01)CA=.01
      VKMH = 3.6*V1/SQRT(ABS(CA))
      VS = VKMH*CWGES/(3.6*ABS(CA))
      GLTZ = CA/CWGES
      IZT=NZPZ(1,0)
84 WRITE(IDRU,86) IZT,ALV(I),CA,CWP,CWGES,VKMH,VS,GLTZ
86 FORMAT (A1,F6.2,F8.3,2F8.4,F8.1,F9.3,F8.2)
```

```
         IF(NF.EQ.0) GO TO 50
     88 CONTINUE
         CWSF = CWSFU
         FF=FAU
         GEW = GAU
         GO TO 50
C    STRK CARD
     90 IF(NUPU)94,100,92
     92 NT = 0
     94 DO 98 J = 1,14
         IF(PUFF(J)) 96,100,96
     96 NT = NT + 1
     98 T(NT) = PUFF(J)*10.
         IF(IABS(NUPU).GT.14) GO TO 11
    100 CALL STRDR(T,NT)
         IF(NUPI.NE.0) GO TO 11
         DO 102 I = 1,NT
    102 CALL STRAAK(T(I),RUA,YBL,MXZ,ISTIFT)
         GO TO 11
C    DIAG CARD
    104 CALL DIAGR(ISTIFT,NUPU,NUPI)
         GO TO 11
C    PUXY CARD
    106 CALL PUDECK
         GO TO 11
C    STRD CARD
    112 IF(NUPU.NE.0) MXZ = NUPU
         IF(PUFF(1).NE.0.) YBL = 100.*PUFF(1)
         IF(PUFF(2).NE.0.) RUA = 100.*PUFF(2)
         GO TO 11
C    ABSZ CARD
    142 IF(NUPA.NE.0) AGAM(3)=FLOAT(NUPE)
         IF(PUFF(2).NE.0.) ABFA=PUFF(2)
         GO TO 11
C    ENDE CARD
    150 IF(MGC.NE.0) CALL GCLOSE
         IF(MPL.NE.0)CALL FINISH
         STOP
C    CDCL CARD
    160 IF(NUPA.EQ.0)GO TO 166
         BL1=PUFF(1)+.005
         BL2=PUFF(2)+.005
         DO 162 K=1,5
         NLINE(K)=INT(BL1*(10.**(K-3)))-10*INT(BL1*(10.**(K-4)))
    162 NPAR(K) =INT(BL2*(10.**(K-3)))-10*INT(BL2*(10.**(K-4)))
         DO 164 K=1,12
    164 BROKL(K)=PUFF(K+2)
         GO TO 11
    166 CALL CDCL(NUPU,JP,ISTIFT)
         GO TO 11
C    FXTR CARD
    180 ITP=NUPU
```

```
          CALL FIXLES
          MSPLI=0
C   PAN   CARD
    170 IF(MSPLI.EQ.0)CALL SPLITZ(X,Y,NQ,XP)
          IF(NUPA.NE.0) AGAM(10)=FLOAT(NUPE)
          IF(NUPA.EQ.9) GO TO 11
          DO 172 I=1,14
          IF(PUFF(I).EQ.0.)GO TO 172
          MEIG=INT(PUFF(I))
          MEI=MEIG/10
          KEI =MEIG-10*MEI
          XSTX=ABS(PUFF(I)-FLOAT(MEIG))
          CALL PADD(X,Y,XP,NQ,MEI,KEI,XSTX)
    172 CONTINUE
          DO 174 I=1,NQ
          XF(I)=X(I)
          YF(I)=Y(I)
    174 BETAF(I)=XP(I)
          DLTR=DLT
          DLTUR=DLTU
          XDA=0.
          YDA=0.
          FLCH=0.
          DEFLG=0.
          NQRS=NQ
    176 NKR=NQ-1
          CALL PANEL(NKR,AMAT,GAMMA,CAE)
          DARG = ALN
          GO TO 11
C    FLAP CARD
    190 CHORD = XF(1)
          FLCH=PUFF(1)
          XDA=(1.-.01*FLCH)*CHORD
          YDA=.01*PUFF(2)*CHORD
          ARCL=.01*PUFF(3)*CHORD
          DEFLG=PUFF(4)
          DLT=DLTR+DEFLG
          DLTU=DLTUR-DEFLG
          DEFL=DEFLG*BOGEN
          ARCLU=.01*PUFF(5)*CHORD
          MSPLI=1
          CALL FLAP(XF,YF,BETAF,NQRS,XDA,YDA,ARCL,ARCLU,DEFL,X,Y,XP,NQ)
          GO TO 176
C    ALFA CARD
    333 IF(NUPA.EQ.0) GO TO 330
          MOMAG=NUPA
          AGAM(2)=FLOAT(NUPE)
          IF(NUPA.EQ.1) AGAM(10)=FLOAT(NUPE+1)
    330 IF(NUPU.EQ.0) GO TO 335
          DO 331 I=1,14
    331 ALCA(I)=PUFF(I)
    328 ITIT1=NUPI/2+1
```

```
      ITIT2=NUPI-2*ITIT1+3
      DARF=0.
      IF(ITIT2.NE.1)DARF=1.
      NAL=IABS(NUPU)
      IF(NAL.GT.14)NAL=4
335 DO 334 I=1,NAL
      PA=ALCA(I)
      IF(PA.LE.-99.) PA=RS(30+I)
      IF(PA.GT.-99.) PA=PA+DARF*DARG
334 ALV(I)=PA
      CALL MOMENT(X,Y,NQ,XDA,YDA,DEFLG,MOMAG)
      IF(AGAM(2).EQ.0.)GO TO 11
      NZF=NQ+3
      IF(ITP.EQ.2.AND.AGAM(10).EQ.1.)NZF=0
      CALL DIA(X,Y,NQ,THK)
      THKP=100.*THK
      DO341 N=1,NQ
      ND=N-1
      XDR=X(N)
      YDR=Y(N)
      DO 340M=1,NAL
      V(M)=ABS(VPR(N,M))
      VQ=1.-V(M)*V(M)
      IF(ITIT1.EQ.2)V(M)=VQ
340 CONTINUE
      NZT=NZPZ(1,NZF)
      IF(NZT.NE.NNESE.AND.N.NE.1)GO TO 341
      NZF=0
      DO  339 M=1,NAL
339 P(M)=ALV(M)-DARF*DARG
332 IF(ITP.EQ.1)WRITE(IDRU,337)NZT,NUPRO,THKP,(P(M),M=1,NAL)
337 FORMAT (A1,8HAIRFOIL ,I4,F8.2,1H%,F9.2,13F8.2)
      IF(ITP.EQ.2)WRITE(IDRU,336)NZT,NAMP,THKP,FLCH,DEFLG,(P(M),M=1,NAL)
336 FORMAT (A1,8HAIRFOIL ,12A1,F8.2,11H% THICKNESS,F10.2,6H% FLAP,
     *F8.2,19H DEGREES DEFLECTION/23X,14F8.2)
      IF(ITP.EQ.2)NZT=NZPZ(1,0)
      NZT=NZPZ(1,0)
      WRITE(IDRU,338)NZT,CPV(ITIT1),(ALTX(M,ITIT2),M=1,4)
338 FORMAT (A1,3H  N,7X,1HX,8X,1HY,5X,A9,60HDISTRIBUTIONS FOR THE ABOV
     *E ANGLES OF ATTACK RELATIVE TO THE,4A4)
      NZT=NZPZ(1,0)
341 WRITE(IDRU,342)ND,XDR ,YDR ,(V(M),M=1,NAL)
342 FORMAT (I4,F10.5,F9.5,14F8.3)
      IF(ITP.EQ.2)GO TO 11
      NZT=NZPZ(1,0)
      WRITE(IDRU,344)NZT,DARG,CM,ETA
344 FORMAT (A1,8HALPHA0 =,F5.2,8H DEGREES,3X,5HCM0 =,F7.4,3X,
     *5HETA =,F6.3)
      GOTO11
      STOP
      END
```

```
      SUBROUTINE TRAPRO
      DIMENSION FLS(2),FLA(2),DRAK(2),DRAM(2),AC(5,4),D(4),
     1WSI(2),WCI(2),FINT(3),A(5),HK(2),R(3),FKERN(30)
      DIMENSION CFP(2),AKK(2),PHIS(2),PHIW(2),AKN1(2),F(2),G(2)
      DIMENSION XRT(2),YRT(2)
      COMMON/EA/ILES,IDRU,ISTA,NNESE
      COMMON/PRAL/DLT,DLTU,ALN,ALV(14),NAL,ITP,NAMP(12),CML(14),CRL(14)
     1 ,CPV(2),ALTX(4,2),DARF,ITIT1,ITIT2
      COMMON P1(121),P(121),XP(121),YP(121),PUFF(14),AGAM(14),X(121),
     1Y(121),DS(122),VF(121),ARG(121),ANI(28),ALFR(29),IZZ,KFU,NQ,NUPRO,
     2JAB,JST,CM,ETA,ABFA,PI,BOGEN,DARG,PURES(13),GAP(450),ALFA(29)
      DATA ABSZ/0./
      CALL WANDEL(NUPRO,NAMP,12,5)
      ALFR(JAB+1)=0.
      ABZT=ANI(JAB)
      IF(ABS(ABZT-ABSZ).LT..1) GO TO 14
      IB=INT(.25*ABZT+.1)
      MQ=2*IB
      NKR=2*MQ
      ABSZ=FLOAT(NKR)
      ABGR=360./ABSZ
      HABGR=.5*ABGR
      PURES(8)=0.0
      DO 8 M=1,IB
      ARI=FLOAT(MQ+1-2*M)*HABGR
    8 FKERN(M)=ABGR*COSG(ARI)/(SING(ARI)*PI)
   14 MAGAM=INT(AGAM(3))
      NQ=NKR+1
      IF(MAGAM.EQ.0) GO TO 22
      NZT=NZPZ(3,0)
      WRITE(IDRU,82)NZT
      MCT=0
   22 DO 23 I=1,29
   23 ALFA(I)=ALFR(I)
      I=1
      J=1
   24 FLS(J)= PURES(I)*ABFA
    4 CALL DRAW(WC,WS,WL,.6,-1.,FLS(J),ABGR,1)
      CALL DRAW(WCI(J),WSI(J),WLI,-.6,-1.,FLS(J),ABGR,1)
      WCI(J)= WCI(J)+WC
      WSI(J)= WSI(J)+WS
      WLI = WLI+WL
      C4=WLI
      C5=-WLI
      FLA(J)= PURES(I+1) * ABFA
      IF(FLA(J))25,25,26
   25 DRAK(J)= 0
      DRAM(J)= 1.
      GOTO 34
   26 IF(J.EQ.2) GO TO 401
      WI = COSG(ABGR*FLA(J))
```

```
      IF(PURES(I+2)-1.)27,30,29
   27 DRAK(J)= .1*PURES(I+3)
   28 DRAM(J)= .1*PURES(I+4)
      GOTO 34
   29 DRAK(J)=((.1*PURES(I+4))**(-10./PURES(I+3))-1.)*(1.+WI)/(1.-WI)
      DRAK(J)= RUND(DRAK(J),1000.)
      DRAM(J) = .1*PURES(I+3)
      GO TO 34
   30 AA = .05*(1.-WI )*PURES(I+3)
      WILN = ALOG(.1*PURES(I+4))
      FMIT = .5
      MIT  = 0
   31 FM = -WILN/ALOG(AA/FMIT +1.)
      MIT=MIT+1
      IF(ABS(FM-FMIT)-1.E-6) 33,32,32
   32 FMIT = FM
      GO TO 31
   33 DRAM(J) = RUND(FM,1000.)
      DRAS = .05*PURES(I+3)*(WI+1.)/FM
      DRAK(J) = RUND(DRAS,1000.)
      GO TO 34
  401 DRAK(J)=.1*PURES(I+3)
      DRAM(J)=1.0
   34 I= I+5
      J= J+1
      IF(J-3)24,38,38
   38 MER = 0
      WSI(2)= -WSI(2)
      IWPPM=INT(PURES(10))
      ITMOD=INT(PURES(11))
      RUF=100.
      IF(ITMOD.GE.4.AND.ITMOD.LE.6)RUF=1000.
      ITMR=ITMOD
      SHKS = .1*PURES(12)
      HKST=.1*ABS(PURES(13))
   35 DO 36 J=1,4
   36 AC(1,J)= 0.
      ALFA(JAB)=ALFA(1)
      ALIV = 0.
      SINAI = 0.
      COSAI = 1.
      FNI = 0.
      TNAI=0.
      J=1
   37 CSAIP = COSG(2.*ALFA(J))
      SNAIP = SING(2.*ALFA(J))
      TNAIP=TNG(ALFA(J))
      IF(J-JST-1)40,39,40
   39 AC(2,1)= SINAI
      AC(2,2)= -1.-COSAI
      AC(2,3)= +1.
      AC(3,1)= -SNAIP
```

```
      AC(3,2)= 1.+CSAIP
      AC(3,3)=-1.
      AC(4,1)= COSAI-CSAIP
      AC(4,2)= SINAI-SNAIP
      AC(4,3)= 0.
      AC(5,1)=0.
      AC(5,2)=0.
      AC(5,3)=0.
      AC(2,4)=-2.*TNAI
      AC(3,4)=2.*TNAIP
      AC(4,4)=0.
      AC(5,4)=2.*(TNAI-TNAIP)
      ALIS = ALIV
      ALISP = ALFA(J)
      GOTO 41
   40 FII = CSLG(HABGR*FNI-90.,ALIV)
      FIIP= CSLG(HABGR*FNI-90.,ALFA(J))
      PB=FNI*HABGR*BOGEN
      AC(1,1)=-FIIP*SNAIP+FII*SINAI+(COSAI-CSAIP)*PB +AC(1,1)
      AC(1,2)=-FII*(1.+COSAI)+FIIP*(1.+CSAIP)+(SINAI-SNAIP)*PB+AC(1,2)
      AC(1,3)=-FIIP + FII + AC(1,3)
      JCK=J-1
      JMI=J-JAB-1
      IF(JCK.EQ.0.OR.JMI.EQ.0) GO TO 402
      FSI=SNLG(HABGR*FNI)
      AC(1,4)=FSI*(2.*TNAI-2.*TNAIP)-2.*TNAI*FII+2.*TNAIP*FIIP+AC(1,4)
  402 CONTINUE
   41 IF(J-JAB-1)42,43,43
   42 ALIV =ALFA(J)
      SINAI=SNAIP
      COSAI=CSAIP
      TNAI=TNAIP
      FNI = ANI(J)
      J=J+1
      GO TO 37
   43 J=1
      IF(FLA(J)) 47,47,49
   49 CALL DRAW(WC,WS,WL,DRAK(J),DRAM(J),FLA(J),ABGR,0)
      AC(1,1)= WC+ AC(1,1)
      AC(1,2) = WS +AC(1,2)
      AC(1,3)=WL+AC(1,3)
   47 J=2
      WWC6=0.0
      WWS6=0.0
      C6=0.0
      IF(FLA(J)) 410,410,411
  411 CALL DRAW(WC,WS,WL,DRAK(J),1.0,FLA(J),ABGR,0)
      WWC6=WC
      WWS6=-WS
      C6=-WL
  410 CONTINUE
      PHIS(1)=FLS(1)*ABGR*BOGEN
```

```
      PHIW(1)=FLA(1)*ABGR*BOGEN
      PHIS(2)=(360.-FLS(2)*ABGR)*BOGEN
      PHIW(2)=(360.-FLA(2)*ABGR)*BOGEN
      DO 425 J=1,2
      G(J)=DRAK(J)/(1.0+COS(PHIW(J)))
      F(J)=1.0-G(J)*COS(PHIW(J))
      IF(G(J)**2-F(J)**2) 420,421,422
420   TARG=((F(J)-G(J))*TAN(PHIW(J)/2.))/SQRT(F(J)**2-G(J)**2)
      TARG1=ATAN(TARG)
      CFP(J)=-((4.*(G(J)-F(J)))/SQRT(F(J)**2-G(J)**2))*TARG1
      GO TO 425
421   CFP(J)=0.0
      GO TO 425
422   GFLN2=SQRT(G(J)**2-F(J)**2)
      GFLN1=(G(J)-F(J))*TAN(PHIW(J)/2.)
      GFLN=ALOG(ABS((GFLN1+GFLN2)/(GFLN1-GFLN2)))
      COEFF=-(2.*(G(J)-F(J))/SQRT(G(J)**2-F(J)**2))
      CFP(J)=COEFF*GFLN
425   CONTINUE
      SRM=.6
      AK=1.0-SRM
      BK=1.0+SRM
      DO 450 J=1,2
      AKN1(J)=SRM/(1.0-COS(PHIS(J)))
      IF(BK-2.*AKN1(J)) 430,431,432
430   AKSR=SQRT(2.*BK*AKN1(J)-BK**2)
      AKT1=2.*AKN1(J)-BK
      COEFK=AKT1/(2.*AKSR)
      AKLN1=AKT1*TAN(PHIS(J)/2.)
      AKLN=ALOG(ABS((AKLN1+AKSR)/(AKLN1-AKSR)))
      AKK(J)=COEFK*AKLN
      GO TO 450
431   AKK(J)=0.
      GO TO 450
432   AKSR1=SQRT(BK**2-2.*AKN1(J)*BK)
      AKT2=2.*AKN1(J)-BK
      AKT3=BK-2.*AKN1(J)
      AKTAN=(AKT3*TAN(PHIS(J)/2.))/AKSR1
      AKATAN=ATAN(AKTAN)
      AKK(J)=(AKT2/AKSR1)*AKATAN
450   CONTINUE
      AC1=-2.*DRAM(1)*PHIW(1)
      AC2=DRAM(1)*CFP(1)
      AC(1,4)=AC(1,4)+AC1+AC2
      C1A=SQRT((AK+2.*AKN1(1))/AK)
      C1C=4.*C1A*ATAN(C1A*TAN(PHIS(1)/2.))
      C1=4.0*PHIS(1)-C1C+4.0*AKK(1)
      C2A=SQRT((AK+2.*AKN1(2))/AK)
      C2C=4.*C2A*ATAN(C2A*TAN(PHIS(2)/2.))
      C2=8.0*PI-4.0*PHIS(2)+C2C-4.0*AKK(2)
      C3=2.0*PHIW(2)-CFP(2)-4.0*PI
      D(1)=WSI(1)*(C3*C5-C2*C6)-WSI(2)*(C3*C4-C1*C6)+WWS6*(C2*C4-C1*C5)
```

```
      D(2)=-(WCI(1)*(C3*C5-C2*C6)-WCI(2)*(C3*C4-C1*C6)+WWC6*(C2*C4-C1*C5
     1))
      D(3)=WCI(1)*(C3*WSI(2)-C2*WWS6)-WCI(2)*(C3*WSI(1)-C1*WWS6)+WWC6*(C
     12*WSI(1)-C1*WSI(2))
      D(4)=-(WCI(1)*(C6*WSI(2)-C5*WWS6)-WCI(2)*(C6*WSI(1)-C4*WWS6)+WWC6*
     1(C5*WSI(1)-C4*WSI(2)))
      A(1)=D(1)*AC(1,1)+D(2)*AC(1,2)+D(3)*AC(1,3)+D(4)*AC(1,4)
      A(2)=D(1)*AC(2,1)+D(2)*AC(2,2)+D(3)*AC(2,3)+D(4)*AC(2,4)
      A(3)=D(1)*AC(3,1)+D(2)*AC(3,2)+D(3)*AC(3,3)+D(4)*AC(3,4)
      A(4)=D(1)*AC(4,1)+D(2)*AC(4,2)
      A(5)=D(4)*AC(5,4)
C     SOLUTION OF TRANSCENDENTAL EQUATION
   53 I=0
      FV = 9.E9
      PHISH =      .5 *(ALIS+ALISP)
   60 CSLI = CSLG(PHISH,ALIS)
      CSLIP= CSLG(PHISH,ALISP)
      SNLI=SNLG(PHISH+90.)
      FP=A(1)+A(2)*CSLI+A(3)*CSLIP+A(4)*BOGEN*(90.+PHISH)+A(5)*SNLI
      IF(I.GE.20) GO TO 66
      IF(ABS(FP)-ABS(FV).LT.-.5E-9) GO TO 62
      I=20
      PHISH = PHISH - PDIF
      GO TO 60
   62 PDIF=-FP/(A(2)/(PHISH-ALIS)+(A(3)/(PHISH-ALISP))+A(5)*PHISH)
      I = I+1
   65 FV=FP
      PHISH = PHISH + PDIF
      IF(PHISH.LT.ALIS.AND.PHISH.GT.ALISP) GO TO 60
      WRITE(IDRU,64)MER,ITMOD
   64 FORMAT (66HOTRANSCENDENTAL EQUATION HAS DIVERGED.  CHECK TRA1 AND
     *TRA2 CARDS.,12H   ITERATION,I2,8H   MODE ,I1)
      STOP
   66 ANI(JST) = (PHISH+90.)/HABGR
      AJC=AC(1,1)+AC(2,1)*CSLI+AC(3,1)*CSLIP+AC(4,1)*BOGEN*(PHISH+90.)
      AJS=AC(1,2)+AC(2,2)*CSLI+AC(3,2)*CSLIP+AC(4,2)*BOGEN*(PHISH+90.)
      AJT=AC(1,3)+AC(2,3)*CSLI+AC(3,3)*CSLIP
      AJ4=AC(1,4)+AC(2,4)*CSLI+AC(3,4)*CSLIP+AC(5,4)*SNLI
      DD=WCI(1)*(WSI(2)*C6-WWS6*C5)-WCI(2)*(WSI(1)*C6-WWS6*C4)+WWC6*(WSI
     1(1)*C5-WSI(2)*C4)
      DRAM(2)=(WCI(1)*(AJS*C5-AJT*WSI(2))-WCI(2)*(AJS*C4-AJT*WSI(1))-AJC
     1*(WSI(1)*C5-WSI(2)*C4))/DD
   69 HK(1)=(-AJC*(WSI(2)*C6-WWS6*C5)-WCI(2)*(AJT*WWS6-AJS*C6)+WWC6*(AJT
     1*WSI(2)-AJS*C5))/DD
      HK(2)=(WCI(1)*(AJT*WWS6-AJS*C6)+AJC*(WSI(1)*C6-WWS6*C4)+WWC6*(AJS*
     1C4-WSI(1)*AJT))/DD
      HKS = HK(1)+HK(2)
C
      WPPWUD=(1.0+DRAK(1)+(1.0-DRAK(1))*COS(PHIW(1)))
      WPPWU=(DRAM(1)*DRAK(1))/WPPWUD
      WPPSU=(1.125*HK(1))/(1.0-COS(PHIS(1)))
      WPPU=WPPWU+WPPSU
```

```
      WPPWLD=(1.0+DRAK(2)+(1.0-DRAK(2))*COS(PHIW(2)))
      WPPWL=(DRAM(2)*DRAK(2))/WPPWLD
      WPPSL=(1.125*HK(2))/(1.0-COS(PHIS(2)))
      WPPL=WPPWL+WPPSL
C
      IF(ITMOD.EQ.0.OR.ABS(HKS-SHKS).LT.HKST) GO TO 74
      IF(MAGAM.LT.2.AND.MAGAM-MER.NE.1) GO TO 100
      GO TO 76
   74 ITMOD =0
      IF(MAGAM.EQ.0) GO TO 300
   76 NZT=NZPZ(2,JAB+4)
      WRITE(IDRU,77)NZT,NUPRO,MER,ITMR
   77 FORMAT (A1,42HTRANSCENDENTAL EQUATION RESULTS   AIRFOIL ,I4,
     *12H   ITERATION,I2,8H   MODE ,I1)
      NZT=NZPZ(1,0)
      WRITE(IDRU,78)NZT
   78 FORMAT (A1,69H    NU    ALPHA*  OMEGA´  OMEGA     K        MU      K H
     *    LAMBDA LAMBDA*)
      JH= 1
      DO 85 JN=1,JAB
   79 NZT=NZPZ(1,0)
      IF(JN.NE.1.AND.JN.NE.JAB) GO TO 83
      X1 = .5*(1.+ COSG(FLA(JH)*ABGR))
      WHK = (1.+DRAK(JH)*(1.-X1)/X1)**(-DRAM(JH))
      WSTR= DRAM(JH)*DRAK(JH)/X1
      WRITE(IDRU,82)NZT,ANI(JN),ALFA(JN),WSTR,WHK,DRAK(JH),DRAM(JH),HK(J
     1H),FLA(JH),FLS(JH)
   82 FORMAT (A1,F6.2,F8.2,F8.3,F7.3,F9.4,F9.4,F8.3,F8.2,F7.2)
      JH=2
      GO TO 85
   83 WRITE(IDRU,82)NZT,ANI(JN),ALFA(JN)
   85 CONTINUE
C
      WRITE(IDRU,2000) WPPU,WPPL,IWPPM,MCT
 2000 FORMAT(/5X,5HWPPU=,F7.3,5X,5HWPPL=,F7.3,5X,11HWPP ITMODE=,I2,3X,
     210HITERATION=,I2/)
C
      IF(ITMOD.EQ.0) GO TO 300
  100 IF(MER)103,102,103
  102 DAL = .1
      GO TO 104
  103 IF(HKS-HKSV.EQ.0.)GO TO 74
      DAL = (SHKS-HKS)*DAL/(HKS-HKSV)
      DALD=DAL
      IF(ITP.EQ.0)DAL=RUND(DAL,RUF)
      IF(MAGAM.EQ.0.)GO TO 1004
      NZT=NZPZ(2,0)
      WRITE(IDRU,1003)NZT,MER,HKS,DALD,DAL
 1003 FORMAT (A1,10H ITERATION,I2,3X,5HK S =,F9.6,3X,7HDELTA =,F12.8,
     *3X,9HROUNDED =,F6.2)
 1004 IF(DAL.EQ.0.)GO TO 74
      IF(MER.GE.3.AND.ABS(DALV).LE.ABS(DAL))GO TO 74
```

```
    104 DALV=DAL
        IF(ITMOD.GE.4)GO TO 113
        DO 111 J=1,JAB
        IF(ITMOD.NE.2.AND.J.LE.JST) ALFA(J)=ALFA(J)+DAL
        IF(ITMOD.NE.1.AND.J.GT.JST) ALFA(J)=ALFA(J)-DAL
    111 CONTINUE
        GO TO 112
    113 IF(ITMOD.GE.7)GO TO 114
        IF(ITMOD.NE.5)DRAK(1)=DRAK(1)+DAL
        IF(ITMOD.NE.4)DRAK(2)=DRAK(2)+DAL
        GO TO 112
    114 IF(ITMOD.NE.8)ALFA(JST)=ALFA(JST)+DAL
        IF(ITMOD.NE.7)ALFA(JST+1)=ALFA(JST+1)-DAL
    112 HKSV=HKS
        MER =MER+1
        GOTO 35
C
    300 DWPP=WPPU-WPPL
        CFUNC=ABS(DWPP)
        WPPTOL=.001
        IF(CFUNC.LE.WPPTOL) GO TO 301
        IF(IWPPM.EQ.0) GO TO 301
        IF(MCT.GT.15) GO TO 301
        IF(MCT.NE.0) GO TO 19
        DEL=.1
        GO TO 20
     19 DEL=-DWPP*DEL/(DWPP-DWPPV)
        IF(DEL.EQ.0.) GO TO 301
     20 IF(IWPPM.EQ.4) GO TO 7
        IF(IWPPM.EQ.3) GO TO 6
        IF(IWPPM.EQ.2) GO TO 9
     15 DRAK(1)=DRAK(1)+DEL
        GO TO 21
      9 DRAK(2)=DRAK(2)+DEL
        GO TO 21
      6 DRAM(1)=DRAM(1)+DEL
        GO TO 21
      7 FLSN=FLS(2)+DEL
        IF (FLSN.LT.0.0.OR.FLSN.GT.FLA(2)) GO TO 12
        FLS(2)=FLSN
        DELV=DEL
        DWPPV=DWPP
        MCT=MCT+1
        I=6
        J=2
        GO TO 4
     12 IWPPM=1
        DEL=.1
        GO TO 15
     21 DELV=DEL
        DWPPV=DWPP
        MER=MER+1
```

```
      IF(ITMOD.EQ.0) MER=0
      MCT=MCT+1
      GO TO 35
C
  301 AK1=.5*(COSG(PHISH-ALFA(JST+1))/SING(PHISH-ALFA(JST+1))
     1       -COSG(PHISH-ALFA(JST))/SING(PHISH-ALFA(JST)))
      AKP  =AK1*180./9.8696044
      PHIM = 0.
      NU=1
      I= 1
      ANU =0.
      JH=0
      VI= 0.
  302 JH=JH+1
      FF1 = COSG(ABGR*FLA(JH))
      FF2 = DRAK(JH)/(1.+FF1)
      FG1 = COSG(ABGR*FLS(JH))
      FG3 = .6/(FG1-1.)
  304 VI= VI - CSLG(PHIM-90., ALFA(I))
      GO TO 310
  306 ARGN = ANU
      IF(ANU.GT..5* ABSZ)ARGN= ABSZ - ANU
      CSP = COSG(ARGN*ABGR)
      F1=0.0
      IF(ARGN.LT.FLA(JH))F1=DRAM(JH)*ALOG((CSP-FF1)*FF2+1.)
      G1=0.
      IF(ARGN.LT.FLS(JH))G1=-HK(JH)*ALOG(1.-((CSP-FG1)*FG3)**2)
      P(NU)= F1+G1+CSLG(ANU*HABGR-90.,ALFA(I)) + VI
      P1(NU)=P(NU)-AK1*ABS(SING((ANU*HABGR - 90.) - PHISH))
      NU = NU + 1
      ANU= ANU+ 1.
  310 IF(ANU-ANI(I))306,306,312
  312 IF(ANU- ABSZ)314,320,320
  314 PHIM = ANI(I)*HABGR
      VI=VI+CSLG(PHIM-90.,ALFA(I))
      I = I+1
      IF(I-1-JST)304,302,304
  320 PS=0.
      B2=0.
      DO 324 I=1,NKR
      PS=PS+P(I)
      BI = 2*(I-1)
  324 B2 = B2 + SING(BI*ABGR)*P(I)
      V1 = 2.*EXP(PS/ABSZ)
      SXI = .00000000
      SY=0.
      DO328 N=1,NQ
      Q=0.
      DO326 M=1,IB
      MN = N + 1 + MQ - 2*M
      MM = 2*N - MN
      IF(MN.GT.NKR) MN = MN - NKR
```

```
      IF(MM.LT.1) MM = MM + NKR
326 Q = Q+ FKERN(M)*(P1(MN)-P1(MM))
      ANU= N-1
      ZP = ANU*HABGR - 90.
      ZL = COSG(ZP - PHISH)
      ZL = ABS((1.-ZL)/(1.+ZL))
      IF(ZL.NE.0.)ZL=ALOG(ZL)
      ARG(N) = Q - AKP*SING(ZP-PHISH)*ZL + ZP
      VF(N) = V1*EXP(-P(N))
      WV = COSG(ZP)/VF(N)
      XP(N)= WV*SING(ARG(N))
      YP(N)=-WV*COSG(ARG(N))
      SXI= SXI+ XP(N)
328 SY = SY + YP(N)
      SX = SXI
      XPK = SX/(ABSZ  - 1.)
      YPK  = SY/(ABSZ -1.)
      DO 329 N=2,NKR
      XP(N)=XP(N)-XPK
329 YP(N)=YP(N)-YPK
      CALL CINT(XP,X,NQ,IZZ)
      CALL CINT(YP,Y,NQ,IZZ)
      RQV = 0.
      DO 330 N=2,NKR
      RQ=X(N)*X(N)+Y(N)*Y(N)
      IF(RQ.GT.RQV)L=N
330 RQV = RQ
      DO 327 I = 1,3
      IEPPL = L-2+I
327 R(I)=SQRT(X(IEPPL)*X(IEPPL)+Y(IEPPL)*Y(IEPPL))
333 TAU = (R(3)-R(1))/(4.*(R(2)+R(2)-R(1)-R(3)))
      XNAS = X(L)+TAU*(X(L+1)-X(L-1)+2.*TAU*(X(L+1)+X(L-1)-X(L)-X(L)))
      YNAS = Y(L)+TAU*(Y(L+1)-Y(L-1)+2.*TAU*(Y(L+1)+Y(L-1)-Y(L)-Y(L)))
      SQ = XNAS*XNAS + YNAS*YNAS
      AT=XNAS/SQ
      B= YNAS/SQ
      STREF = 1./SQRT(SQ)
      ETA =  ABSZ*STREF/PI
      CM = .5*ETA*STREF*B2
      DARG = 19.09859 *(3.*YNAS/XNAS - (YNAS/XNAS)**3)
      IF(ABS(SX)+ABS(SY).LT..0001*ABSZ) GO TO 335
      SX=STREF*SX*200.
      SY=STREF*SY*200.
      NZT=NZPZ(2,0)
      WRITE (IDRU,334) NZT,SX,SY
334 FORMAT (A1,14HWARNING - SX =,F6.3,3X,4HSY =,F6.3)
335 CONTINUE
C
      IF(IWPPM.EQ.0) GO TO 605
      CHORD=(4.0*PI)/(ABSZ*STREF)
      PHIW1=COSG(FLA(1)*ABGR)
      PHIS1=COSG(FLS(1)*ABGR)
```

```
      PHIWF=1.0+DRAK(1)*((1.0-PHIW1)/(1.0+PHIW1))
      WO=(PHIWF**(-DRAM(1)))*(.64)**HK(1)
      APO=-ALOG(V1)-ALOG(WO)+ALOG(2.0)
      QO=(ARG(1)+90.)*(PI/180.)
      ALFA1=ALFA(1)*(PI/180.)
      DELTE=.5*(ATAN(Y(2)/X(2))+ATAN(Y(NKR)/X(NKR)))
      GAMMA=ALFA1-DELTE
C
  605 DO 331 N=2,NQ
      XR=X(N)
      X(N)= 1.-B*Y(N)-AT*XR
      Y(N)= B*XR -AT*Y(N)
      ARG(N) = ARG(N) - DARG
      WQ = (XP(N)+XP(N-1)-XPK-XPK)**2 + (YP(N)+YP(N-1)-YPK-YPK)**2
  331 DS(N-1) = STREF*SQRT(WQ)*(1.+.6666667*((XP(N)*YP(N-1)
     1-XP(N-1)*YP(N))/WQ)**2)
      NHKW=NQ/12
      DLT = Y(NHKW)/(BOGEN*(1.-X(NHKW)))
      NHKW=NQ-NHKW+1
      DLTU=-Y(NHKW)/(BOGEN*(1.-X(NHKW)))
      X(1) = 1.
  332 ARG(1) = ARG(1) - DARG
  346 ITP=1
C
      IF(IWPPM.EQ.0) GO TO 606
      XT=X(1)*CHORD
      YT=Y(1)*CHORD
      XRT(1)=X(2)*CHORD
      XRT(2)=X(NKR)*CHORD
      YRT(1)=Y(2)*CHORD
      YRT(2)=Y(NKR)*CHORD
      CALL RCAL(XT,YT,XRT,YRT,APO,QO,ALFA1,PXT,PYT,NKR)
      PST=PXT*COS(GAMMA)+PYT*SIN(GAMMA)
      PNT=-PXT*SIN(GAMMA)+PYT*COS(GAMMA)
      CPST=2.0*CHORD*PST
      CPNT=2.0*CHORD*PNT
      WRITE(IDRU,602)
  602 FORMAT("0",11X,45HTHE TRAILING EDGE PRESSURE GRADIENT IS FINITE)
      WRITE(IDRU,603) ALFA(1)
  603 FORMAT(15X,25HWHEN THE ANGLE OF ATTACK=,F4.1,1X,7HDEGREES)
      WRITE(IDRU,604) CPST,CPNT
  604 FORMAT(8X,19HIN THAT CASE, CPST=,F10.3,7X,5HCPNT=,F10.3)
C
  606 ALN=DARG
      IF(PURES(13).GE.0.)GO TO 11
      PURES(12)=10.*HKS
      PURES(13)=.00001
   11 RETURN
      END
```

```
FUNCTION TNG(A)
TNG=SING(A)/COSG(A)
RETURN
END
```

```
FUNCTION SNLG(A)
SNLG=ALOG(ABS(SING(A)))
RETURN
END
```

```
      SUBROUTINE RCAL(XT,YT,X,Y,APO,QO,ALFA1,PXT,PYT,NKR)
      DIMENSION PX(4),PY(4),X(2),Y(2),THETA1(2)
      COMPLEX CEXP,CMPLX,CONJG,ZETA,EIA,EMIA,ZTEXP,
     1ZETA2,WZ,ZT2P,ZT3P,WTP,WT2P,ZETA1,Z,ZT4P,ZT,
     2ZT2PC,PTCAL,C(2),ZETA1P(2),WT3P,WTPC,PTCOEF
      PI=3.141592653589
      ANKR=FLOAT(NKR)
      THETDEG=360./ANKR
      THETA1(1)=THETDEG
      THETA1(2)=360.-THETDEG
      ZTEXP=CMPLX(APO,QO)
      ZT2P=CEXP(ZTEXP)
      COSA=COS(ALFA1)
      SINA=SIN(ALFA1)
      EIA=CMPLX(COSA,SINA)
      EMIA=CMPLX(COSA,-SINA)
      WTP=(EIA+EMIA)
      WT2P=(-4.0*EIA-2.0*EMIA)
      WTPC=CONJG(WTP)
      WT3P=6.0*(3.0*EIA+EMIA)
      ZT3P=ZT2P*(WT2P/WTP)
      ZT=CMPLX(XT,YT)
      ZT4P=0.0
      M=1
      DO 20 I=1,2
      Z=CMPLX(X(I),Y(I))
      THETA=THETA1(I)*(PI/180.)
      XI=COS(THETA)
      ETA=SIN(THETA)
      ZETA=CMPLX(XI,ETA)
      ZETA1P(M)=(ZETA-1.0)
      C(M)=(120./ZETA1P(M)**4)*(Z-ZT-.5*ZT2P*ZETA1P(M)**2
     1-(ZT3P/6.)*ZETA1P(M)**3)
      M=2
   20 CONTINUE
      ZT4P=.10*(C(1)+C(2))+ZT4P
      ZT2PC=CONJG(ZT2P)
      PTCOEF=-(WTPC)/(3.0*ZT2PC*ZT2P**3)
      PTCAL=CONJG(PTCOEF*(ZT2P*WT3P-ZT4P*WTP))
      PXT=REAL(PTCAL)
      PYT=AIMAG(PTCAL)
      RETURN
      END
```

REFERENCES

1. Wortmann, F. X., "A Contribution to the Design of Laminar Profiles for Gliders and Helicopters," Ministry of Aviation Translation TIL/T 4903, February 1960. (Translated from Z. Flugwiss, Vol. 3, 1955, pp. 333-345).

2. Wortmann, F. X., "Progress in the Design of Low Drag Airfoils," Boundary Layer and Flow Control, edited by G. V. Lachmann, Pergamon Press, London, 1961, pp. 748-770.

3. Wortmann, F. X., "A Critical Review of the Physical Aspects of Airfoil Design at Low Mach Number," Motorless Flight Research - 1972, edited by J. L. Nash-Weber, NASA CR-2315, November 1973, pp. 179-196.

4. Wortmann, F. X., "The Quest for High Lift," AIAA Paper No. 74-1018, Second International Symposium on Technology and Science of Low Speed and Motorless Flight, September 1974.

5. Eppler, R., "Direct Calculation of Airfoils From Pressure Distribution," NASA TT F-15,417. 1974. (Translated from Ingenieur-Archiv., Vol. 23, No. 1, 1957, pp. 32-57).

6. Eppler, R., "Laminar Airfoils for Reynolds Numbers Greater Than 4×10^6," B-819-35, April 1969. (Available from NTIS as N69-28178) (Translated from Ingenieur-Archiv., Vol. 38, 1969, pp. 232-240).

7. Eppler, R., "Some New Airfoils," Science and Technology of Low Speed and Motorless Flight, NASA CP-2085, Part 1, 1979, pp. 131-153.

8. Miley, S. J., "An Analysis of the Design of Airfoil Sections for Low Reynolds Numbers," Ph.D. Dissertation, Mississippi State College, 1972.

9. Lighthill, M. J., "A New Method of Two-Dimensional Aerodynamic Design," R & M 2112, Aeronautical Research Council, London, April 1945.

10. Arlinger, B., "An Exact Method of Two-Dimensional Airfoil Design," TN-67, Saab, Linkoping, Sweden, October 1970.

11. Smith, A.M.O., "High-Lift Aerodynamics," Wright Brothers Lecture, AIAA Paper No. 74-939, August 1974.

12. Liebeck, R. H., "On the Design of Subsonic Airfoils for High Lift," AIAA Paper No. 76-406, July 1976.

13. Liebeck, R. H. and Ormsbee, A. I., "Optimization of Airfoils for Maximum Lift," Journal of Aircraft, Vol. 7, No. 5, September-October 1970, pp. 409-415.

14. Stratford, B. S., "The Prediction of Separation of the Turbulent Boundary Layer," Journal of Fluid Mechanics, Vol. 5, 1959, pp. 1-16.

15. Ormsbee, A. I. and Chen, A. W., "Multiple Element Airfoils Optimized for Maximum Lift Coefficients," Journal of Aircraft, Vol. 10, No. 12, December 1972, pp. 1620-1624.

16. Abbott, I. H. and von Doenhoff, A. E., Theory of Wing Sections, Dover, New York, 1959.

17. Edwards, T. E., "An Approximate Numerical Method for the Optimization of Flap Design for Maximum Lift Coefficients," Ph.D. Thesis, University of Illinois, Urbana, 1975.

18. Kennedy, J. L. and Marsden, D. J., "The Development of High Lift, Single-Component Airfoil Sections," Aeronautical Quarterly, February 1979, pp. 343-359.

19. Thompson, W. G., "Design of High Lift Airfoils with a Stratford Distribution by the Eppler Method," University of Illinois Technical Report AAE 75-5, Urbana, June 1975.

20. Nonweiler, T., "The Design of Wing Sections," Aircraft Engineering, July 1956, pp. 216-227.

21. Mead, H. R. and Melnik, R. E., "GRUMFOIL – A Computer Code for the Viscous Transonic Flow Over Airfoils," Grumman Research Department Report, March 1980.

22. McMasters, J. H. and Henderson, M. L., "Low-Speed Single-Element Airfoil Synthesis," Science and Technology of Low Speed and Motorless Flight, NASA CP-2085, Part 1, 1979, pp. 1-31.

23. Sivier, K. R., Ormsbee, A. I. and Awker, R. W., "Low Speed Aerodynamic Characteristics of a 13.1 Percent Thick, High-Lift Airfoil," SAE Paper Number 740366, April 1974.

24. Moore, W. A., "The Experimental Evaluation of a Maximized-Lift Single Element Airfoil," M.S. Thesis, University of Illinois, Urbana, 1979.

25. Eppler, R. and Somers, D. M., "A Computer Program for the Design and Analysis of Low-Speed Airfoils," NASA TM 80210, August 1980.

26. Karamcheti, K., Principles of Ideal Fluid Aerodynamics, Wiley, New York, 1966.

27. Sapuppo, J. and Archer, R. D., "Fully Laminar Flow Airfoil Sections," Journal of Aircraft, Vol. 19, No. 5, May 1982, pp. 406-409.

28. Tolstov, G. P., Fourier Series, Dover, New York, 1976.

29. Preston, J. H. and Sweeting, N. E., "The Experimental Determination of the Boundary Layer and Wake Characteristics of a Simple Joukowsky Aerofoil with Particular Reference to the Trailing Edge Region," R & M 1998, Aeronautical Research Council, London, March 1943.

30. Preston, J. H., "The Effect of the Boundary Layer and Wake on the Flow Past a Symmetrical Aerofoil at Zero Incidence," R & M 2107, Aeronautical Research Council, London, July 1945.

31. Preston, J. H., "The Calculation of Lift Taking Account of the Boundary Layer," R & M 2725, Aeronautical Research Council, London, November 1949.

32. Cebeci, T. and Bradshaw, P., Momentum Transfer in Boundary Layers, McGraw-Hill, New York, 1977.

33. Melnik, R. E., Chow, R. R., Mead, H. R. and Jameson, A., "An Improved Viscid/Inviscid Interaction Procedure for Transonic Flow Over Airfoils," Grumman Research Department Report, February 1980.

34. Strand, T., "Exact Method of Designing Airfoils With Given Velocity Distribution in Incompressible Flow," Journal of Aircraft, Vol. 10, No. 11, November 1973, pp. 651-659.

35. Liebeck, R. H., "A Class of Airfoils Designed for High-Lift in Incompressible Flow," Journal of Aircraft, Vol. 10, No. 10, October 1973, pp. 610-617.

36. Wortmann, F. X., "On the Optimization of Airfoils with Flaps," Soaring, May 1970, pp. 23-27.

37. Somers, D. M., "NASA Research Related to Sailplane Airfoils," Proceedings of the 1981 Soaring Society of America National Convention, Phoenix, Arizona, January 1981, pp. 99-109.

Figure 1. Form of the velocity distribution for maximum lift on a
single-element airfoil.

Figure 2.   Kennedy and Marsden High Lift Airfoil and Design
Velocity Distribution [18]. $RE = 1 \times 10^6$.

Figure 3. Kennedy and Marsden airfoil potential flow velocity distribution (Eppler panel method code) compared with viscous analysis (GRUMFOIL code) and experimental results [18]. ALPHA = 4.2 DEG (relative to chord-line), RE = 1 x 10^6.

Figure 4. Thompson high-lift airfoil and design velocity distribution [19].

Figure 5. Conformal transformation of the flow around an infinite
circular cylinder into the flow around an airfoil.

ZT= 1.000	0.000		Z2= -1.000	0.000
Z3= 0.370	-0.471		Z4= -0.370	0.471
Z5= 0.000	0.000		Z6= 0.000	0.000
C1= 0.91506	-0.34854		C2= 0.00000	0.00000
C3= 0.02831	0.11618		C4= 0.00000	0.00000
C5= 0.00000	0.00000		URMAX=0.000	

R=1.111   UR= -0.072   UI=0.290   VTE=0.76274

Figure 6.   Example of von Mises airfoil generated using a
four-term transformation.

ZT= 1.000   0.000 $Z2$= -1.000   -0.330

$Z3$= 0.283   -0.142 $Z4$= -0.283   0.472

$Z5$= 0.000   0.000 $Z6$= 0.000   0.000

$C1$= 0.90416 0.15624 $C2$= 0.08312 -0.16284

$C3$= -0.02347 0.05648 $C4$= 0.00000 0.00000

$C5$= 0.00000 0.C0000   URMAX= -0.027

R= 1.131   UR= -0.131   UI= 0.000   VTE= 0.87305

Figure 7. Example von Mises airfoil generated using a
four-term transformation.

ZT= 1.000   0.000 $Z2$= -1.000   0.000

$Z3$= 0.030   -0.300 $Z4$= 0.020   0.300

$Z5$= 0.025   0.000 $Z6$= 0.025   0.000

$C1$= 1.00627   -0.00300 $C2$= -0.04772 0.00007

$C3$= 0.03122   0.00100 $C4$= -0.00114 -0.00004

$C5$= 0.00001   0.00000   URMAX=0.000

R=1.123 UR= -0.120 UI=0.088   VTE=0.85389

Figure 8.   Example von Mises airfoil generated using a
            six-term transformation.

ZT= 1.000   0.000   Z2= -1.000   -0.240

Z3= 0.300   -0.150   Z4= -0.400   0.300

Z5= 0.150   0.090   Z6= -0.050   0.000

C1= 1.04840 0.08850   C2= 0.03719 -0.10349

C3= -0.04847 0.04072   C4= 0.00530 -0.00079

C5= 0.00029 -0.00010   URMAX= -0.118

R= 1.118   UR= -0.118   UI= 0.000   VTE= 0.96515

Figure 9. Example von Mises airfoil generated using a
six-term transformation and a mapping circle radius
equal to the minimum allowable for a physically
realizable airfoil.

```
ZT= 1.000     0.000         Z2= -0.744   0.000

Z3= -0.461    0.000         Z4= 0.205    0.000

Z5= 0.000     0.000         Z6= 0.000    0.000

C1= 0.90415  0.00000        C2= 0.08313  0.00000

C3= -0.02347 0.00000        C4= 0.00000  0.00000

C5= 0.00000  0.00000             URMAX= -0.011

R= 1.131     UR= -0.131   UI= 0.000    VTE= 0.87307
```

Figure 10. Symmetrical von Mises airfoil having real transformation
coefficients equal to those of the airfoil shown in
Figure 7.

$ZT=$ 1.000	0.000	$Z2=$ -1.000	-0.240
$Z3=$ 0.300	-0.150	$Z4=$ -0.400	0.300
$Z5=$ 0.150	0.090	$Z6=$ -0.050	0.000
$C1=$ 1.04840	0.08850	$C2=$ 0.03719	-0.10349
$C3=$ -0.04847	0.04072	$C4=$ 0.00530	-0.00079
$C5=$ 0.00029	-0.00010	URMAX= -0.118	

$R=$ 1.040 $UR=$ -0.040 $UI=$ 0.000 $VTE=$ 1.03779

Figure 11. Von Mises airfoil generated with a mapping circle
radius less than the minimum allowable for a physically
realizable airfoil.

$ZT=$ 1.000   0.000 $Z2=$ -1.000   -0.240

$Z3=$ 0.300   -0.150 $Z4=$ -0.400   0.300

$Z5=$ 0.150   0.090 $Z6=$ -0.050   0.000

$C1=$ 1.04840 0.08850 $C2=$ 0.03719   -0.10349

$C3=$ -0.04847 0.04072 $C4=$ 0.00530   -0.00079

$C5=$ 0.00029 -0.00010   URMAX= -0.118

$R=$ 1.180   UR= -0.180   UI= 0.000   VTE= 0.91466

Figure 12. Von Mises airfoil generated with a mapping circle
            radius greater than the minimum allowable for a
            physically realizable airfoil.

$ZT=$ 1.000   0.000 $Z2=$ -1.000   0.000

$Z3=$ 0.000   0.000 $Z4=$ 0.000   0.000

$Z5=$ 0.000   0.000 $Z6=$ 0.000   0.000

$C1=$ 1.00000   0.00000 $C2=$ 0.00000   0.00000

$C3=$ 0.00000   0.00000 $C4=$ 0.00000   0.00000

$C5=$ 0.00000   0.00000 $URMAX=$ 0.000

$R=$ 1.000 $UR=$ 0.000 $UI=$ 0.000 $VTE=$ 1.00000

Figure 13.   Flat plate airfoil generated by simplifying the
von Mises transformation to that of Joukowsky.

$ZT=$ 1.000   0.000 $Z2=$ -1.100   0.000

$Z3=$ 0.100   0.000 $Z4=$ 0.000   0.000

$Z5=$ 0.000   0.000 $Z6=$ 0.000   0.000

$C1=$ 1.11000 0.00000 $C2=$ -0.05500 0.00000

$C3=$ 0.00000 0.00000 $C4=$ 0.00000   0.00000

$C5=$ 0.00000 0.00000 $URMAX=$ -0.062

$R=$ 1.062 $UR=$ -0.062 $UI=$ 0.000 $VTE=$ 0.99661

Figure 14.   Von Mises airfoil resulting from small perturbation
of zero locations giving the flat plate result.

$ZT=$ 1.000   0.000 $Z2=$ -0.900   0.000

$Z3=$ -0.100   0.000 $Z4=$ 0.000   0.000

$Z5=$ 0.000   0.000 $Z6=$ 0.000   0.000

$C1=$ 0.91000   0.00000 $C2=$ 0.04500   0.00000

$C3=$ 0.00000   0.00000 $C4=$ 0.00000   0.00000

$C5=$ 0.00000   0.00000   URMAX=0.041

R=0.959   UR=0.041   UI=0.000   VTE=0.99814

Figure 15.   Von Mises airfoil resulting from small perturbation
             of zero locations giving the flat plate result.

ZT= 1.000   0.000   Z2= -0.600   0.00C

Z3= -C.100   0.000   Z4= -0.100   0.000

Z5= -0.100   0.C00   Z6= -0.100   0.000

C1= 0.70000   0.00000   C2= 0.13000   0.00000

C3= 0.01250   0.00000   C4= 0.00061   0.00C00

C5= 0.00001   0.00000   URMAX=0.137

R=0.863   UR=0.137   UI=0.000   VTE=0.98959

Figure 16. Von Mises airfoil having largest VTE attainable
for the given real parts of the transformation
coefficients.

ZT= 1.000   0.000   Z2= -0.600   0.000

Z3= -0.120   0.000   Z4= -0.080   0.000

Z5= -0.100   0.000   Z6= -0.100   0.000

C1= 0.70040   0.00000   C2= 0.12996   0.00000

C3= 0.01241   0.00000   C4= 0.00060   0.00000

C5= 0.00001   0.00000   URMAX=0.137

R=0.863   UR=0.137   UI=0.000   VTE=0.98958

Figure 17. Von Mises airfoil resulting from the small perturbation
            of the zero locations used in generating the airfoil
            of Figure 16.

145

Figure 18. Thickness ratio and maximum trailing edge velocity ratio as a function of ξ_2 for three-term, symmetrical von Mises airfoils.

Figure 19. Thickness ratio and maximum trailing edge velocity ratio as a function of ξ_2 for six-term, symmetrical von Mises airfoils.

Figure 20. Approximate relationship between the maximum trailing edge velocity ratio and the thickness ratio for reasonable symmetrical airfoils.

ζ-plane

$r = 1$

ϕ

2α

$U = 1$

α

$z = f(\zeta)$

θ

$U = 1$

α

z-plane

Figure 21. Transformation of a unit circle at angle of attack
into an airfoil.

ZT= 1.000   0.000   Z2= -1.500   0.000

Z3= 0.125   0.000   Z4= 0.125   0.000

Z5= 0.125   0.000   Z6= 0.125   0.000

C1= 1.65625 0.00000   C2= -0.39453 0.00000

C3= 0.04810 0.00000   C4= -0.00296 0.00000

C5= 0.00007 0.00000   URMAX= -0.458

R= 1.458   UR= -0.458   UI= 0.000   VTE= 0.93584

Figure 22.   Von Mises airfoil having finite trailing edge
pressure gradients, CPXT = - 1.37, CPYT = 0.0.

Figure 23.   Segmentation of the interval $(0, 2\pi)$ in the circle
and airfoil planes.

Figure 24.   Typical pressure recovery distribution.

Figure 25. Airfoil obtained using Eppler and Somers code [25] in which no iteration is performed for achieving a desired trailing edge closure angle. ALPHA = 8.0 DEG (relative to zero-lift line).

Figure 26. Airfoil obtained using the modified Eppler and Somers code
in which the integral constraint required for finite
trailing edge pressure gradients is satisfied.
ALPHA = 8.0 DEG (relative to zero-lift line).

Figure 27. Airfoil resulting from Eppler and Somers code in which K
is iterated to achieve a desired trailing edge angle.
ALPHA = 8.0 DEG (relative to zero-lift line).

Figure 28. Airfoil having finite trailing edge pressure gradients
obtained using modified Eppler and Somers code.
ALPHA = 8.0 DEG (relative to zero-lift line).

CPST = - 7.2   CPNT = - 57.0

Figure 29. Airfoil obtained from Eppler and Somers code in which K is iterated to achieve the desired trailing edge closure angle. ALPHA = 12.0 DEG (relative to zero-lift line).

Figure 30. Airfoil having finite trailing edge pressure gradients
obtained using modified Eppler and Somers code.
ALPHA = 12.0 DEG (relative to zero-lift line).

CPST = - 12.6   CPNT = - 72.4

Figure 31. Symmetrical airfoil having finite trailing edge pressure
gradients. CPST = - .71, CPNT = 0.0, ALPHA = 0.0 DEG.

Figure 32. Potential flow velocity distribution of Strand airfoil,
Reference [34], calculated using the panel method analysis
capability of the Eppler and Somers code, shown along with
the finite trailing edge pressure gradient airfoil and its
design velocity distribution. ALPHA = 12.0 DEG (relative
to zero-lift line).

Figure 33. Liebeck L1004 airfoil redesigned to have finite trailing
edge pressure gradients. CL = 1.31, CD = .0071, CM = - .0276
CPST = - 38, CPNT = - 227, ALPHA = 8.9 DEG

Figure 34. Liebeck L1003 airfoil redesigned to have finite trailing edge pressure gradients. CL = 1.07, CD = .0270, CM = - .0228, CPST = - 45, CPNT = - 225, ALPHA = 11.3 DEG. Separated flow on upper surface.

ORIGINAL PAGE IS
OF POOR QUALITY

Figure 35. Aerodynamically smoothed Wortmann FX 67-K-150 airfoil,
Reference [37], and calculated velocity distribution.
ALPHA = 10.0 DEG (relative to zero-lift line).

ORIGINAL PAGE IS
OF POOR QUALITY

Figure 36. Viscous analysis of Wortmann FX 67-K-150 using Eppler and Somers code. Pitching moment coefficient is taken about the quarter-chord point.

Figure 37. Velocity distribution at the design point and finite trailing
edge pressure gradients airfoil based on FX 67-K-150 of
Wortmann.
ALPHA = 10.0 DEG (relative to zero-lift line).

T. = Boundary layer transition
S. = Boundary layer separation
u. = Upper surface
l. = Lower surface

Figure 38. Viscous analysis of airfoil based on Wortmann FX 67-K-150 using Eppler and Somers code. Pitching moment coefficient is taken about the quarter-chord point.

Figure 39. Pressure distribution from GRUMFOIL analysis. Wortmann FX 67-K-150. CL = 1.1676
CD = .0066   CM = -.1203   CPTE = .2602   ALPHA = 5.56   RE = 2x10^6

167

ORIGINAL PAGE IS
OF POOR QUALITY

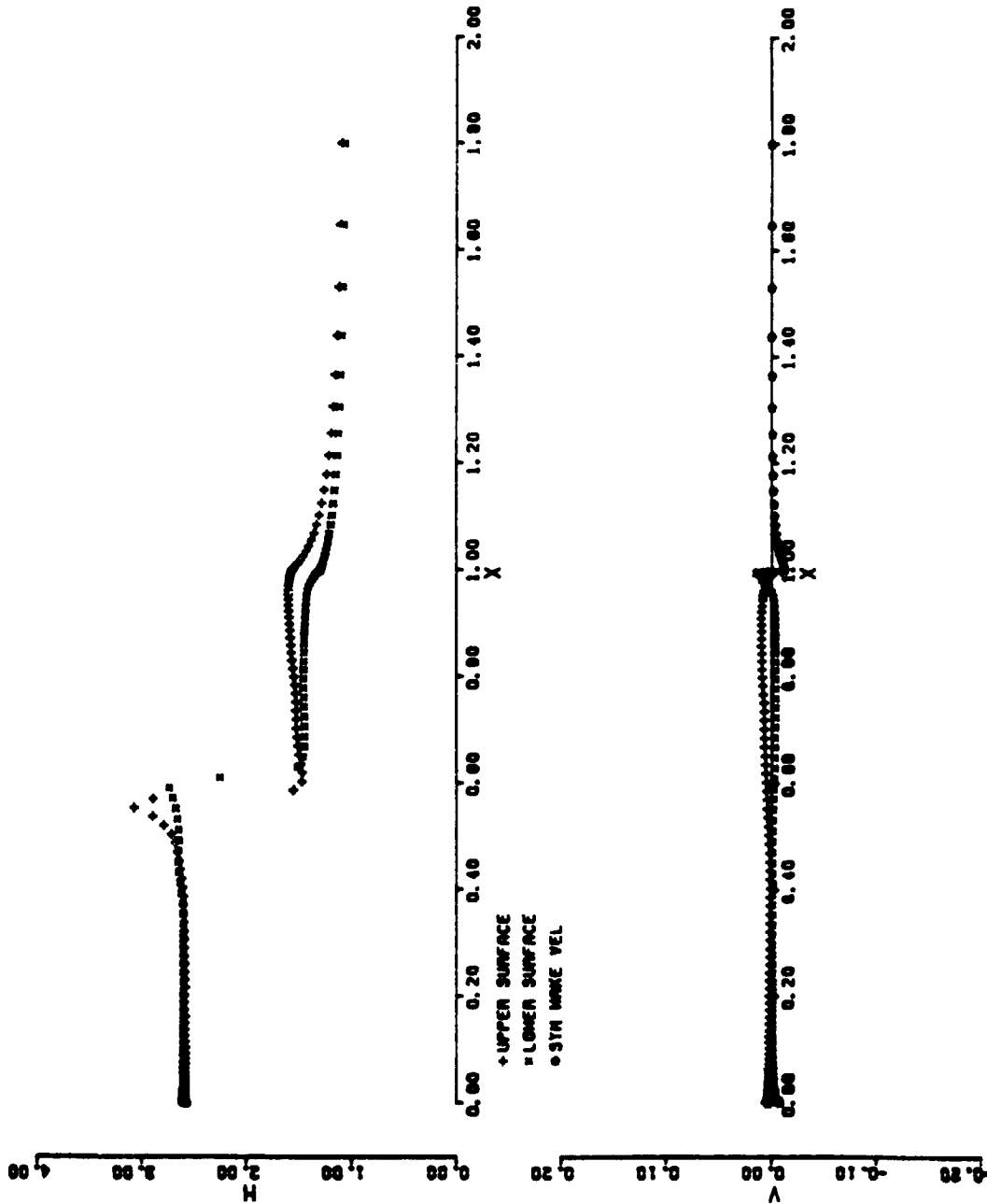Figure 40. Skin friction coefficient and displacement thickness. Wortmann FX 67-K-150.

Figure 41. Local boundary layer form factor, H_{12}, and equivalent surface source velocity distribution to account for displacement thickness. Wortmann FX 67-K-150.

ORIGINAL PAGE IS
OF POOR QUALITY

Figure 42. Pressure distribution from GRUMFOIL analysis. Airfoil based on Wortmann FX 67-K-150 but having finite trailing edge pressure gradients.

CL = 1.1684   CD = .0064   CM = -.1308   CPTE = .2012   ALPHA = 4.98   RE = 2x10^6

Figure 43. Skin friction coefficient and displacement thickness. Airfoil based on Wortmann FX 67-K-150 but having finite trailing edge pressure gradients.

Figure 44. Local boundary layer form factor, H_{12}, and equivalent surface source velocity distribution to account for displacement thickness. Airfoil based on Wortmann FX 67-K-150 but having finite trailing edge pressure gradients.
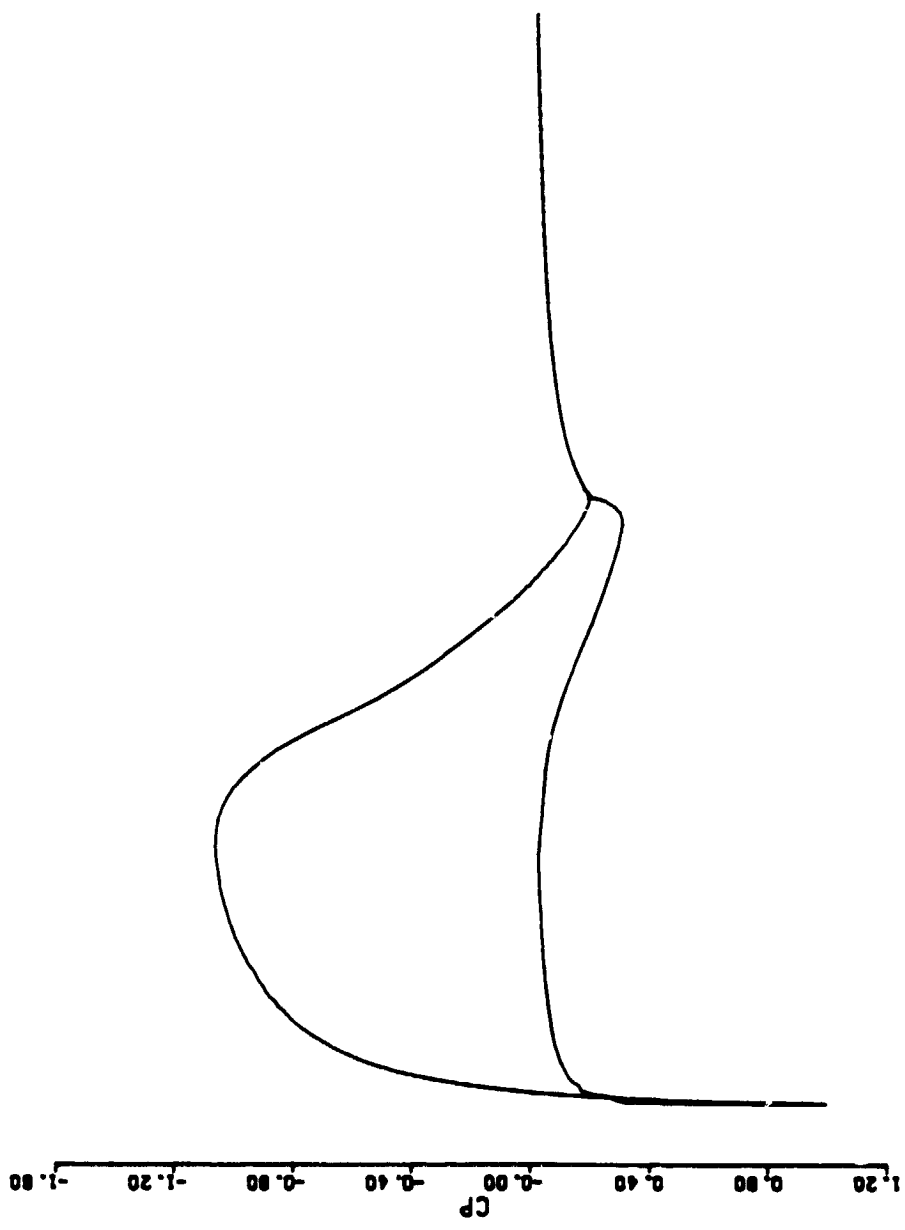
ORIGINAL PAGE IS
OF POOR QUALITY

Figure 45. Off-design pressure distribution from GRUMFOIL analysis. Airfoil based on Wortmann FX 67-K-150 but having finite trailing edge pressure gradients. CL = .7019
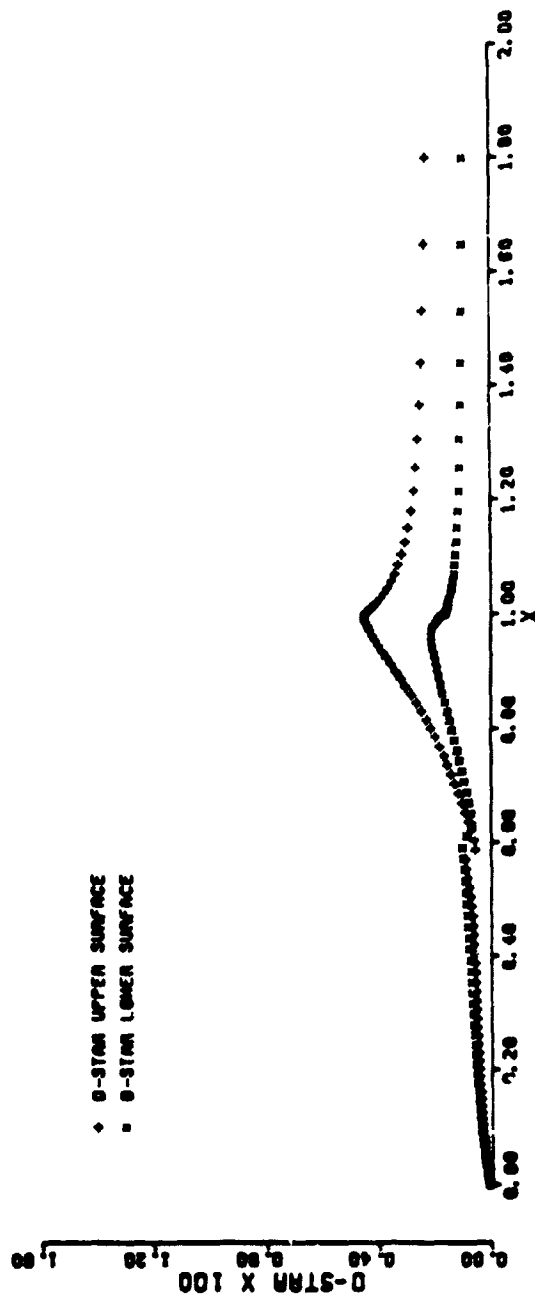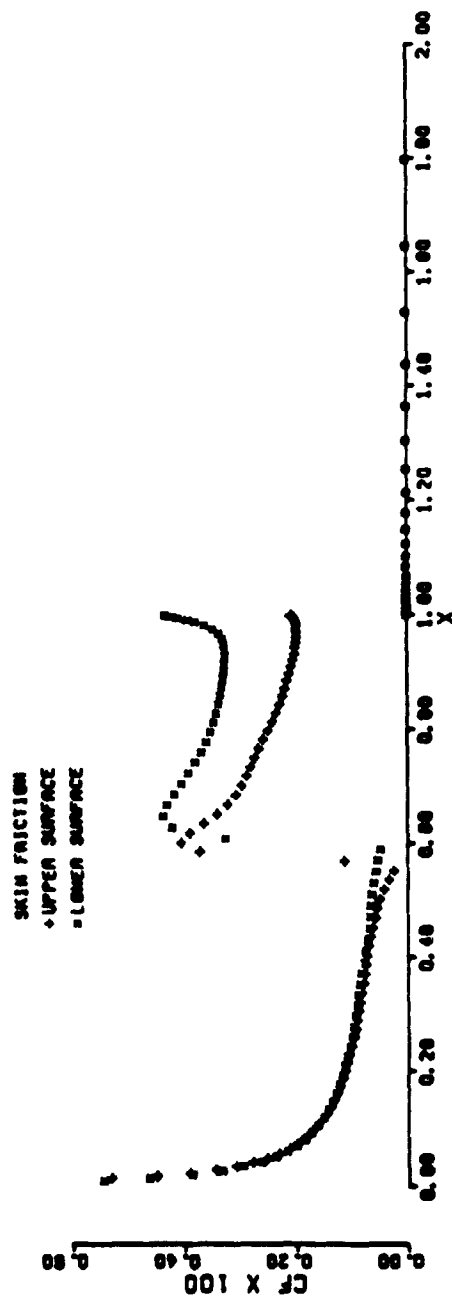CD = .0055 CM = -.1211 CPTE = .2019 ALPHA = 0.98 RE = 2x10^6

Figure 46. Off-design skin friction coefficient and displacement thickness. Airfoil based on Wortmann FX 67-K-150 but having finite trailing edge pressure gradients.
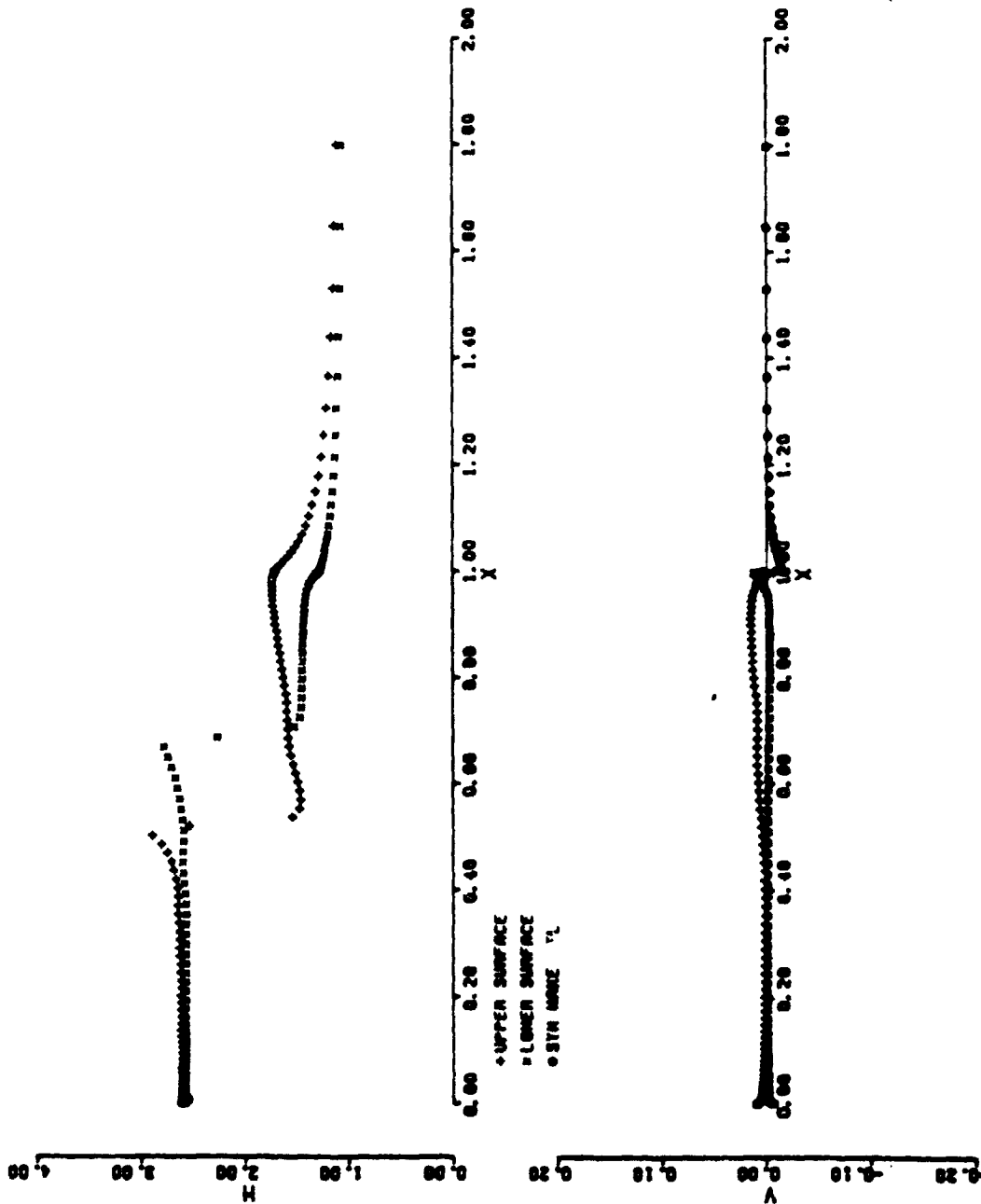
Figure 47. Off-design local boundary layer form factor, H_{12}, and equivalent surface source velocity distribution to account for displacement thickness. Airfoil based on Wortmann FX 67-K-150 but having finite trailing edge pressure gradients.
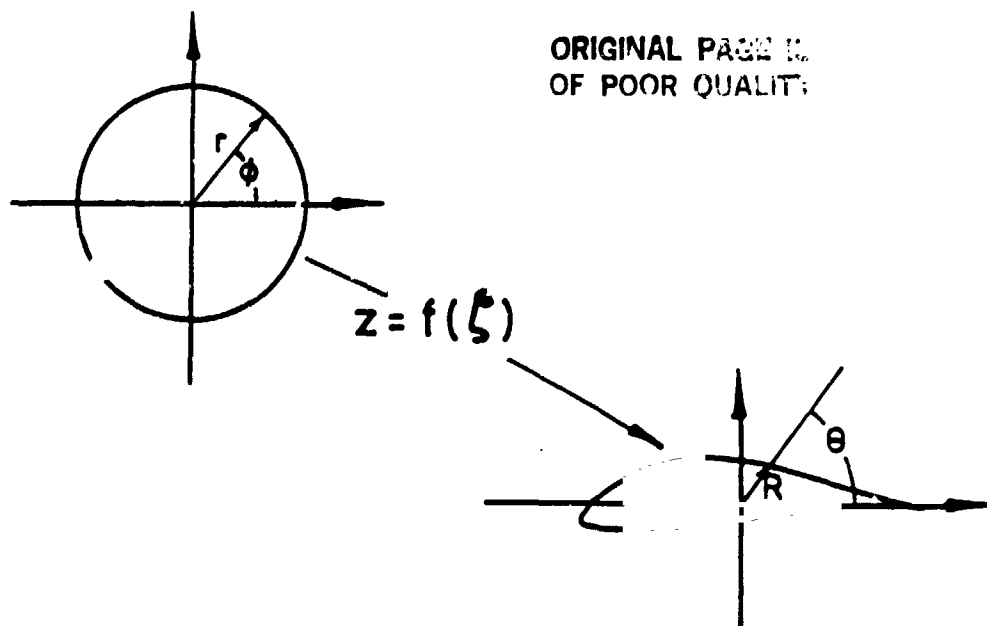
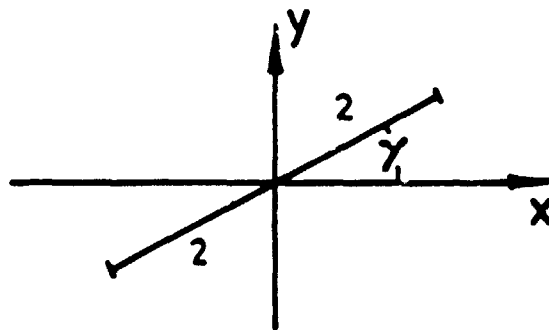Figure 48. General transformation of a circle to an airfoil.

Figure 49. Mapping of the unit circle using the transformation of
equation (A-13).

```
ABS?          180
TRA1  9030  950 1C00 1650-2400 1150-2400 1250-2400 1350-1600 1450 1550 -100
TRA1  9030 1650  400 1750  700 1850  800 1950  850 2050  900 2450 1000 2750 1075
TRA1  9030 2950 1125  000 1150 3250  450 3350  500 4050  500 4450  500 4750  800
TRA1  9030 4850 1200 4950 1600 5045 2000 5C50 2400 6000 1000
TRA2  9030   30  940  000  100 6000  550  940  000  100  300
ALFA100 14  100  200  300  400  500  600  700  800  900 1000 1100 1200 1300 1400
DIAG
RE  100   03      100003    200003    3000
CDCL
ENDE
```

Figure 50. Sample input to modified Eppler and Somers code which yields an airfoil based on the Wortmann FX 67-K-150 but having finite trailing edge pressure gradients.

RECENT AERONAUTICAL AND ASTRONAUTICAL ENGINEERING DEPARTMENT TECHNICAL REPORTS (Continued)

Technical Report Number	Title	Author	Journal Publication
AAE 77-16 UILU-ENG 77 0516	The Effects of Energy Distribution Rates and Density Distribution on Blast Wave Structure	R. A. Strehlow L. H. Sentman	
AAE 77-17 UILU ENG 77 0517	Modeling of Convective Mode Combustion Through Granulated Propellant to Predict Transition to Detonation	H. Krier J. A. Kezerle	17th Combustion Symposium: In Press
AAE 78-1 UILU ENG 78 0501	Unsteady Internal Boundary Layer Flows with Application to Gun Barrel Heat Transfer and Erosion	M. J. Adams H. Krier	
AAE 78-2 UILU ENG 78 0502	Extracting Burning Rates for Multiperforated Propellant from Closed Bomb Testing	H. Krier	
AAE 78-3 UILU ENG 78 0503	Lean Limit Flammability Study of Methane-Air Mixtures in a Square Flammability Tube	J. Jarosinski R. A. Strehlow	
AAE 78-4 UILU ENG 78 0504	Interim Technical Report AFOSR 77-3336: "An Investigation of the Ignition Delay Times For Propylene Oxide-Oxygen-Nitrogen Mixtures"	E. E. Meister	
AAE 78-5 UILU ENG 78 0505	Final Report: A Distribution Model for the Aerial Application of Granular Agricultural Particles	S. T. Fernandes A. I. Ormsbee	
AAE 78-6 UILU ENG 78 0506	The Thermal Structure of a Methane-Air Flame Propagating in a Square Flammability Tube	J. Jarosinski R. A. Strehlow	
AAE 78-7 UILU ENG 78 0507	The Effects of Energy Distribution Rates and Density Distribution on Blast Wave Structure	R. A. Strehlow L. H. Sentman	
AAE 78-8 UILU ENG 78 0508	The Effect of a Zero G Environment on Flammability Limits as Determined Using a Standard Flammability Tube Apparatus	R. A. Strehlow D. L. Reuss	

RECENT AERONAUTICAL AND ASTRONAUTICAL ENGINEERING DEPARTMENT TECHNICAL REPORTS (Continued)

Technical Report Number	Title	Author	Journal Publication
AAE 79-1 UILU-ENG 79 0501	An Approximate Finite Element Method of Stress Analysis of Non-Axisymmetric Bodies with Elastic-Plastic Material	J. N. Craddock A. R Zak	
AAE 79-2 UILU-ENG 79 0502	Stability of Bridge Motion in Turbulent Winds	Y. K. Lin S. T. Ariaratnam	
AAE 79-3 UILU ENG 79 0503	Rotor Blade Dynamics in Hovering Flights	C.Y.R. Hong	
AAE 79-4 UILU ENG 79 0504	Finite Element Analysis of A Dynamically Loaded Flat Laminated Plate	D. W. Pillasch A. R. Zak	
AAE 79-5 UILU ENG 79 0505	An Efficient Rotational Nonequilibrium Model of a CW Chemical Laser	L, H, Sentman	
AAE 79-6 UILU ENG 79 0506	Column Response to Vertical-Horizontal Earthquakes	Y. K. Lin T. Y. Shih	
AAE 79-7 UILU ENG 79 0507	Users Guide for Programs MNORO & AFOPTMNORO	L. H. Sentman	
AAE 79-8 UILU ENG 79 0508	The Blast Wave from Deflagrative Explosions, an Acoustic Approach	R. A. Strehlow	
AAE 80-1 UILU ENG 80 0501	Gas Flow Resistance Measurements Through Packed Beds at High Reynolds Numbers	S. F. Wilcox H. Krier	
AAE 80-2 UILU ENG 80 0502	Fluid Mechanical Processes of Deflagration to Detonation Transition in Beds of Porous Reactive Solids	S. Hoffman H. Krier	
AAE 80-3 UILU ENG 80 0503	Dynamic Analysis of Orthotropic, Layered Plates Subject to Explosive Loading	D. W. Pillasch A. R. Zak	

RECENT AERONAUTICAL AND ASTRONAUTICAL ENGINEERING DEPARTMENT TECHNICAL REPORTS (continued)

Technical Report Number	Title	Author	Journal Publication
AAE 81-1 UILU ENG 81 0501	Shock Development and Transition to Detonation Initiated by Burning in Porous Propellant Beds	P. B. Butler H. Krier	
AAE 81-2 UILU ENG 81 0502	Development of a Single Species Equation of State for Determining Products Suitable for Hydrocode Calculations	L. H. Sentman R. A. Strehlow B. Haeffle A. Eckstein	
AAE 81-3 UILU ENG 81 0503	Large Deformation Dynamic Analysis of Laminated Plates by Finite Element Method	A. R. Zak	
AAE 81-4 UILU ENG 81 0504	Computer Programs for Automatic Input Data Generation for Finite Element Structural Codes ADINA and NASTRAN	A. R. Zak	
AAE 81-5 UILU ENG 81 0505	Nonlinear Interactions Between the Pumping Kinetics, Fluid Dynamics and Optical Resonator of cw Fluid Flow Lasers	L. H. Sentman M. H. Nayfeh	
AAE 81-6 UILU ENG 81 0506	An Algorithm for Minimum Weight Design of Structures Based on Optimality Criteria	W. Li	
AAE 81-7 UILU ENG 81 0507	Test and Evaluation of an Advanced Dynagun Ballistic Simulator	H. Krier D. W. Meeks	
AAE 81-8 UILU ENG 81 0508	A Theoretical and Experimental Study of cw HF Chemical Laser Performance	L. H. Sentman W. O. Mosebach	
AAE 82-1 UILU ENG 82 0501	A Subroutine for Calculating High Temperature CHONI Equilibrium	R. A. Strehlow	
AAE 82-2 UILU ENG 82 0502	Gaskinetics and Thermodynamic Aspects in Evaporation and Condensation Knudsen Layers	T. Ytrehus	

RECENT AERONAUTICAL AND ASTRONAUTICAL ENGINEERING DEPARTMENT TECHNICAL REPORTS (continued)

Technical Report Number	Title	Author	Journal Publication
AAE 83-1 UILU ENG 83 0501	MNORO3: An Efficient Rotational Nonequilibrium cw HF Chemical Laser Model	L. H. Sentman P. Schmidt	
AAE 83-2 UILU ENG 83 0502	Concepts of a General Substructuring System for Structural Dynamics Analyses	A. L. Hale L. V. Warren	
AAE 83-3 UILU ENG 83 0503	Approximate Modal Control of Distributed-Parameter Structures	A. L. Hale G. A. Rahn	
AAE 83-4 UILU ENG 83 0504	Users Guide for Program MNORO3	L. H. Sentman P. Schmidt	
AAE 83-5 UILU ENG 83 0505	Nonlinear Interactions Between the Pumping Kinetics, Fluid Dynamics and Optical Resonator of cw Fluid Flow Lasers	L. H. Sentman M. H. Nayfeh	
AAE 83-6 UILU ENG 83 0506	Effects of the HF Rate Package and the Optical Resonator on cw HF Chemical Laser Performance	L. H. Sentman P. F. Schmidt G. M. Marinos L. H. Sentman	
AAE 83-7 UILU ENG 83 0507	The Effects of Cavity Losses on the Performance of a Subsonic cw HF Chemical Laser	P. Renzoni S. Townsend M. H. Nayfeh K. K. King	
AAE 83-8 UILU ENG 83 0508	The Dynamic Synthesis of General Nonconservative Structures From Separately Identified Substructure Models	A. L. Hale L. A. Bergman	
AAE 83-9 UILU ENG 83 0509	Finite Element Model for Nonaxisymmetric Structure With Rate Dependent Yield Conditions	A. R. Zak	
AAE 83-10 UILU ENG 83 0510	Nonlinear Interactions Between the Pumping Kinetics, Fluid Dynamics and Optical Resonator of cw Fluid Flow Lasers	L. H. Sentman M. H. Nayfeh	

RECENT AERONAUTICAL AND ASTRONAUTICAL ENGINEERING DEPARTMENT TECHNICAL REPORTS (continued)

Technical Report Number	Title	Author	Journal Publication
AAE 84-1 UILU ENG 84 0501	Trailing Edge Flow Conditions as a Factor in Airfoil Design	A. I. Ormsbee M. D. Maughmer	